INORGANIC SYNTHESIS AND CRYSTAL CHEMISTRY AT MULTIMEGABAR PRESSURES

Leonid Dubrovinsky and
Natalia Dubrovinskaia

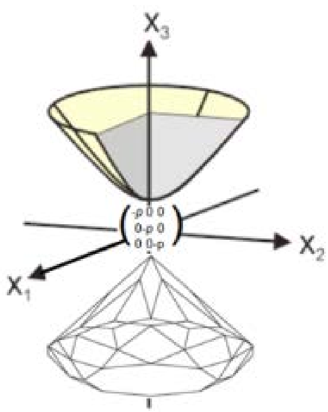

in incudibus veritas

UNIVERSITÄT BAYREUTH

BGI Bayerisches Geoinstitut

Haber-Bosch High Pressure Process

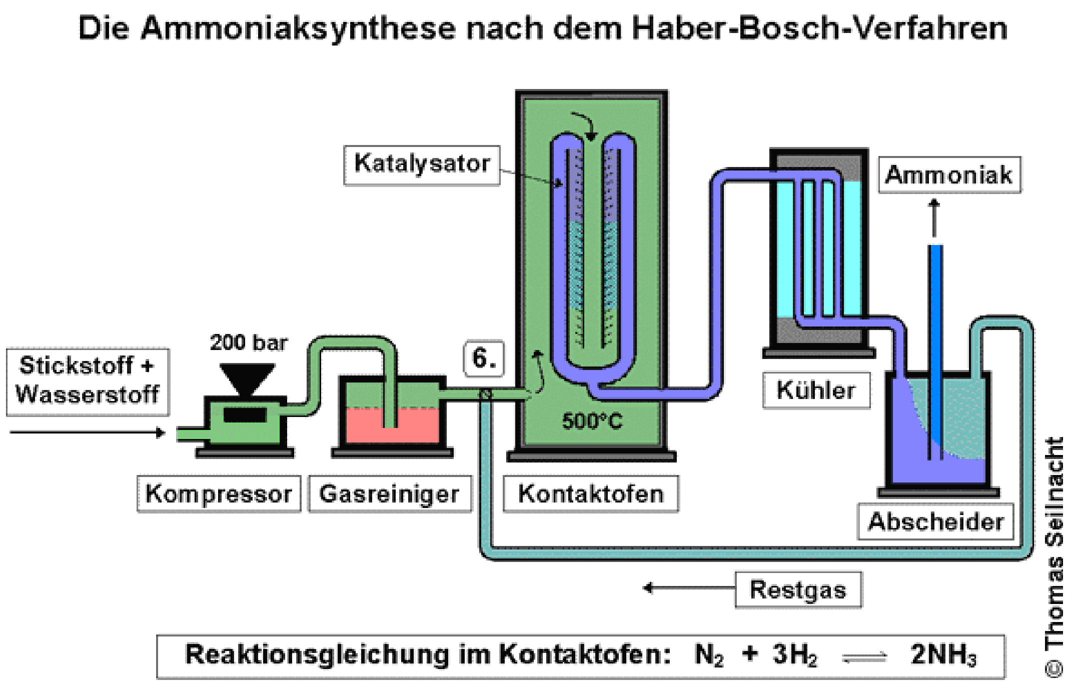

A historical (1921) high-pressure steel reactor for production of ammonia via the Haber process is displayed at the Karlsruhe Institute of Technology, Germany

High-Pressure Chemistry

DOI: 10.1002/anie.200602485

The Chemical Imagination at Work in *Very* Tight Places

Wojciech Grochala, Roald Hoffmann,* Ji Feng,* and Neil W. Ashcroft**

Keywords:
chemical bonding · electronic structure · high-pressure chemistry · metals · solid-state structures

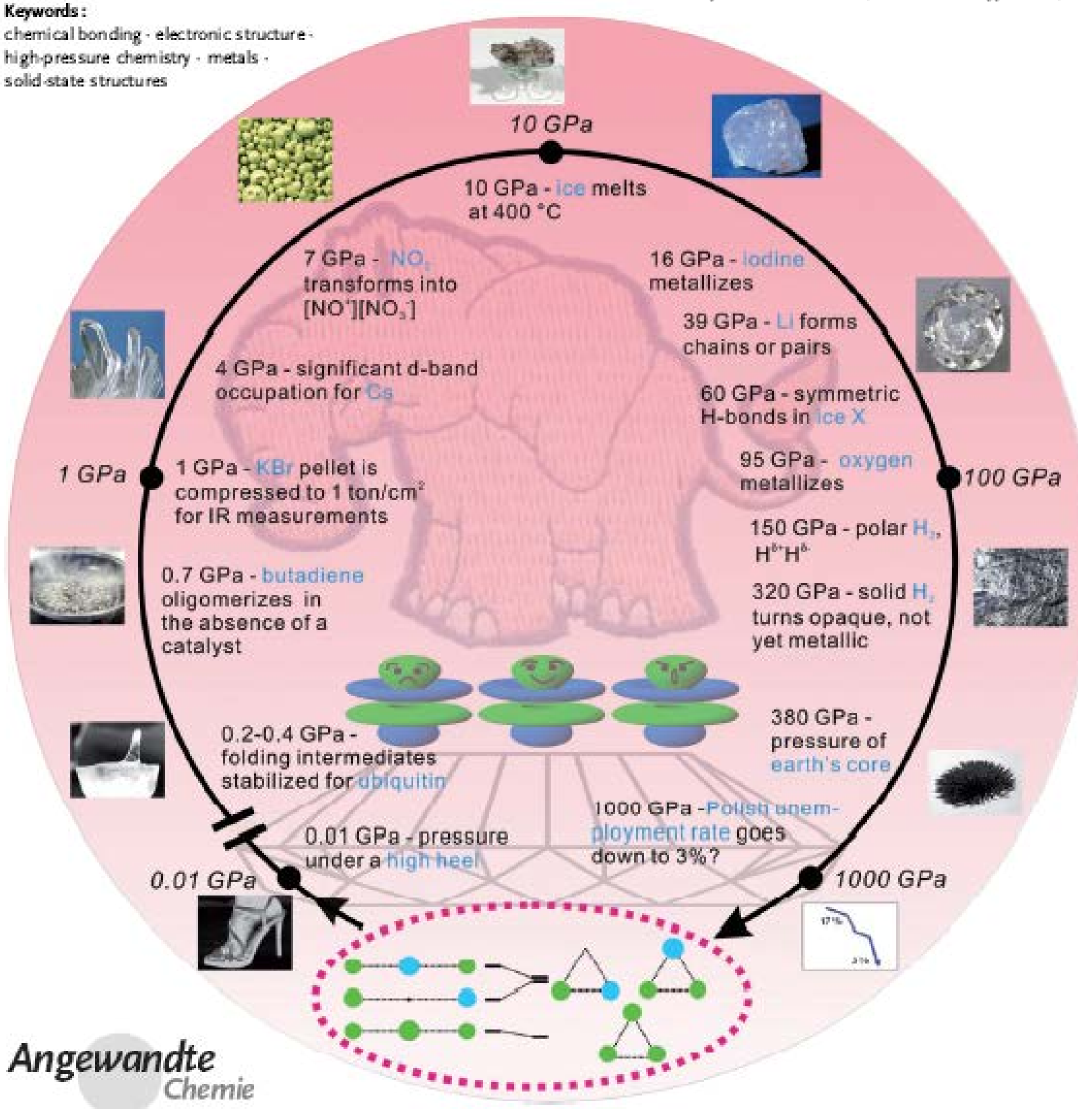

Angewandte Chemie

What are we searching for in extreme environments?

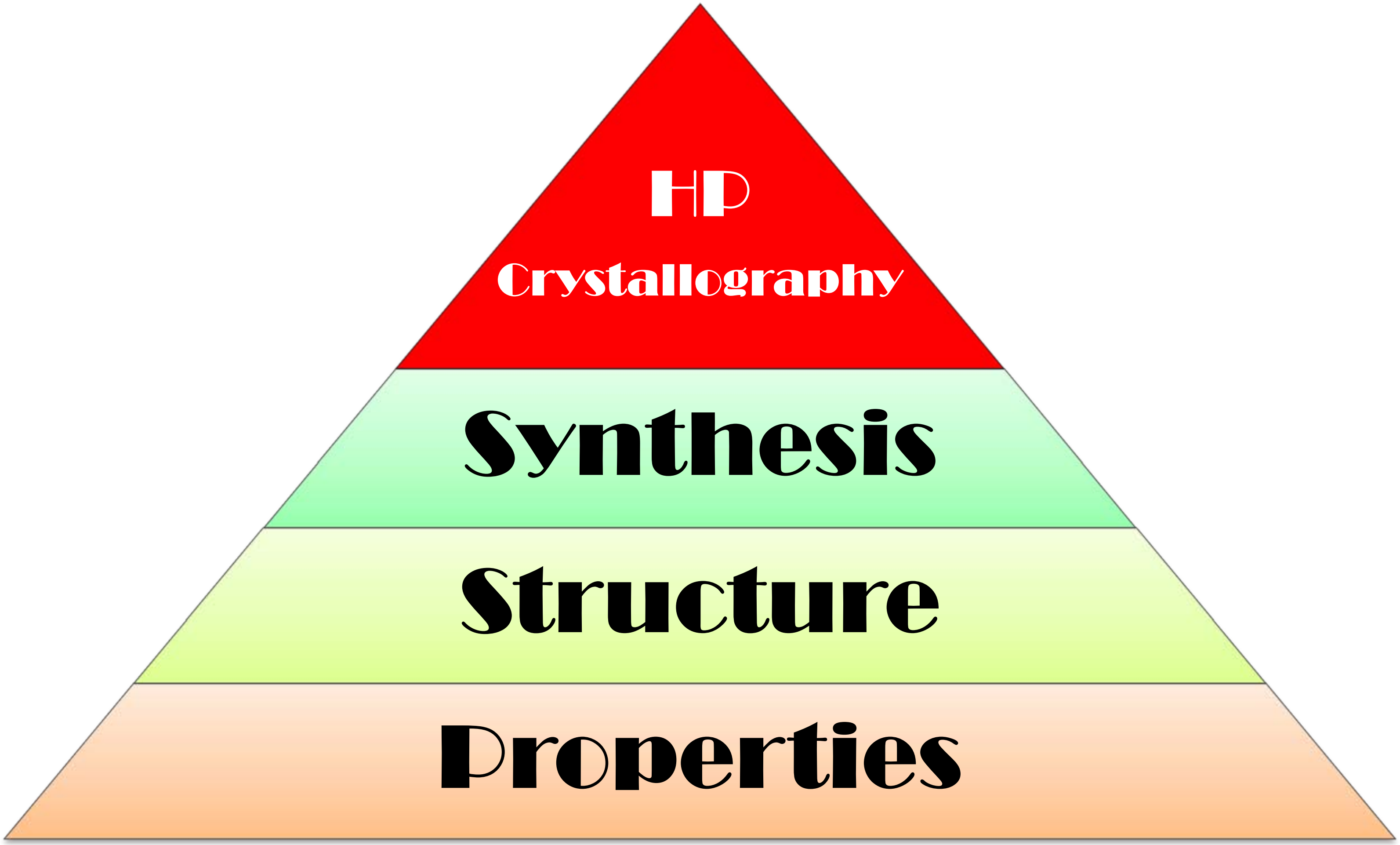

Diamond Anvil Cell (DAC) Technique

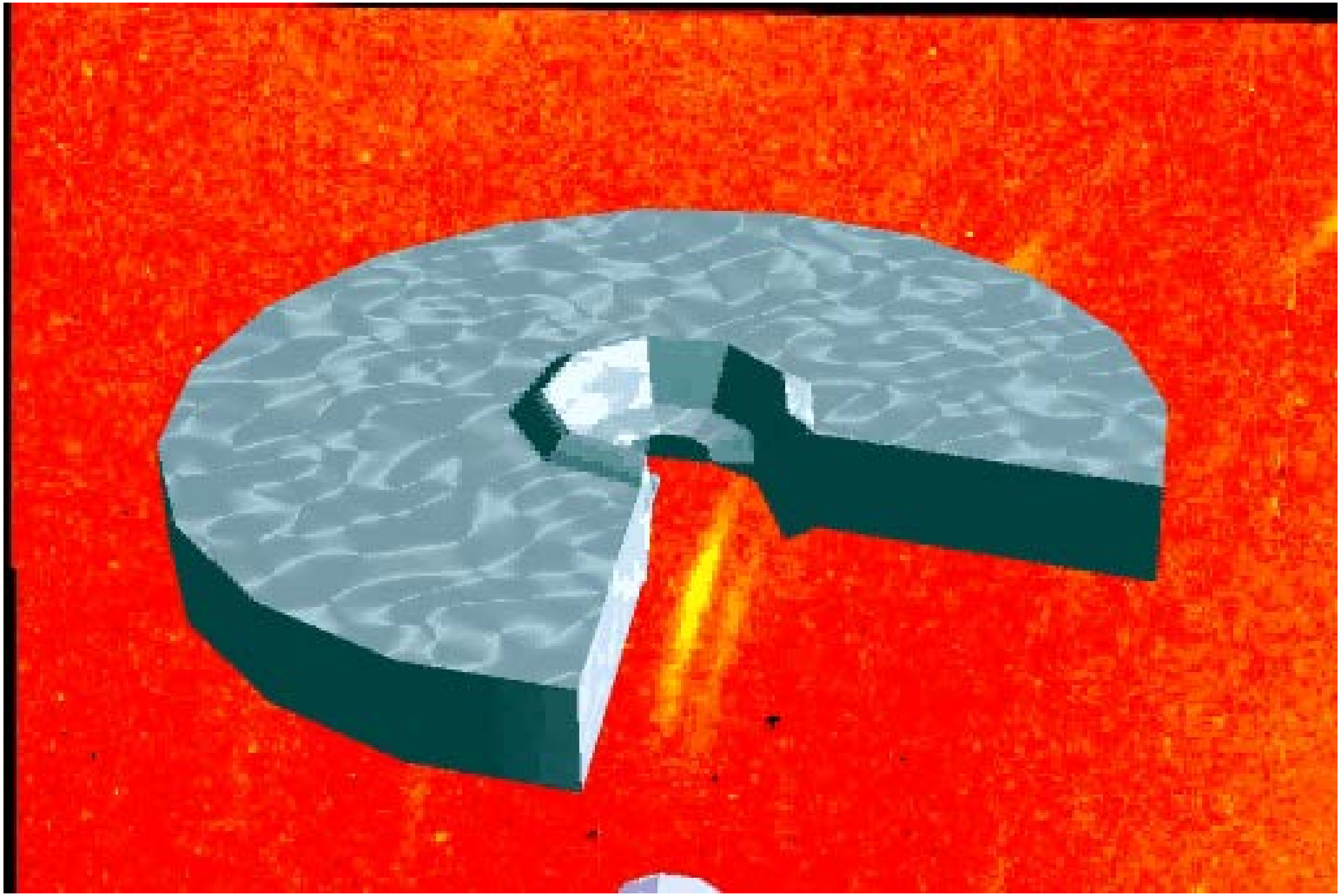

DAC Technique

DAC

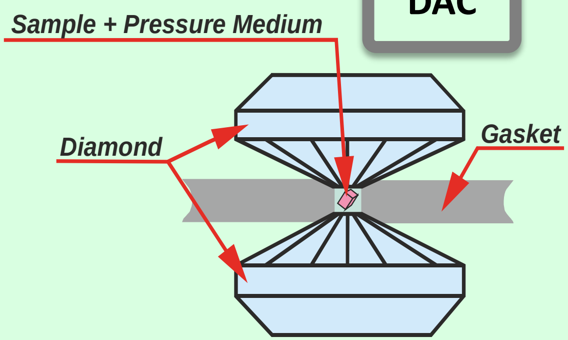

BX90 type DAC

How to heat the sample inside DAC?

- Direct temperature measurement
- Possibility to heat any substance

- Maximum T ~ 1200 K

Resistive Heating

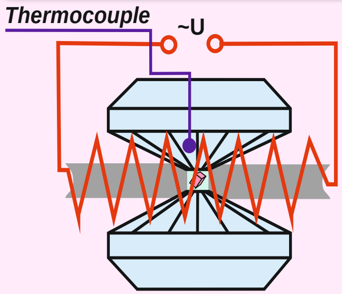

Laser Heating

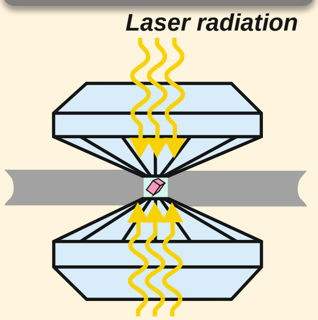

- Very high maximum T

- Temperature is estimated using the gray body approximation of Planck's law
- Impossibility to heat materials with low absorption at laser wavelength
- High temperature gradients

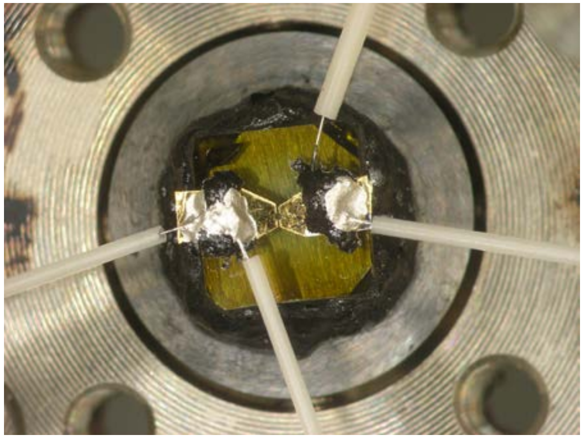

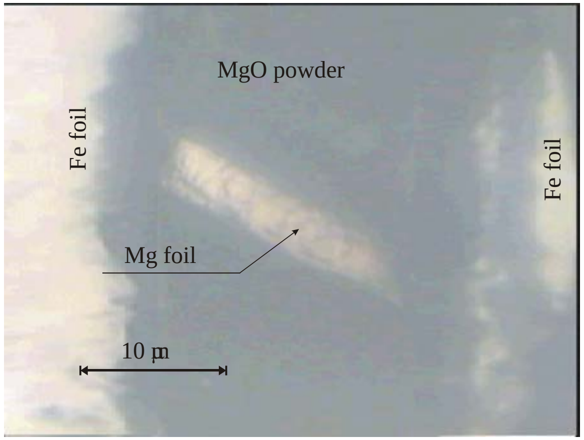

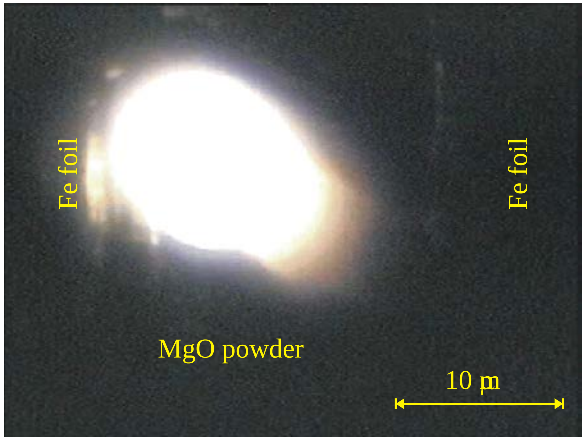

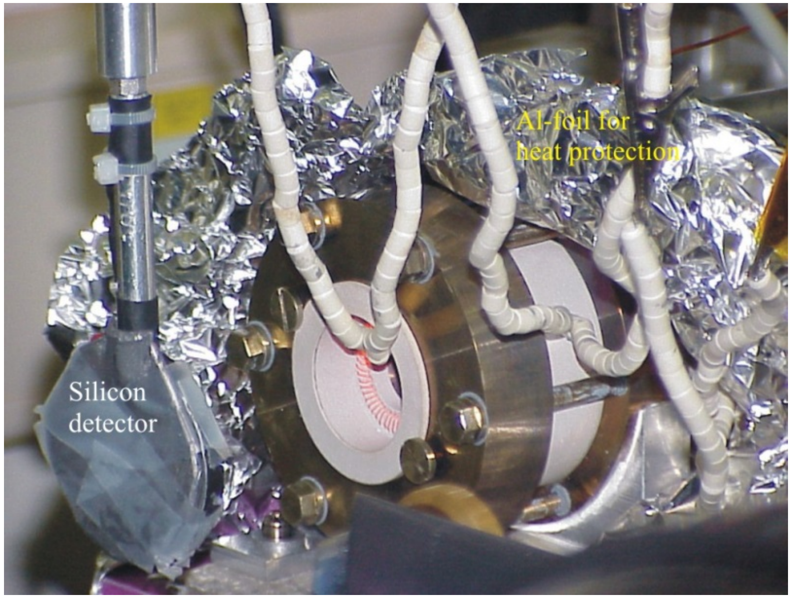

Dubrovinskaia et al., 2003

Dubrovinskaia et al., 2005

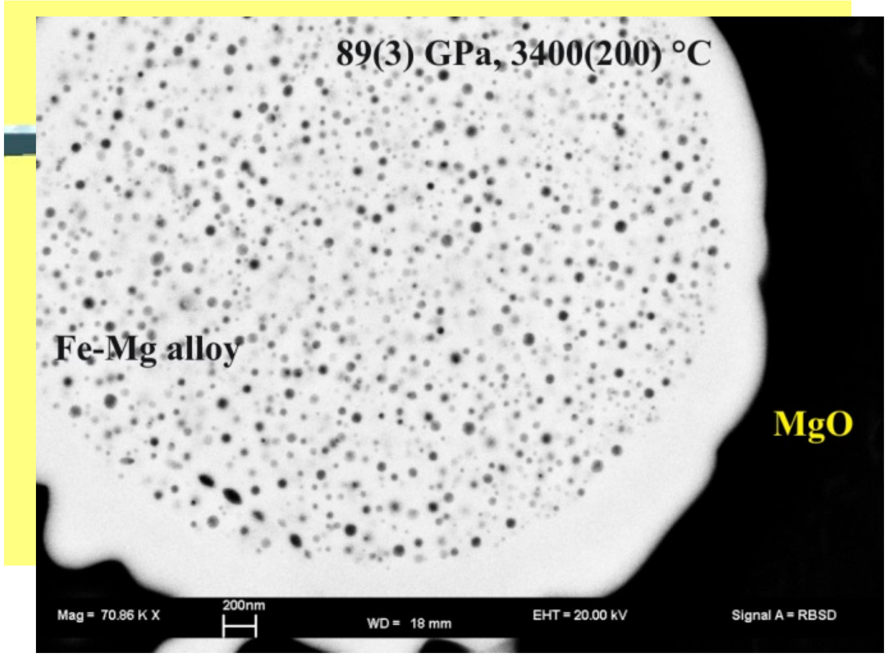

Fe-Mg alloying

Powder XRD

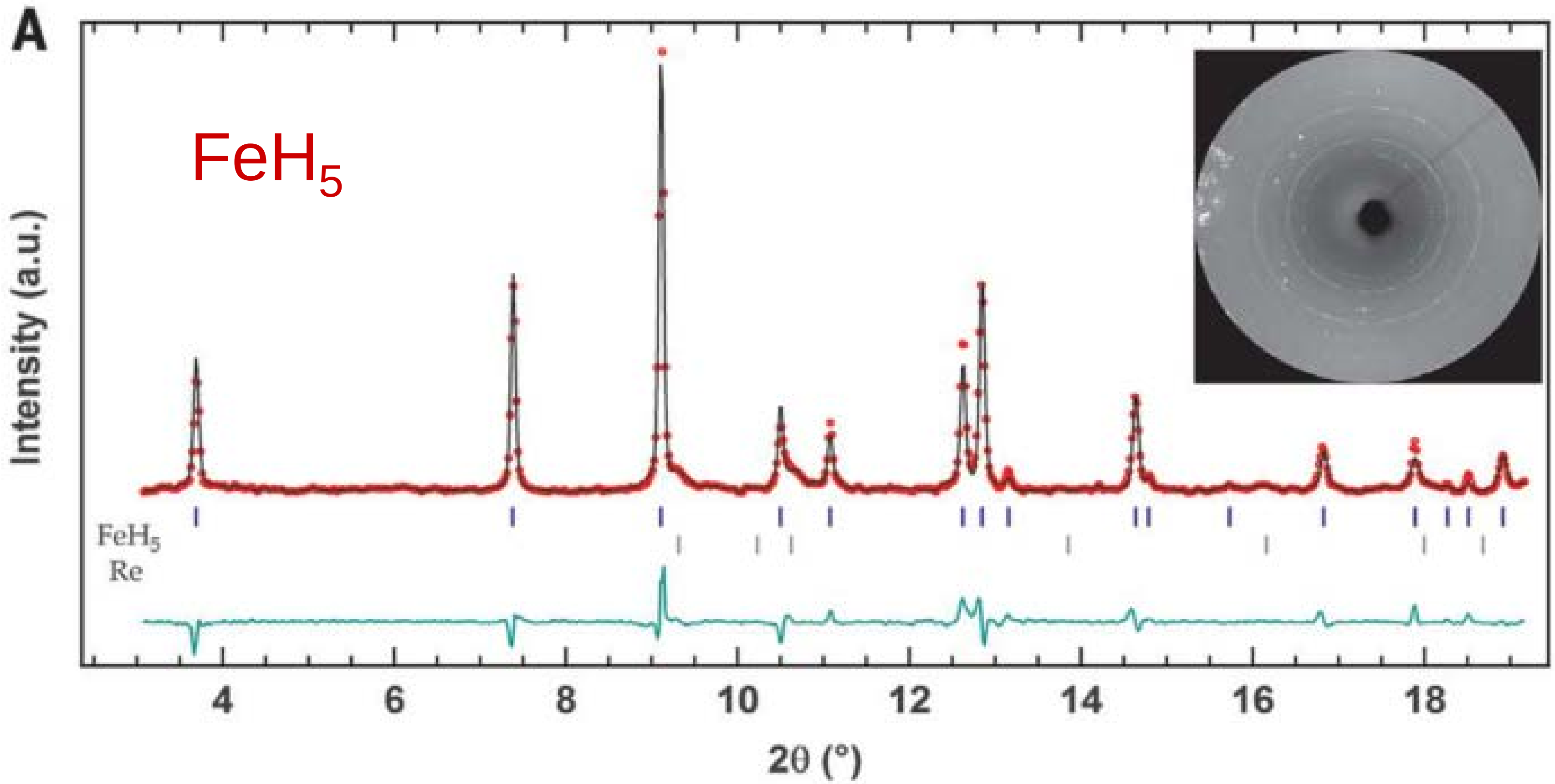

Pépin et al. Science, 2016

Powder XRD

218 J.W.E. Drewitt et al. / Earth and Planetary Science Letters 511 (2019) 213–222

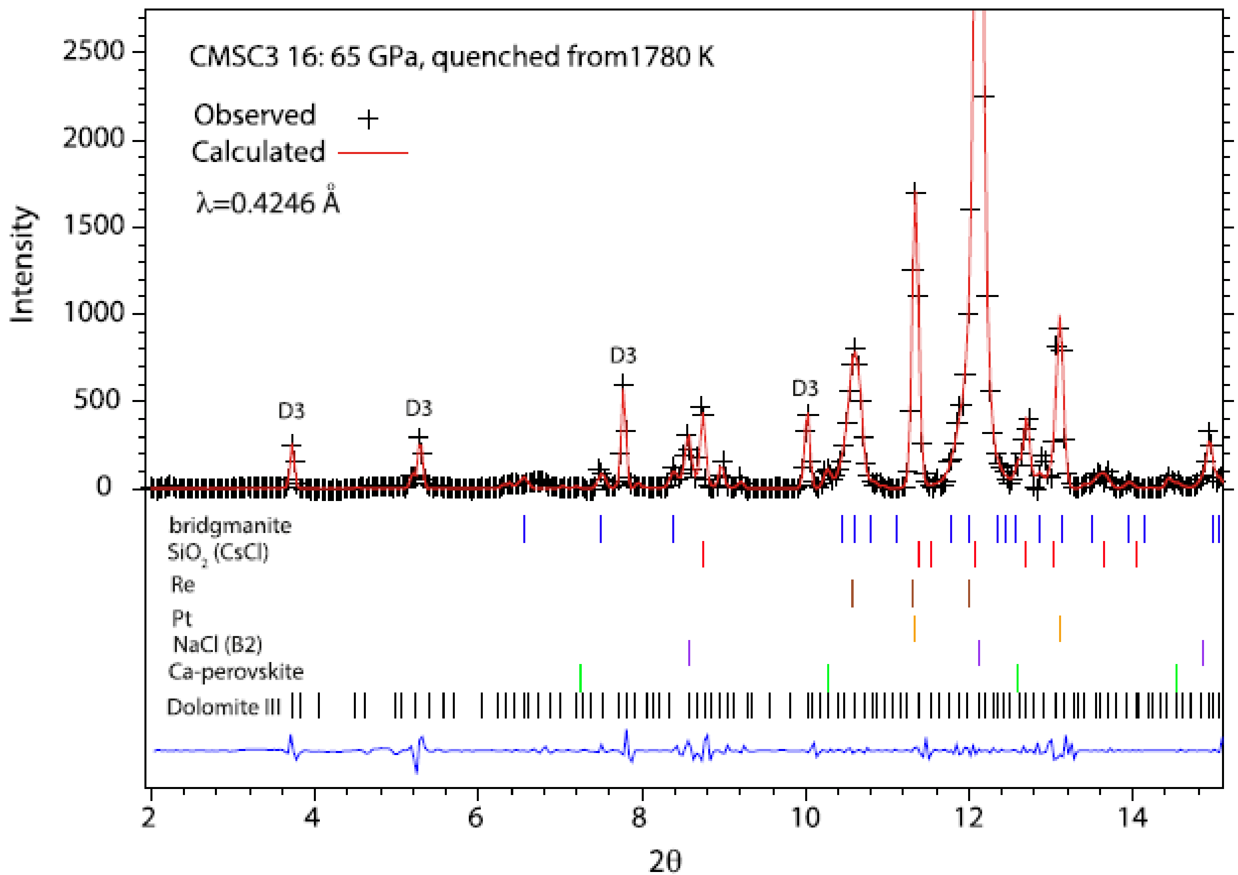

Fig. 5. Full profile GSAS fit to a diffraction pattern in sample CMSC3_16 taken at 65 GPa and quenched from 1780 K. The diffraction pattern shows the presence of a carbonate phase with multiple peaks that index to a dolomite III structured phase (Merlini et al., 2012). The pattern also shows the presence of bridgmanite and Ca-perovskite, which are products of a decarbonation reaction between carbonate and stishovite (also present).

Srtucture solution
Single-crystal XRD

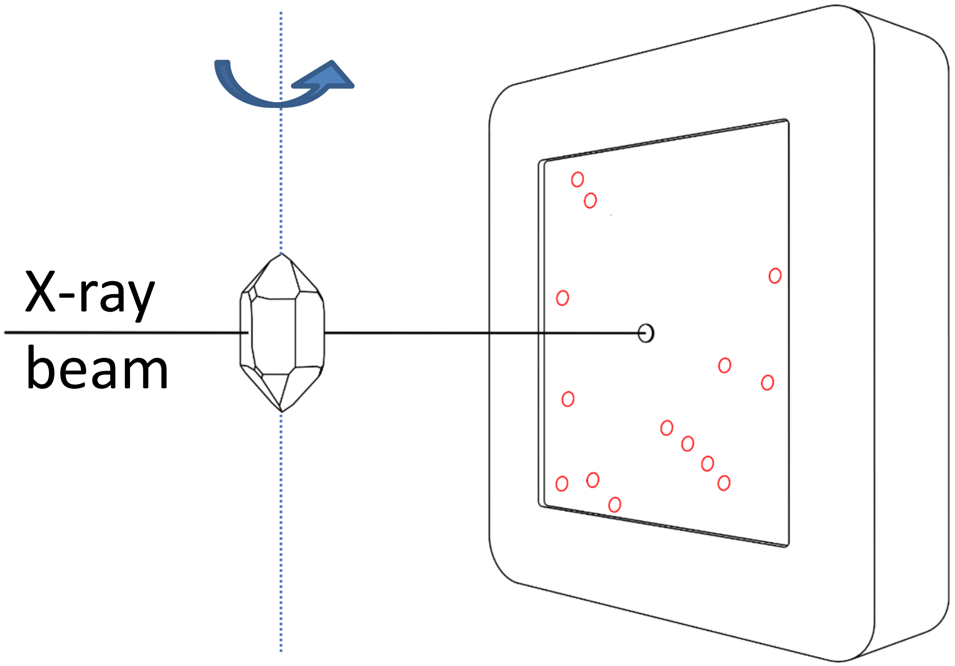

ω = 0°

2D detector

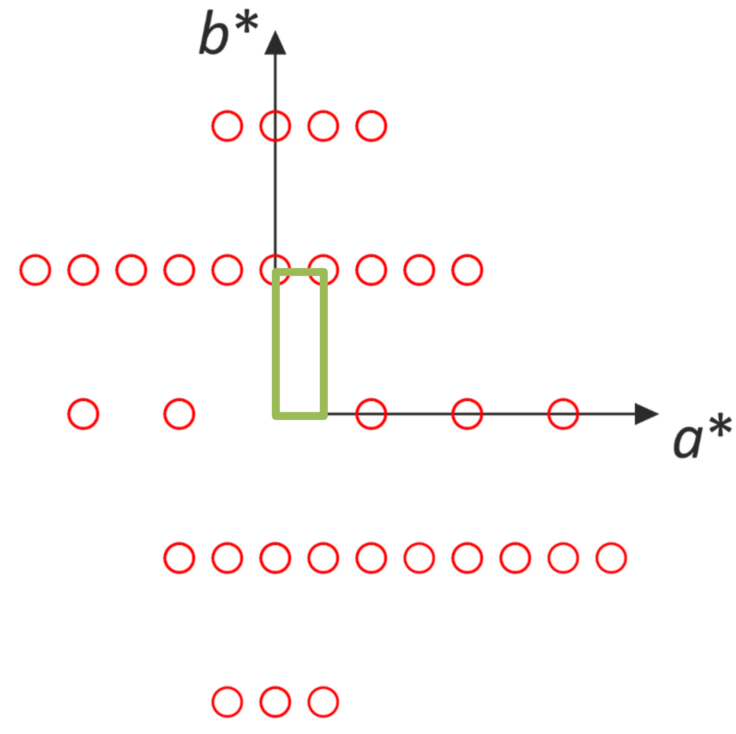

reciprocal space reconstruction

Principle of DAC Technique

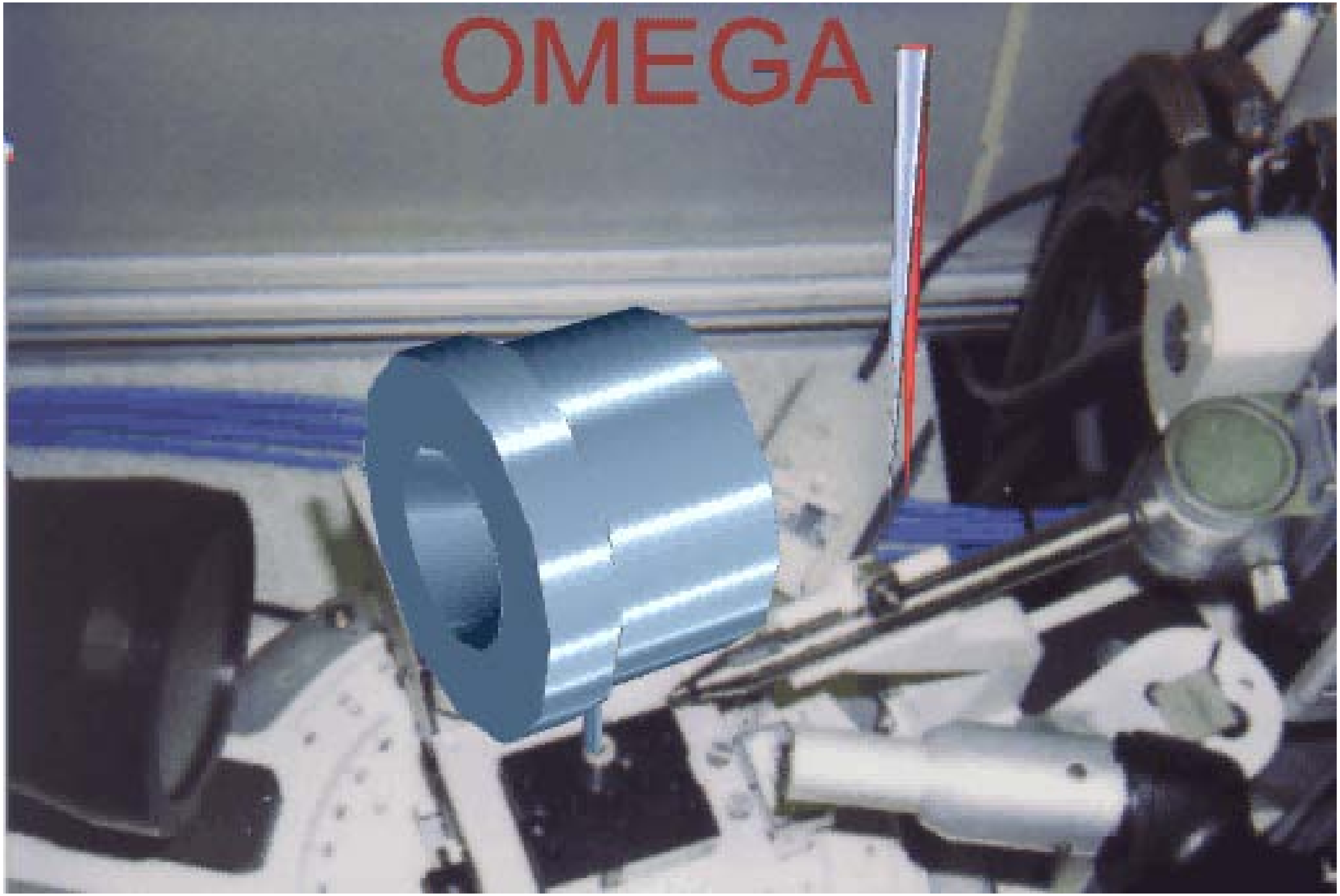

Uppsala, 1999

Principals of DAC Technique

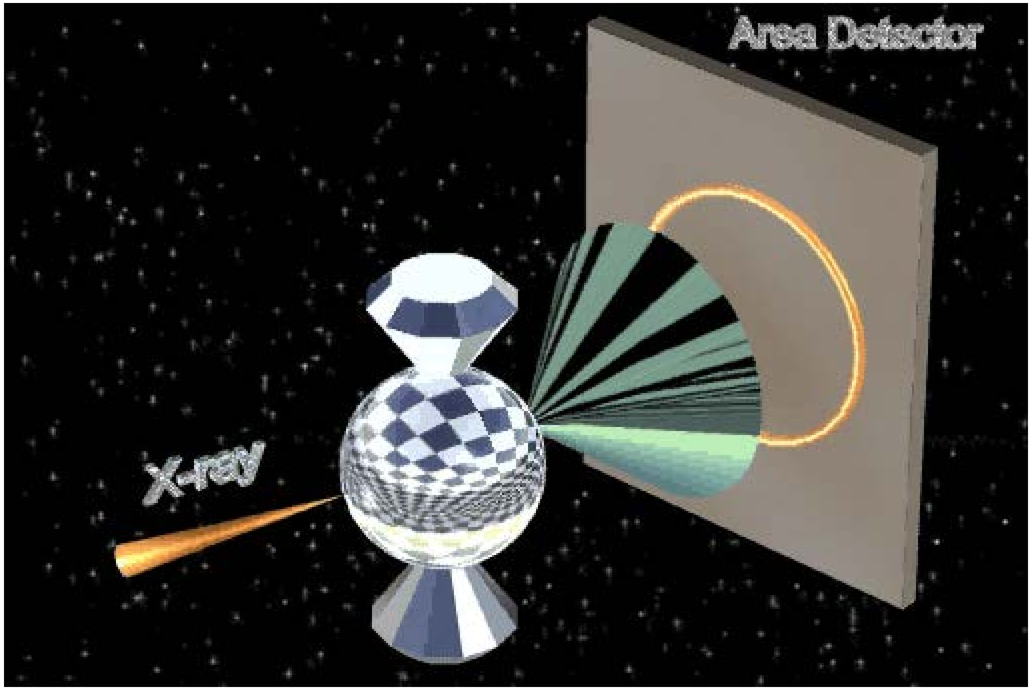

Large stresses in DACs tend to destroy crystals…

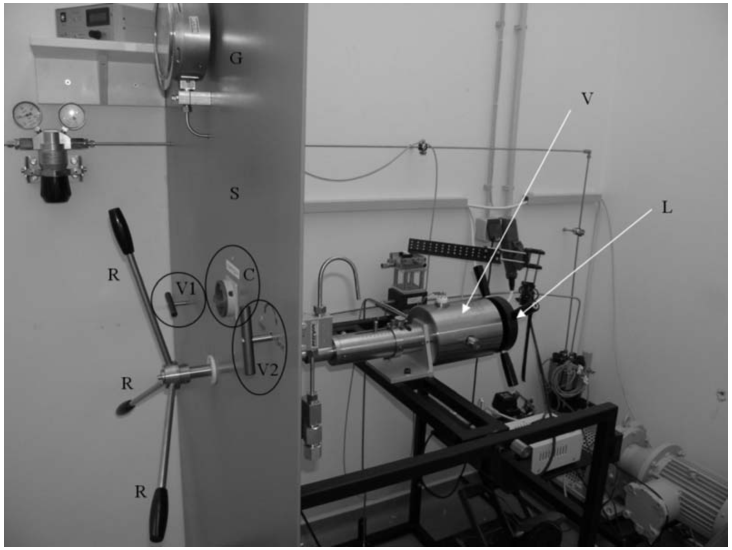

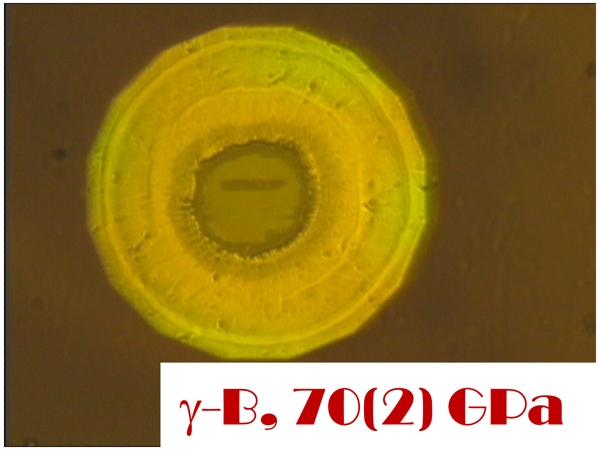

γ-B, 70(2) GPa

…but quasi-hydrostatic nobel gases (He, Ne) pressure transmitting media preserve them!

Kurnosov et al., Rev. Sci. Inst., 2007
Zarechnaya et al., PRB 2010

Principals of DAC Technique

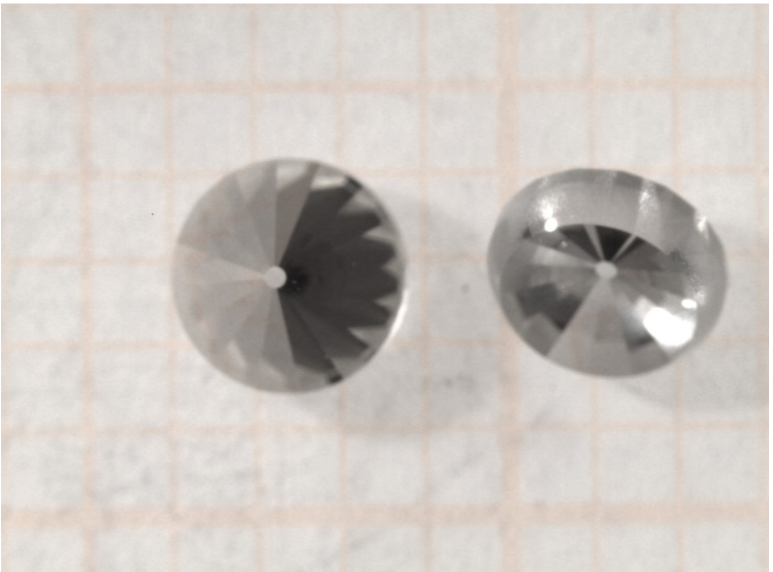

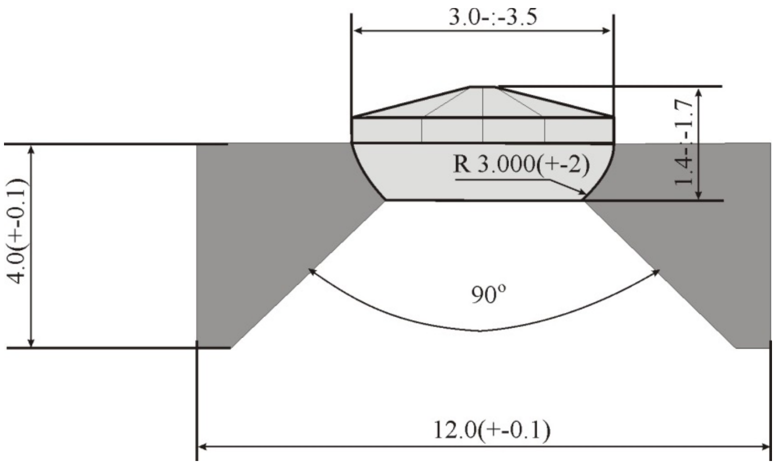

Boehler, Rev. Sci. Inst., 2006
Dubrovinskaia et al., High Pressure, 2012

Principals of DAC Technique

Kantor et al., 2012

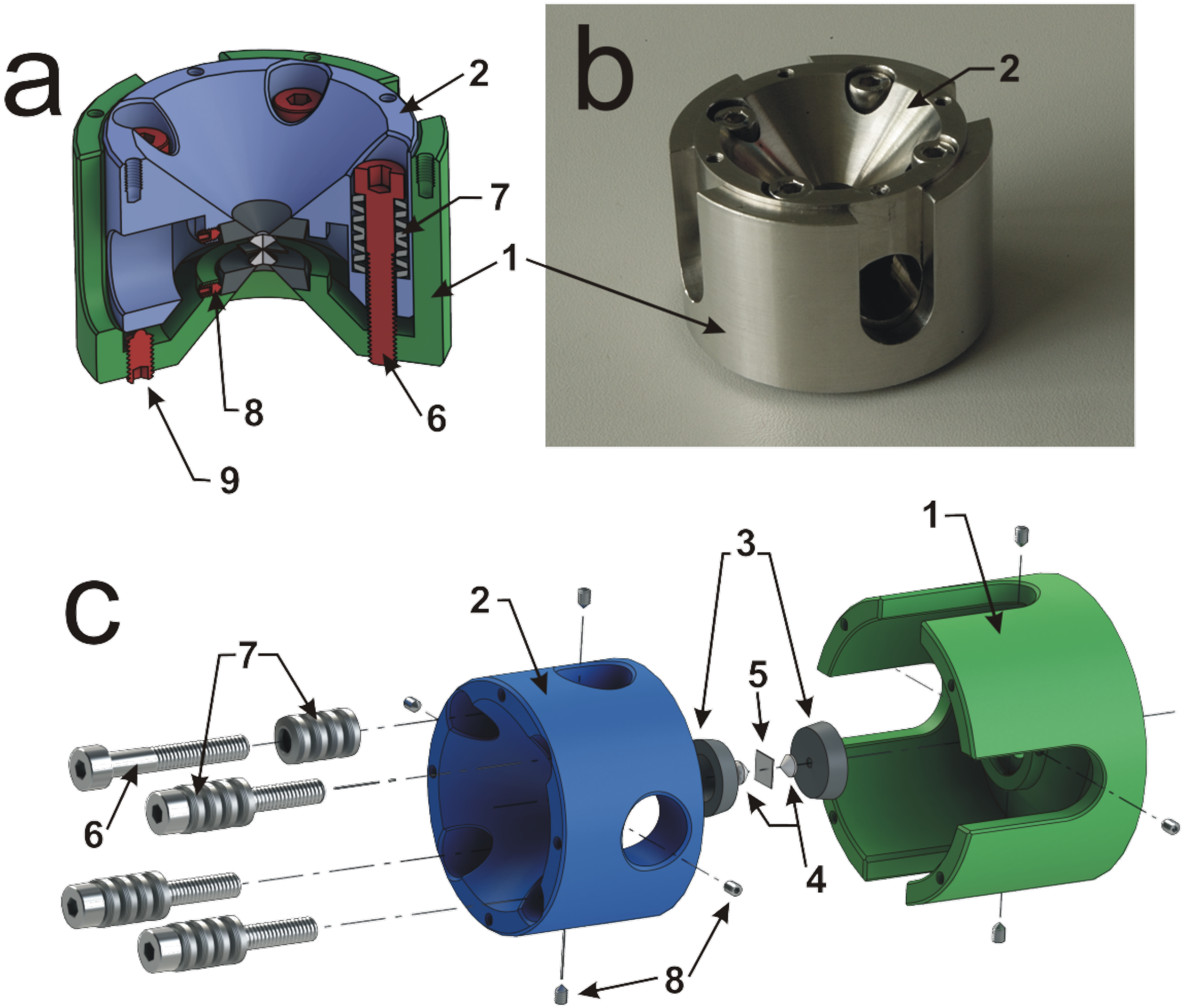

BX90 diamond anvil cell design

a – section view, b – photograph of a loaded cell, c – exploded view. (1 – outer cylinder part; 2 – inner piston part; 3 – diamond supporting plates; 4 – diamond anvils; 5 – metallic gasket; 6 – M4 (#8-32) screws for generating loading force; 7 – pack of conical spring washers (Belleville springs); 8 – setscrews for diamond anvils alignment; 9 – safety setscrews

Srtucture solution

Powder XRD *vs* Single-crystal XRD

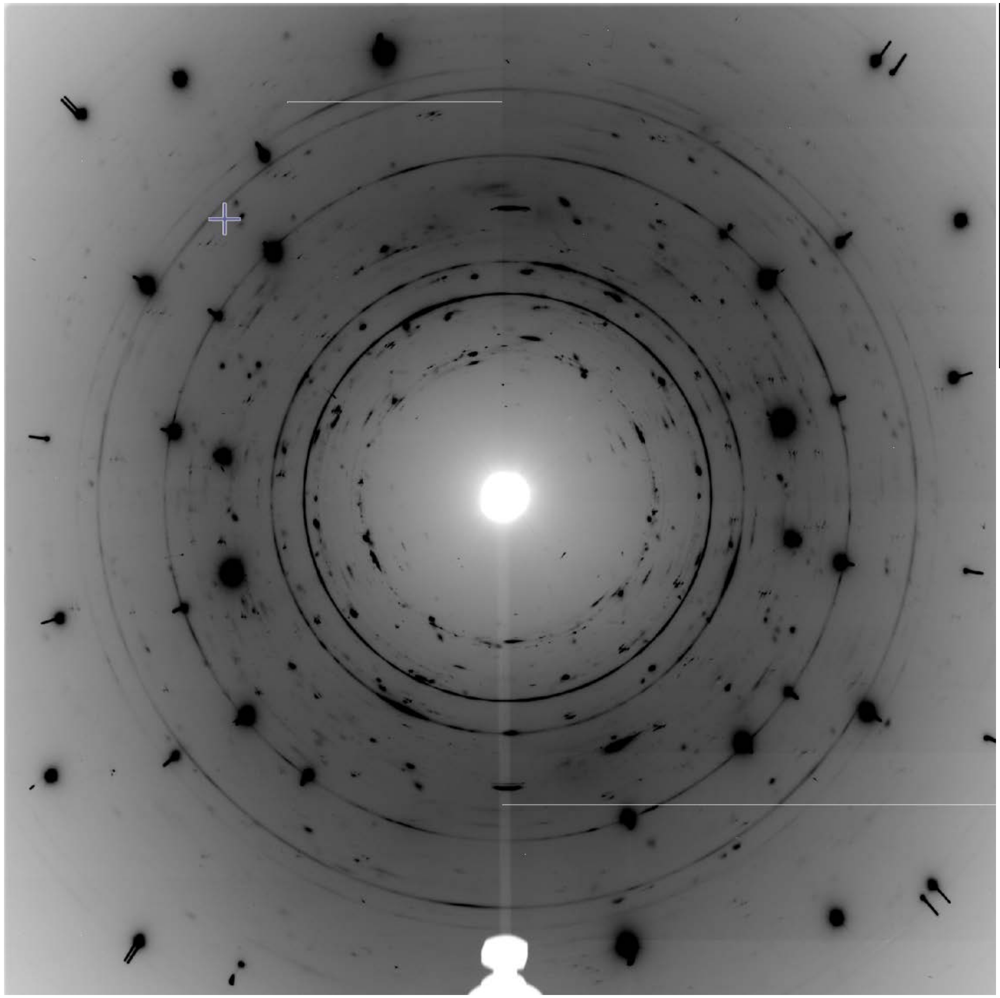

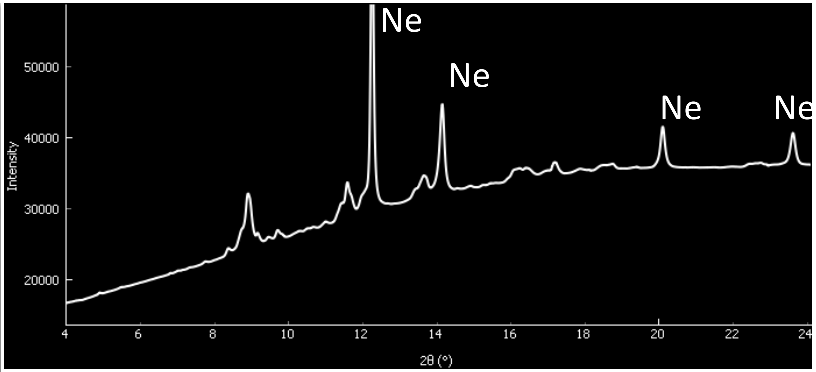

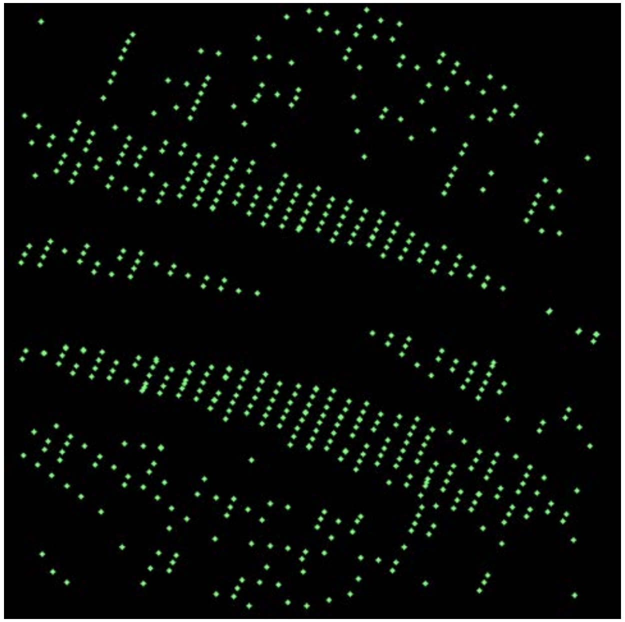

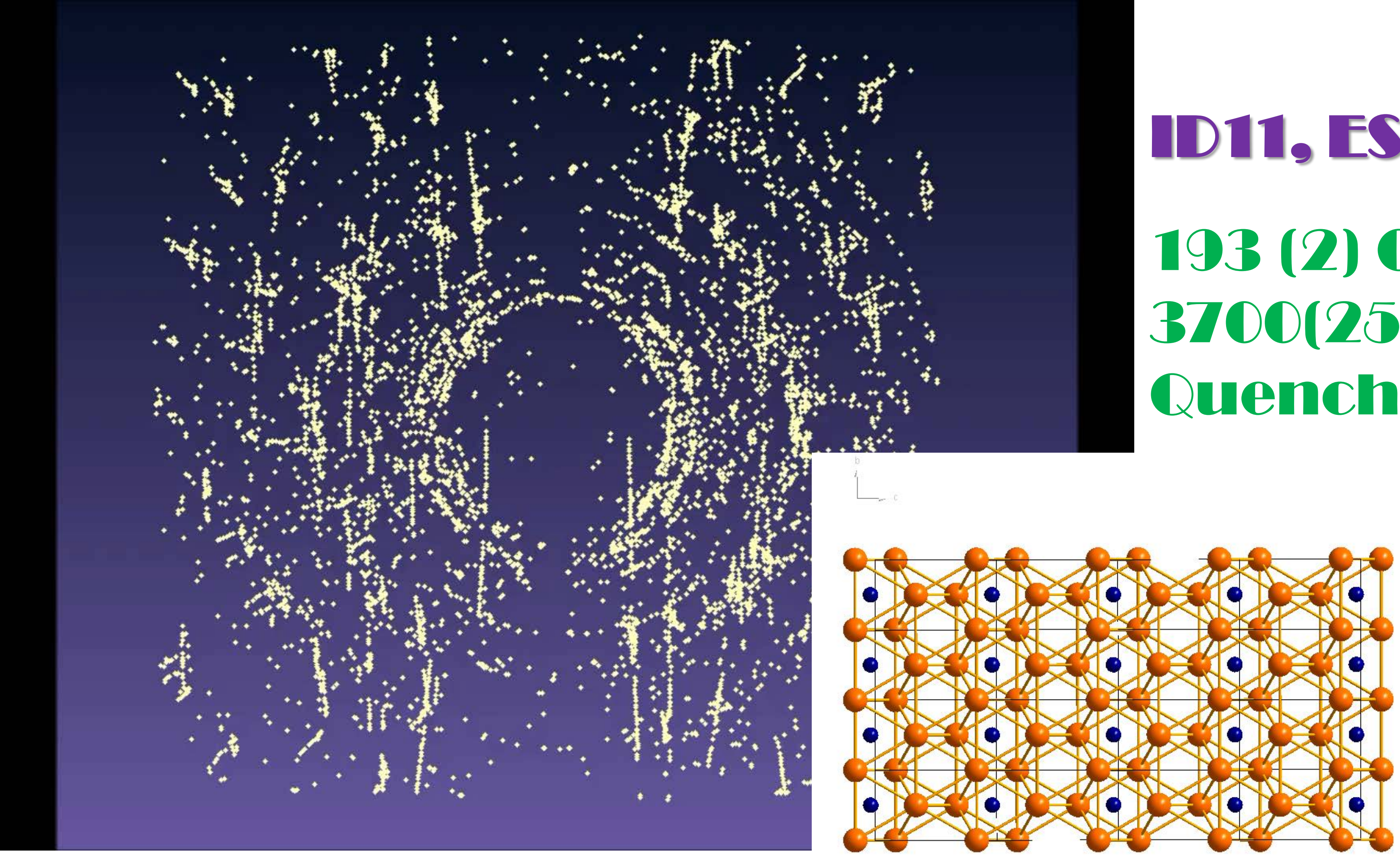

ID11, ESRF

193 (2) GPa
3700(250) K
Quenched

CrysAlisPro (c) 39.43c

Re_2C, $P2_1/n$, 187 reflections, R_{int}=2.1%, R1=6.6%

Reciprocal space

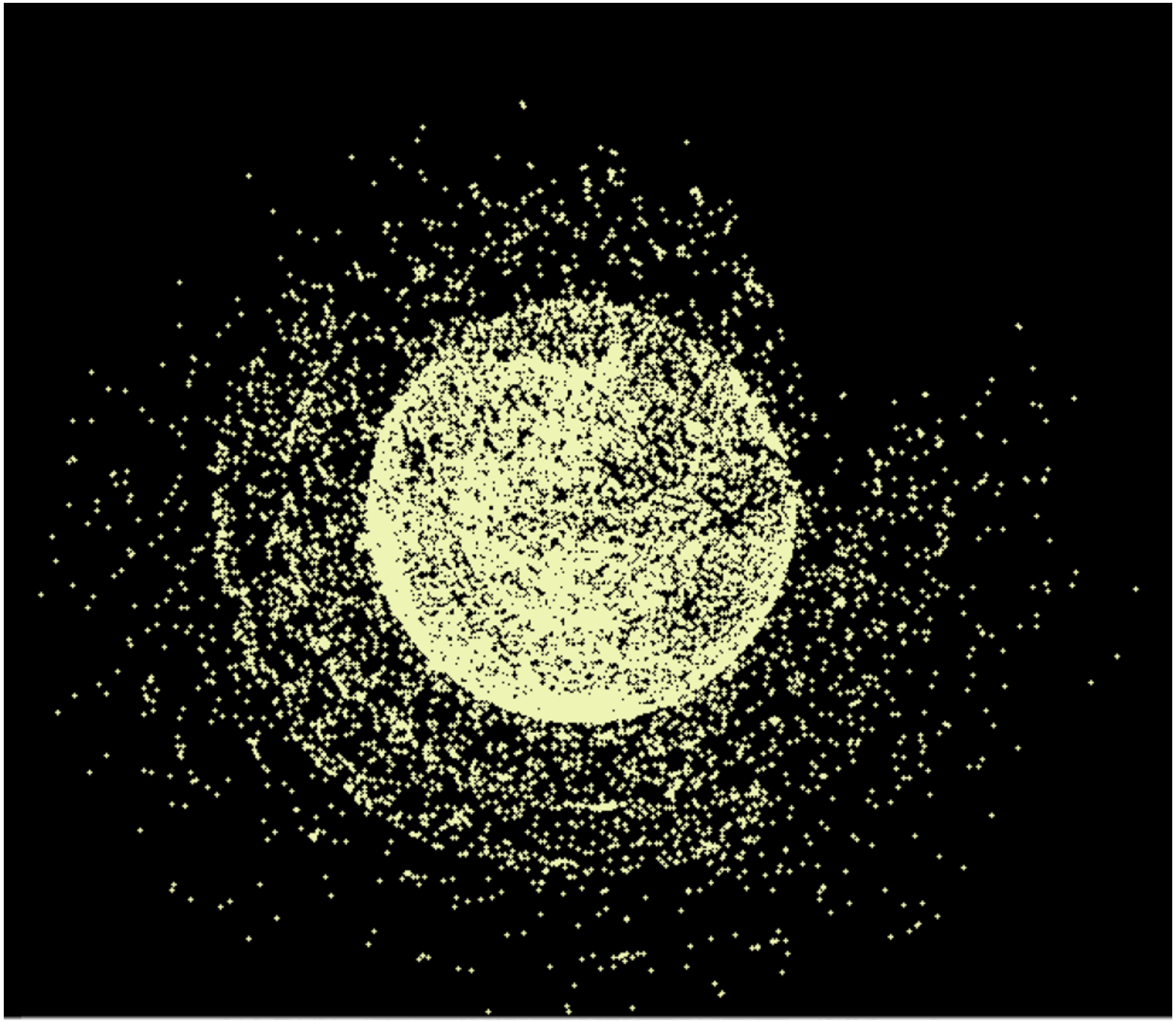

Single-crystal XRD with ω–2θ setup

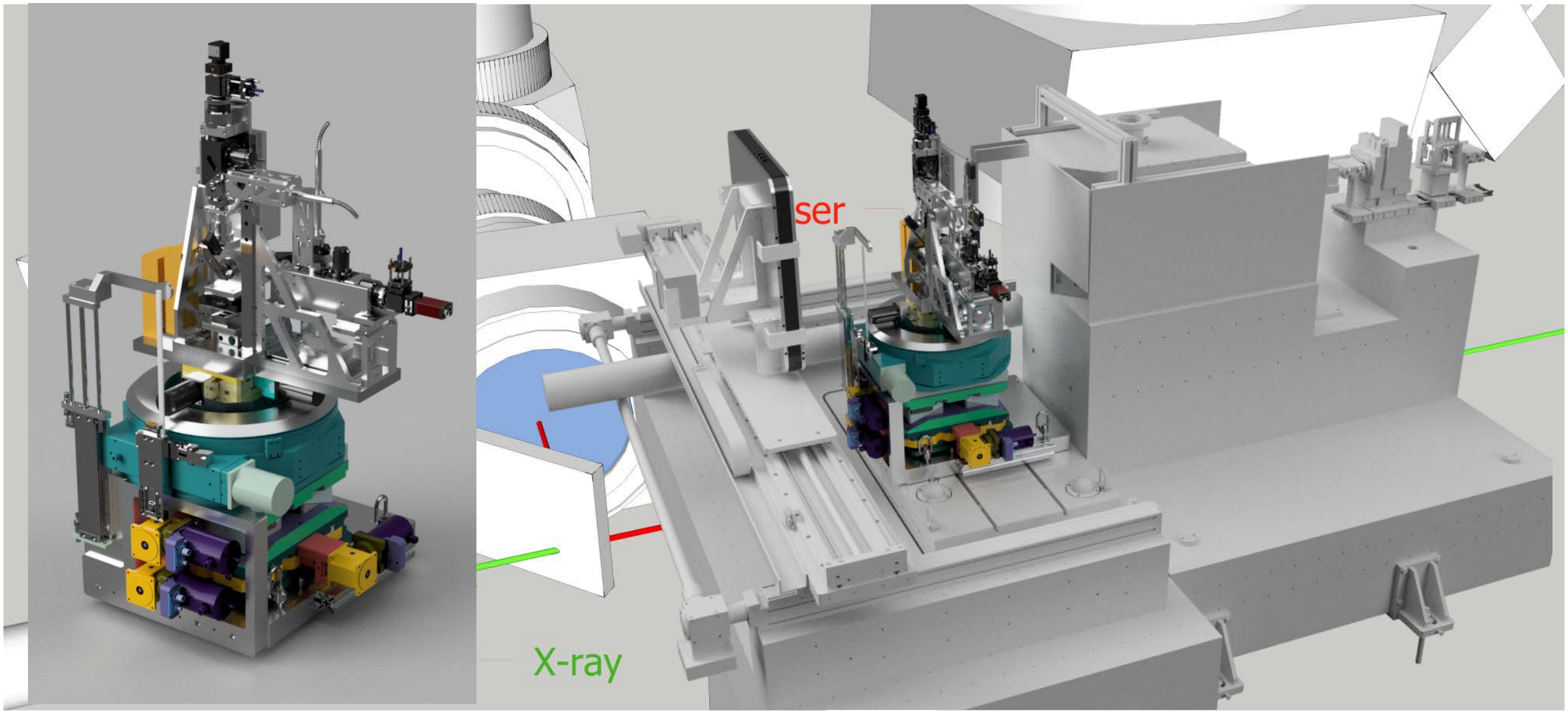

Bykova et. al. (2019), RSI *to be published*

Single Crystal Diffraction at high-P,T

P02.2, PETRA III

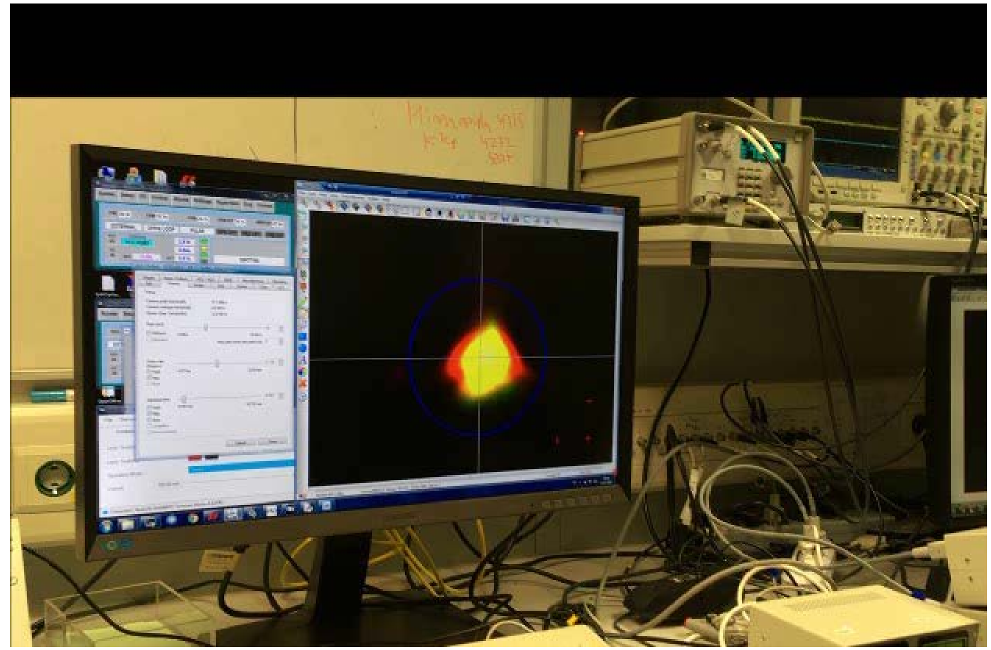

Available for general users since 2017

Bundesministerium für Bildung und Forschung

Single-crystal XRD with ω–2θ setup

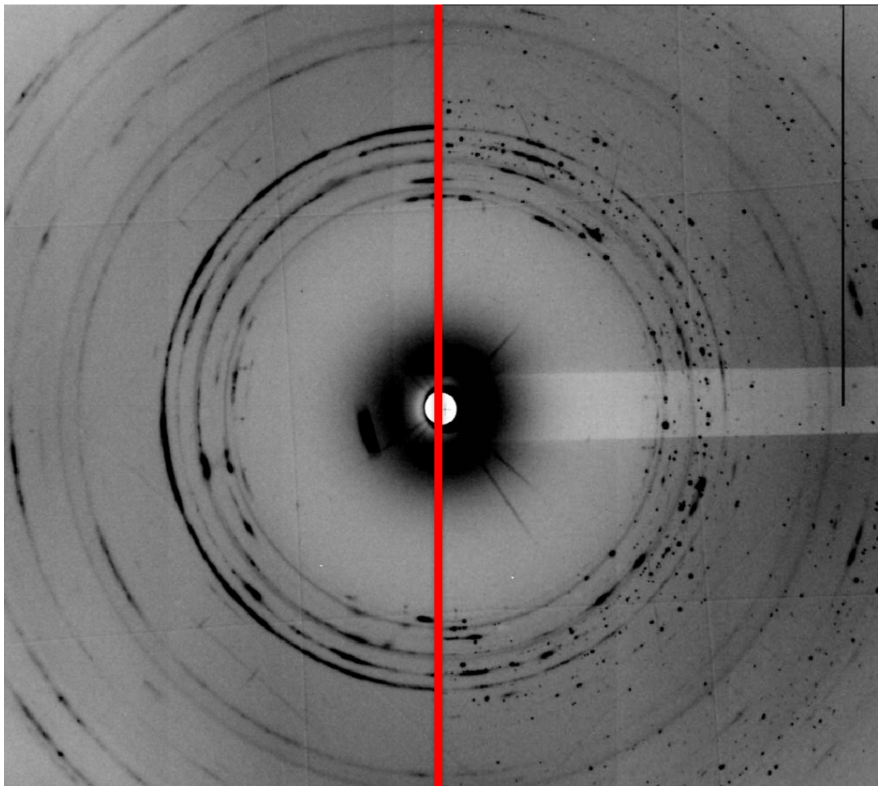

Cold diffraction. 55 GPa
FeN + ε-N_2 + Fe_3N_2

Hot diffraction. 55 GPa
FeN + FeN_2

HPHT behavior of iron nitrides

Bykova et. al. (2019),* RSI *to be published

Crystal structure of B8-FeN at 55 GPa

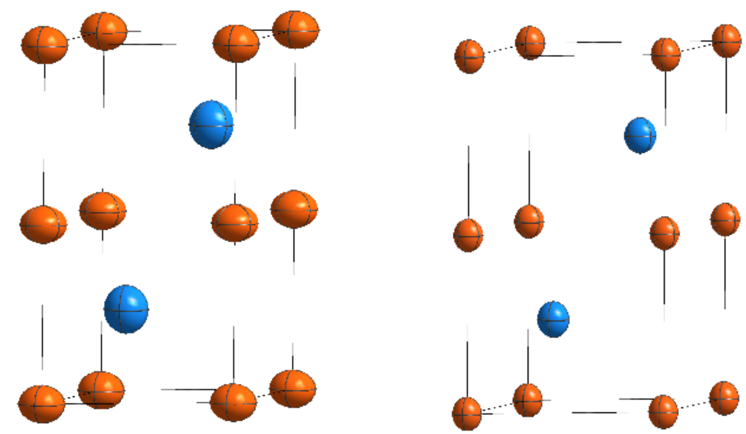

T ~ 1900 K	T = 293 K (quenched)
a = 2.6689(4) Å	a = 2.6392(4) Å
c = 4.8394(6) Å	c = 4.8142(15) Å
V = 29.85(1) Å^3	V = 29.04(1) Å^3
R_1/wR_2 = 7.7/7.9%	R_1/wR_2 = 4.3/4.5%
$< U_{eq} >$ = 0.025(4) Å^2	$< U_{eq} >$ = 0.013(4) Å^2

Both the unit cell volume and thermal displacement parameters become larger, thus giving evidence that we indeed collected single-crystal XRD during laser heating.

Diamond Anvil with Round Table

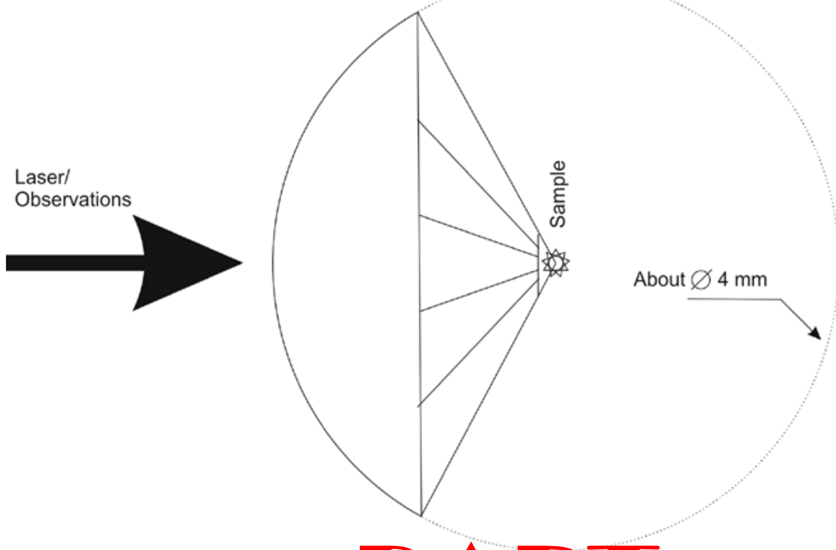

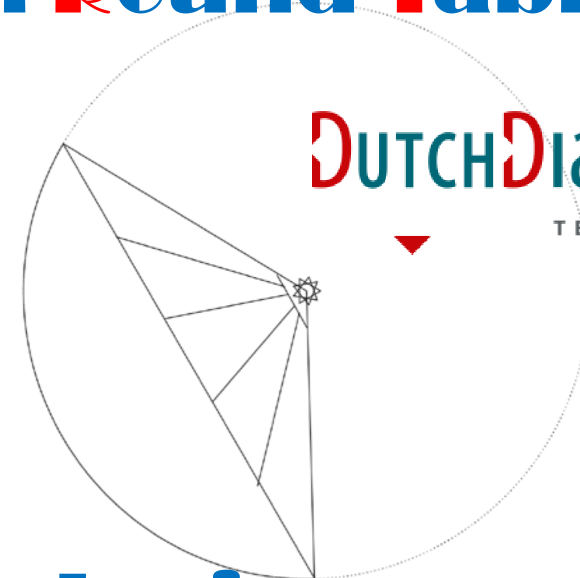

DART anvil design

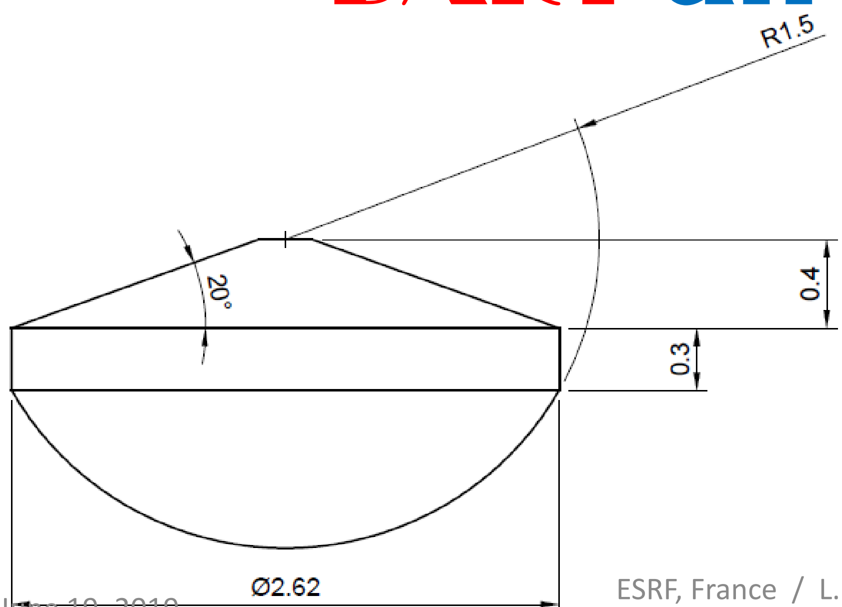

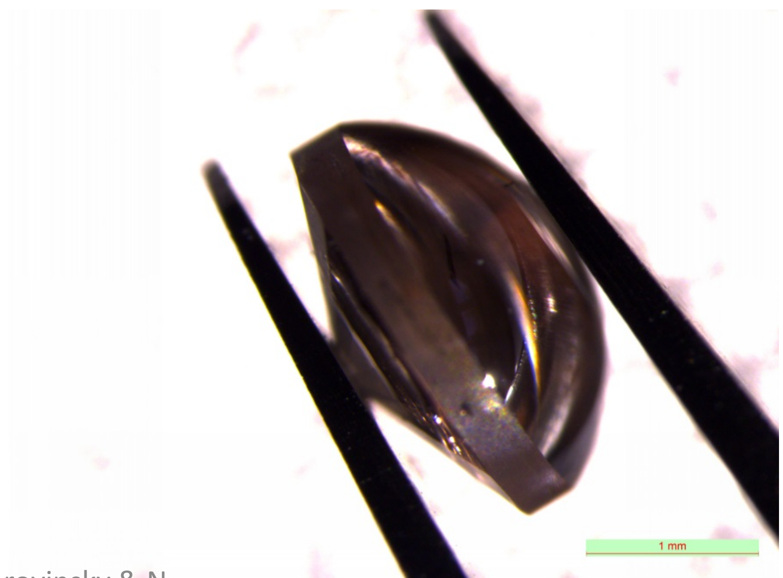

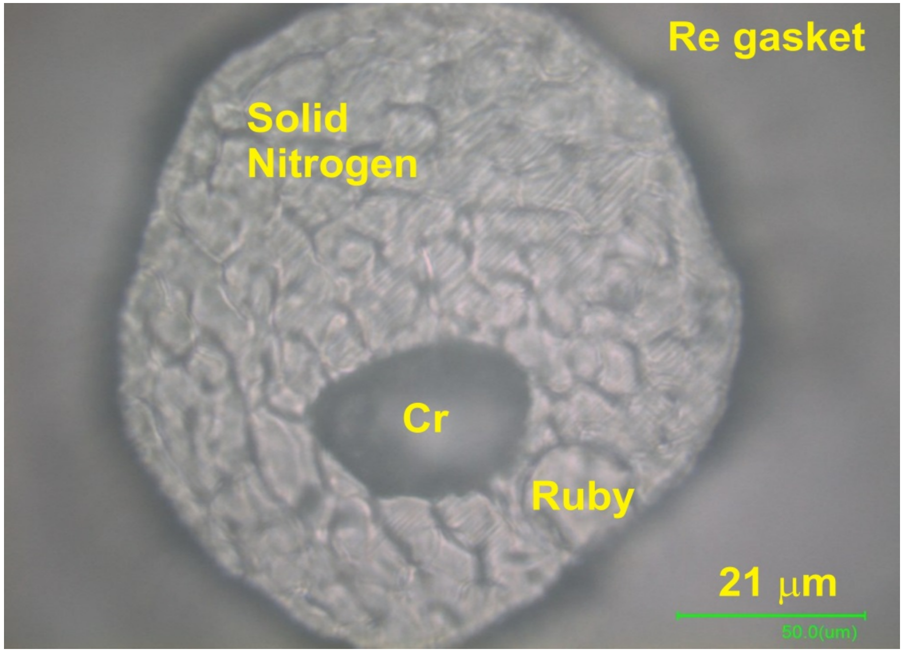

38(1) GPa,
ECB-P02 PETRA III

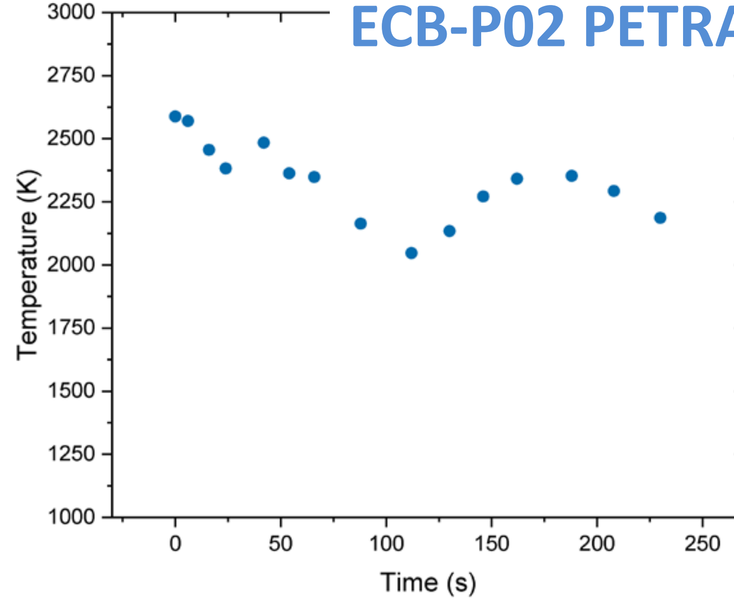

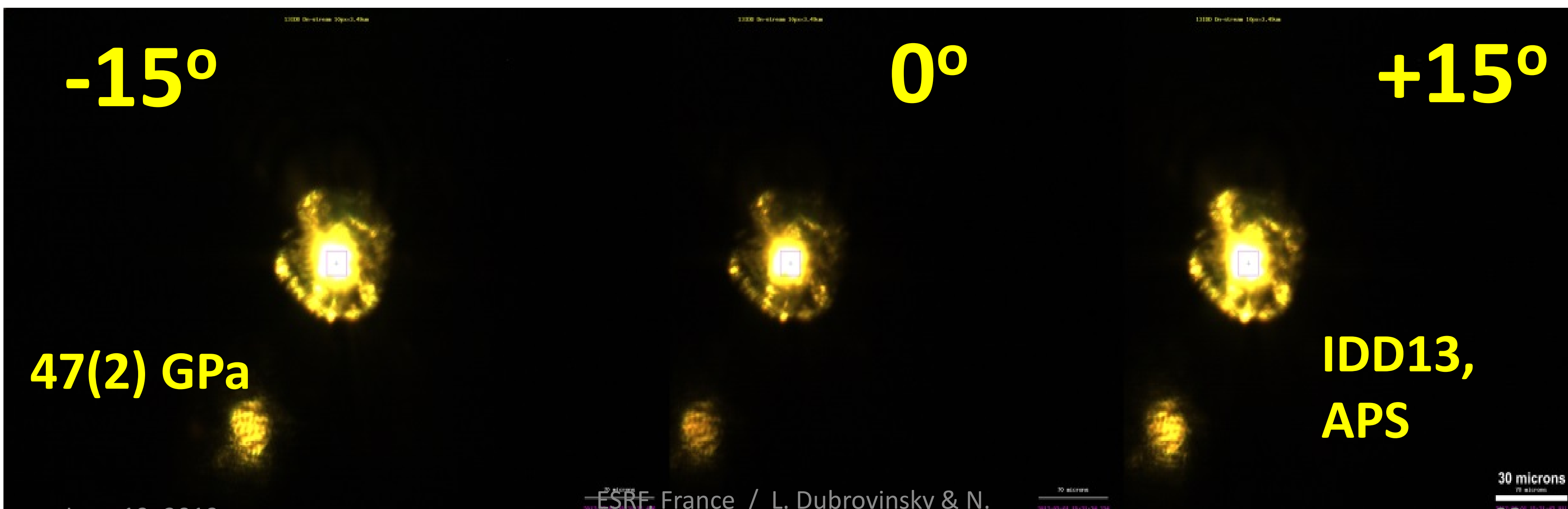

Examples of studied materials

Boron modifications and boron-rich borides (Al-, Fe-, Mg-, Co-borides)

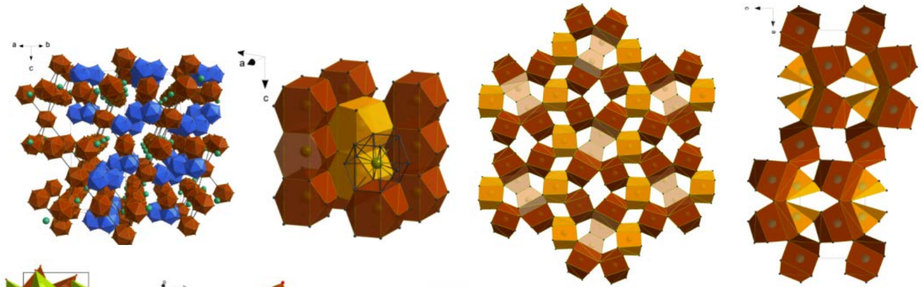

Silica and silicates

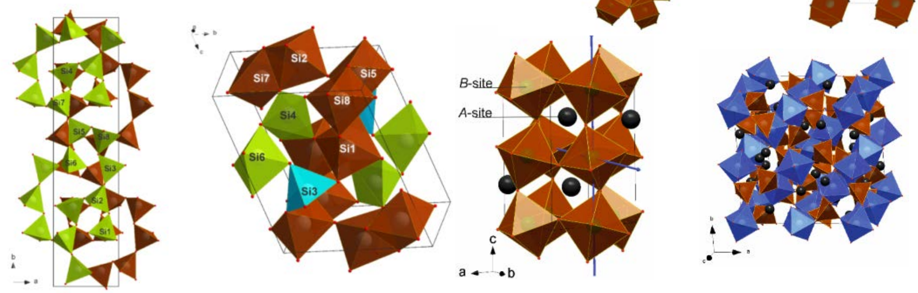

Oxides and oxyhydroxides of iron

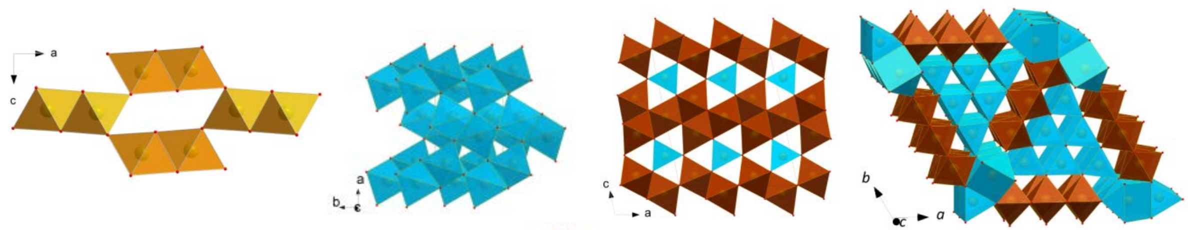

Carbonates (Fe, Mn, Co…)

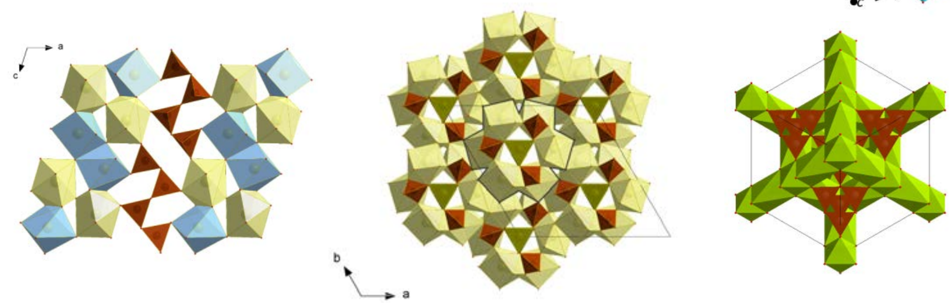

Cerantola, V., *et al.* (2017) *Nat. Commun.*, 8, 15960.
Chariton, S., *et al.* (2017) *Phys. Chem. Miner.*, 45, 59.

Scientific Case: Silica

Pressure-induced amorphization of crystalline silica

R. J. Hemley*, A. P. Jephcoat*, H. K. Mao*, L. C. Ming† & M. H. Manghnani†

* Geophysical Laboratory, Carnegie Institution of Washington, 2801 Upton Street, NW, Washington, DC 20008, USA
† Hawaii Institute of Geophysics, University of Hawaii, 2525 Correa Road, Honolulu, Hawaii 96822, USA

The crystalline-to-amorphous transformation in the solid state is currently the subject of intense study. With the seminal discovery of amorphization of H_2O ice I under pressure[1], interest has focused on the possible occurrence of pressure-induced amorphization in other systems, the thermodynamic and mechanistic basis of the process, and the relationship between amorphization by pressure and by other means[2–5]. Here we report *in situ* synchrotron X-ray diffraction measurements of α-quartz and coesite in a diamond-anvil cell that demonstrate that these crystalline materials transform to amorphous solids at 25–35 GPa and 300 K. We show that an internally consistent thermodynamic description of the process is possible, extending into the pressure domain recent thermodynamic calculations of thermally-induced amorphization of silica polymorphs[4]. The measurements provide constraints on the equations of state and melting relations in this system at high pressures, shed light on the mechanism for glass formation in SiO_2 in laboratory shock-wave experiments and meteorite-impact events, and provide insights into the thermoelastic stability of tetrahedral network structures at high compression.

the
rem:
men
the
stres
stud
occu
pres
We
by r
the
scop
larg
Th
are
Fig.
and
phiz
18 c
of si
to 1
a di
com
high
(shc
pres
ted
rece
regi
A
to u
in a

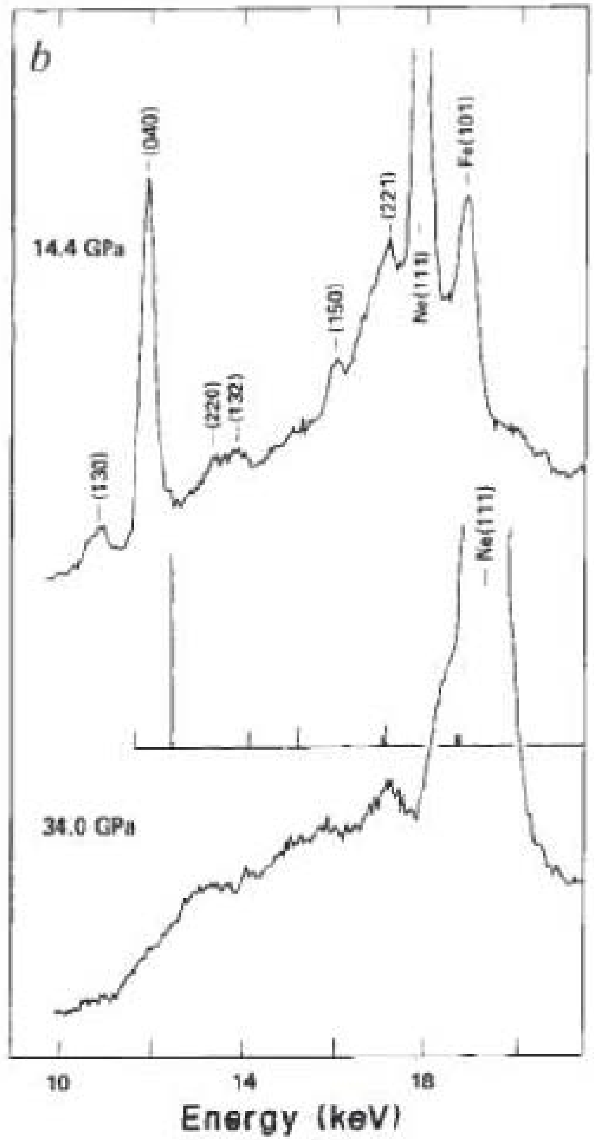

ium, which
hese experi-
the neon in
-hydrostatic
The Raman
n in quartz
, even when
neasurable[2].
ion is driven
contacts in
ous spectro-
occurs when
re used.
X-ray data
ca phases in
e for quartz
h the amor-
es at 17–
molar volume
nt *P*-*V* data
Jeanloz[19] in
0 K, are also
the glass at
compression
rial at high
s (uncorrec-
om the more
igh-pressure
it is possible
tion process
ent pressure

Scientific Case : Silica

Coesite, SiO_2

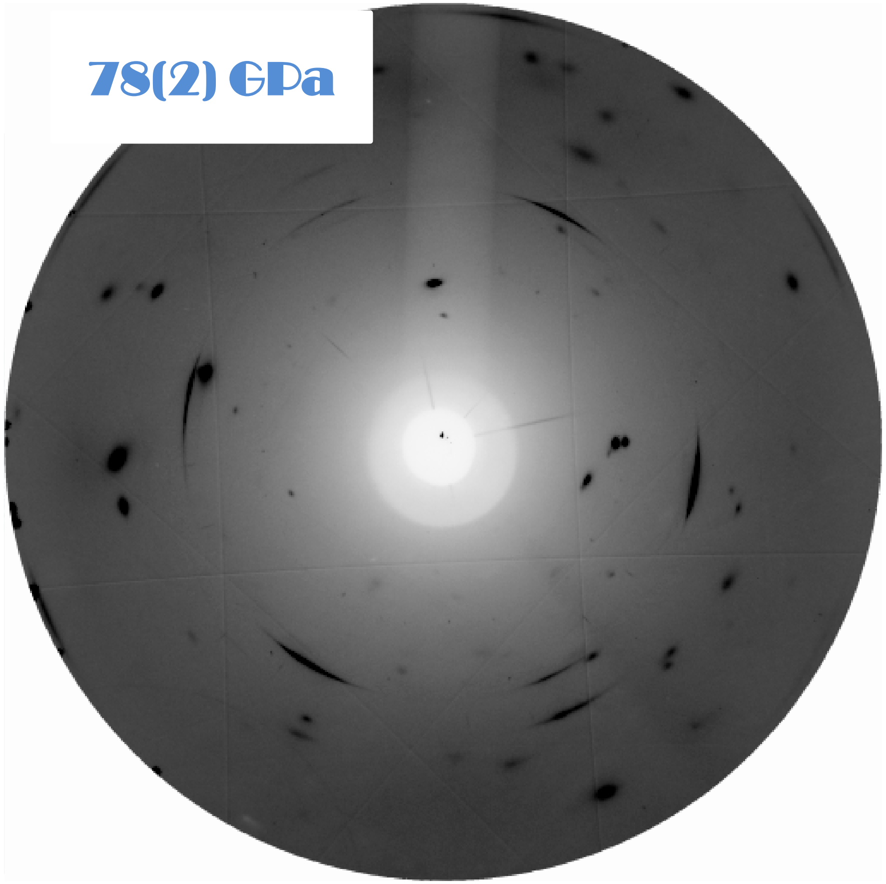

High pressure behavior of coesite

Spectroscopic and energy dispersive XRD data: amorphization above 20 GPa.

Single crystal: crystal survives till 80 GPa, 4 phase transitions to phases unknown before

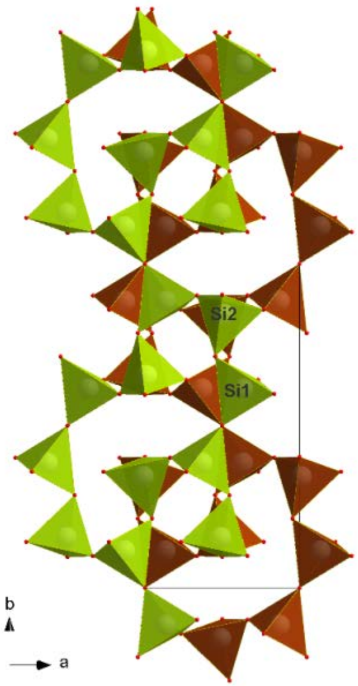

Coesite-I at 6.5 GPa

*C*2/*c*, *V* = 467.2(8) Å^3

R_1 = 5.1 %

7 atoms in asymmetric unit; 302 independent reflections

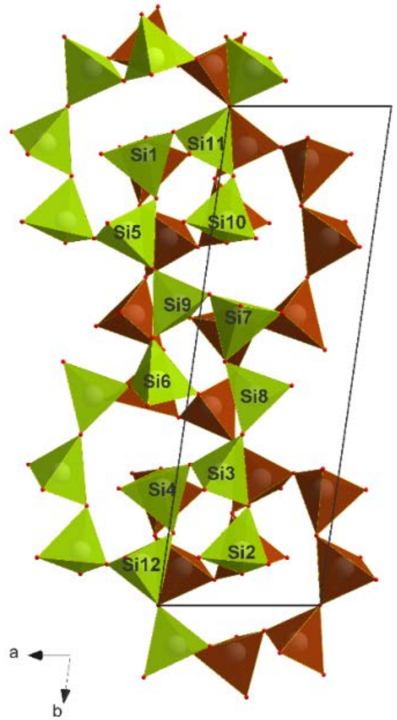

Coesite-II at 27 GPa

$P2_1/n$, *V* = 886.8(4) Å^3

R_1 = 4.2 %

24 atoms in asymmetric unit; 1535 independent reflections

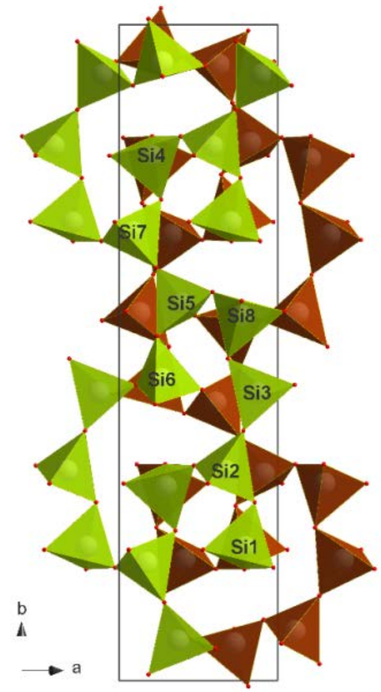

Coesite-III at 28 GPa

P-1, *V* = 666.2(7) Å^3

R_1 = 13.6 %

37 atoms in asymmetric unit; 833 independent reflections

Bykova E. *et al.*, **Metastable silica high pressure polymorphs as structural proxies of deep Earth silicate melts.** *Nature Commun.* (2018).

High pressure behavior of coesite

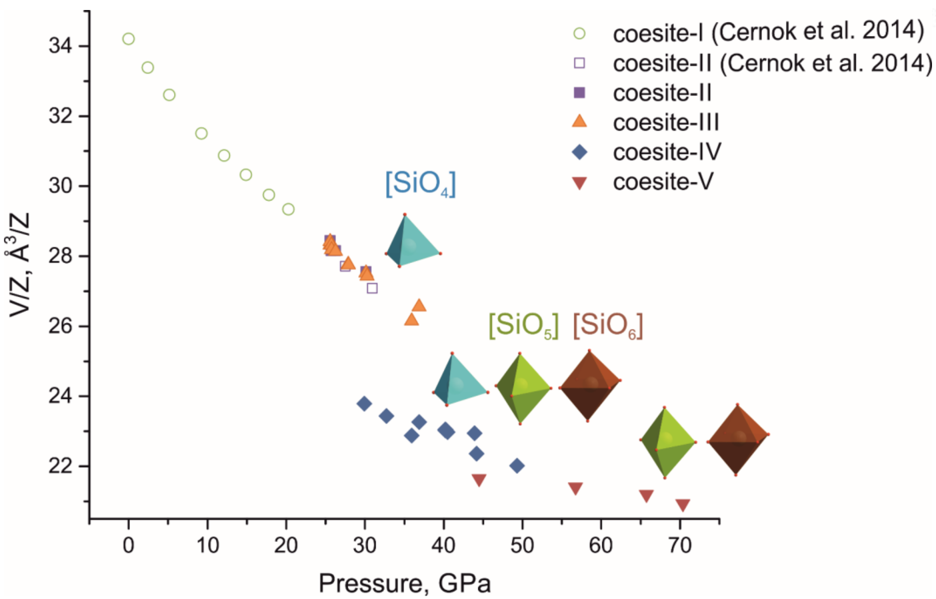

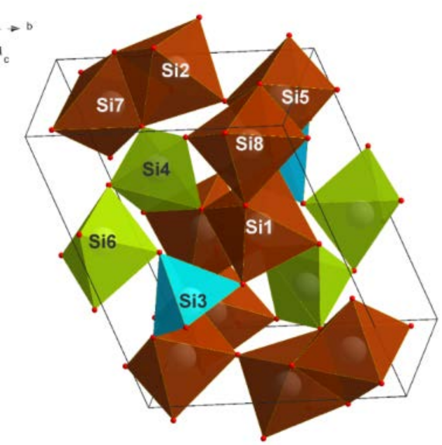

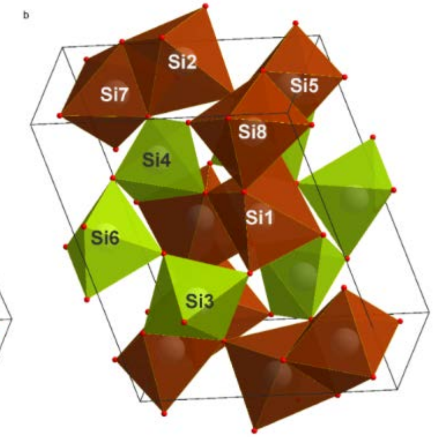

Coesite-IV at 49 GPa *P*-1, *V* = 366.1(8) Å^3

R_1 = 6.3 %

24 atoms in asymmetric unit; 968 independent reflections

4, 5, 6 coordinated Si

Coesite-V at 57 GPa *P*-1, *V* = 342.6(2) Å^3

R_1 = 7.3 %

24 atoms in asymmetric unit; 672 independent reflections

4, 6 coordinated Si

Face-shared [SiO_6]

Close-packed fragments

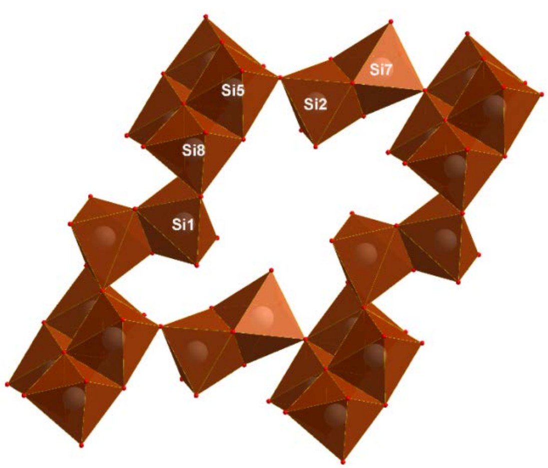

Observed for the first time:

- ***Shared SiO6 octahedra;***
- ***Crystalline silica phase with silicon in 3 different coordinations;***
- ***Crystalline silica phase with 5-coordinted Si***

Bykova E. *et al.*, **Metastable silica high pressure polymorphs as structural proxies of deep Earth silicate melts.** *Nature Commun.* (2018).

Breaking Pauling's rules

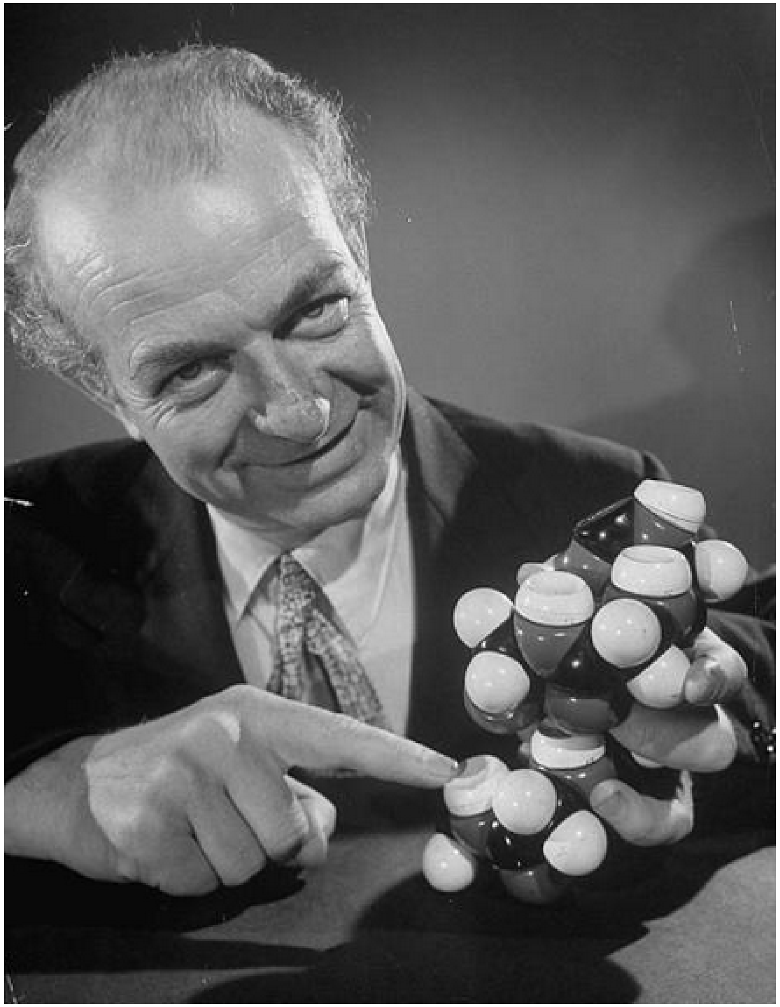

- **3rd rule:** **The sharing of edges and particularly faces by two anion polyhedra decreases the stability of an ionic structure.**

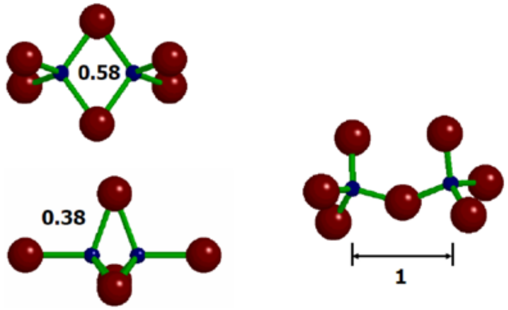

- **5th rule:** **(the rule of parsimony) The number of essentially different kinds of constituents in a crystal tends to be small.**

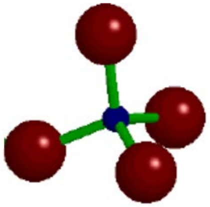

Silica and silicate melts in the deep Earth's interiors

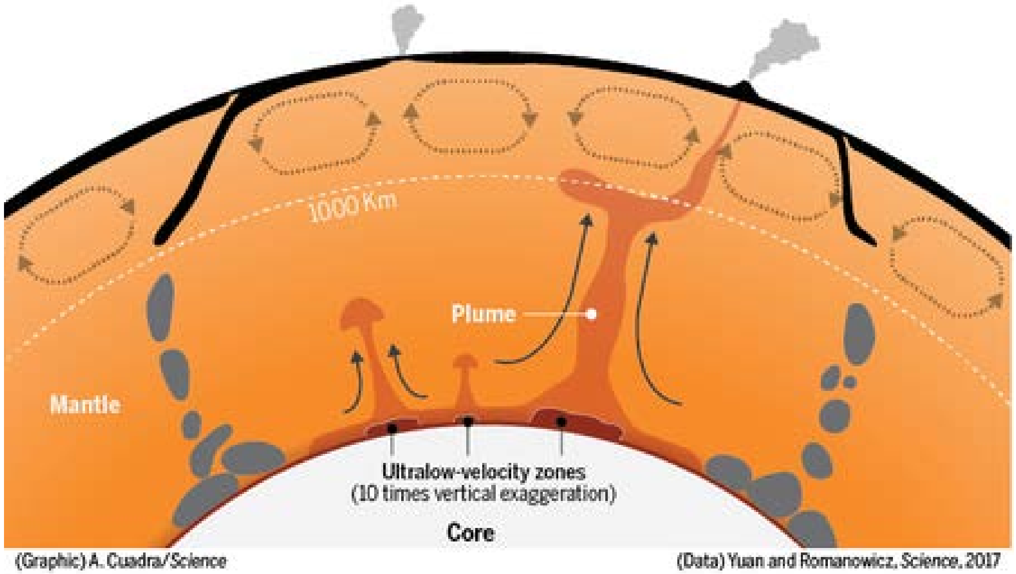

- Silica and silicate melts may exist at the top of the transition zone and at the core–mantle boundary.
- Local structure of the melts is still under debates.
- Structure of the melts influences on such important properties as density and compressibility, and also on the ability of the melt to incorporate other elements (like Mg and Fe).
- Elastic properties of the melts are important for understanding the dynamic behavior of the past and present Earth.

High pressure behavior of coesite and structure of silica glass

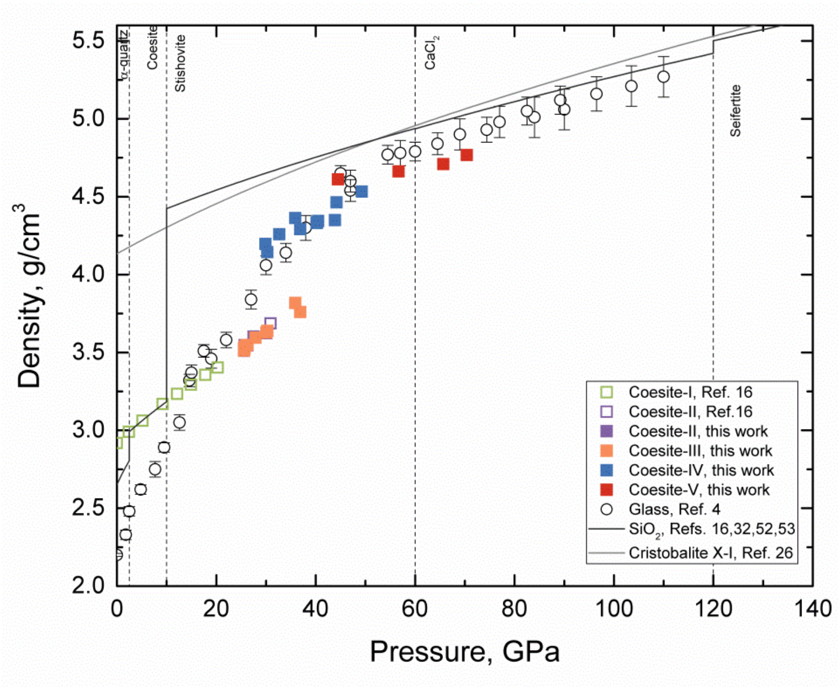

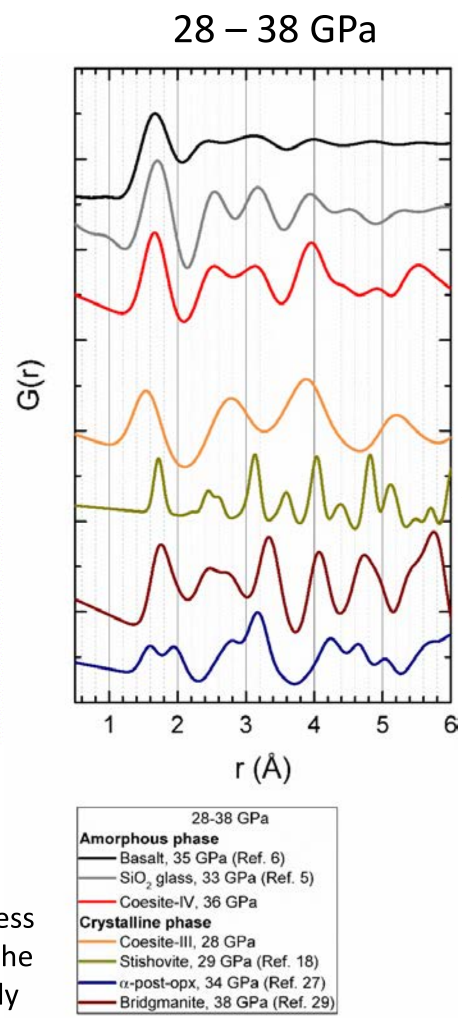

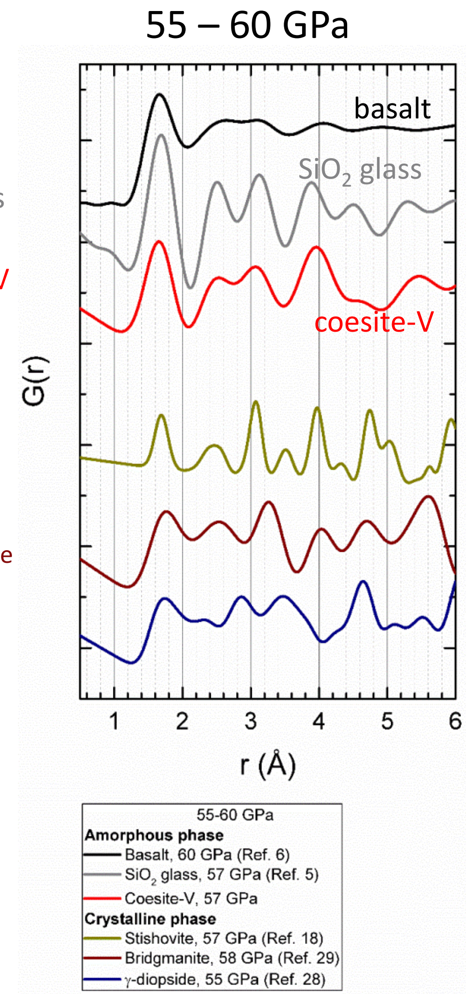

- Silica glass indeed contains shared octahedra and SiO_5 polyhedra (and not just a mixture of tetrahedra and octahedra in certain proportion)
- Densities of silica liquids with complex structures will be less than densities of crystalline high-pressure SiO_2 phases at the corresponding pressures. Such liquids should be seismically detectable.

Bykova E. *et al.*, **Metastable silica high pressure polymorphs as structural proxies of deep Earth silicate melts.** *Nature Commun.* (2018).

High Pressure Crystal Chemistry of Mixed Valence Iron Oxides

Building blocks:

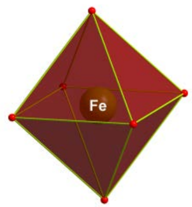

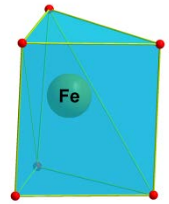

FeO

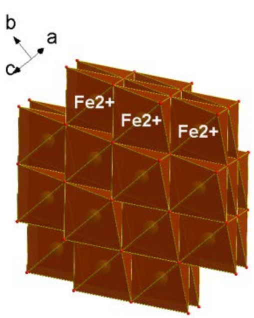

Fe_4O_5 ($2FeO \cdot Fe_2O_3$)

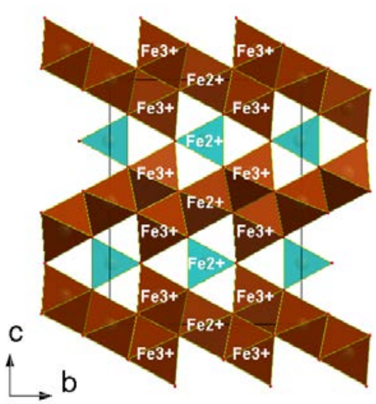

Lavina et al., 2011
Guignard and Crichton, 2014

Fe_3O_4 ($FeO \cdot Fe_2O_3$)

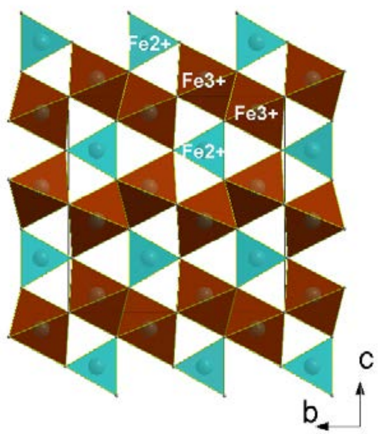

Dubrovinsky et al., 2003

Fe_5O_7 ($FeO \cdot 2Fe_2O_3$)

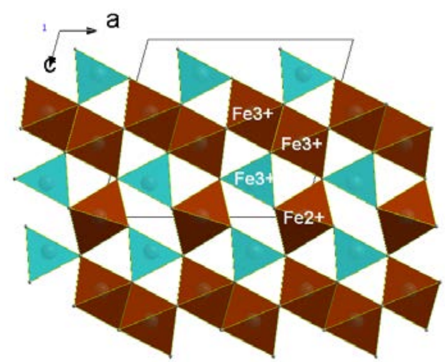

Bykova et al., 2016

ppv-Fe_2O_3

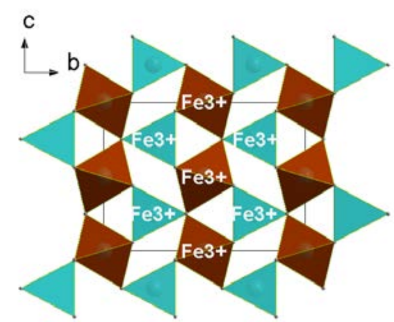

Bykova et al., 2013

Compounds in the Fe-O system

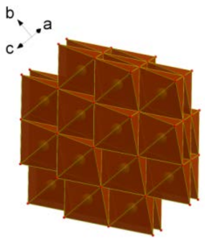

FeO
+ polymorphs

series
of polymorphs
with distorted
wuestite
structures:
R-3*m*
*I*2/*m*
*P*2$_1$/*m*
Pmcn
Pmmn

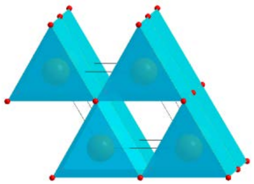

WC-type FeO

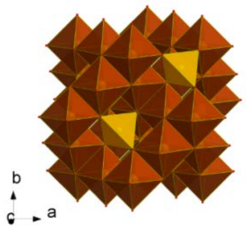

Fe_3O_4
+ polymorphs

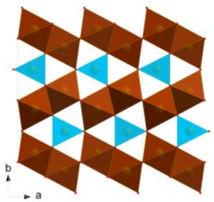

$CaTi_2O_4$-type

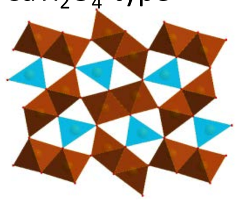

$CaFe_2O_4$-type

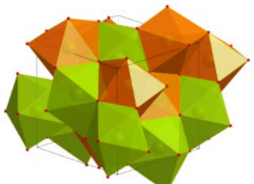

distorted Th_3P_4
structures:
*I*2, *I*4$_1$/*amd*-Fe_3O_4

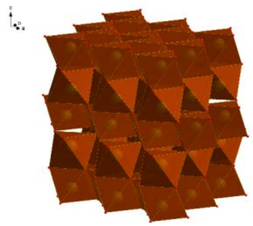

Fe_2O_3
+ polymorphs

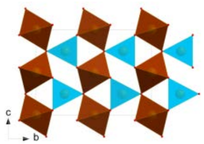

$CaIrO_3$-type

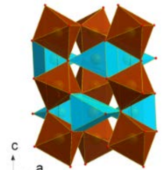

distorted perovskite type

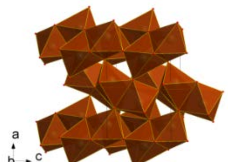

Rh_2O_3-II-type

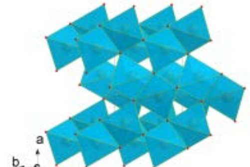

*Aba*2-Fe_2O_3

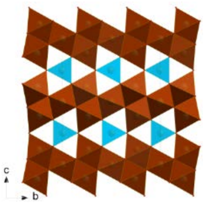

Fe_4O_5

distorted
polymorph
*P*2$_1$/*m*-Fe_4O_5

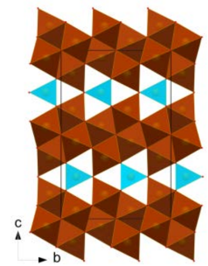

Fe_5O_6

distorted
polymorph
*C*2/*m*-Fe_5O_6

2-fold-Fe_5O_6

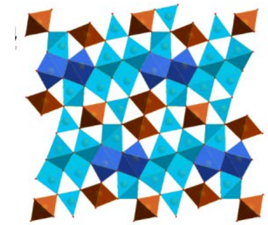

$Fe_{13}O_{19}$

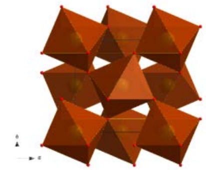

FeO_2

Fe_5O_7

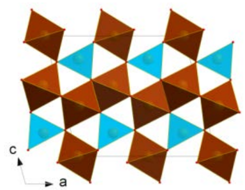

$Fe_{13}O_{18}$

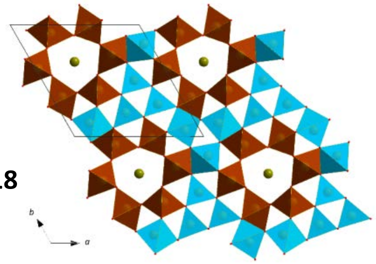

Fe_7O_9

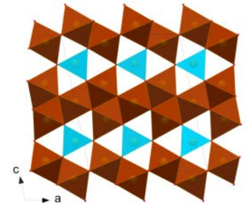

$Fe_{25}O_{32}$

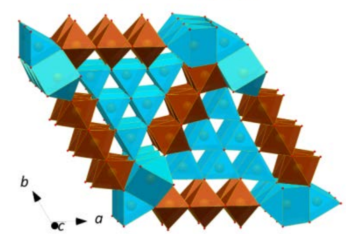

High Pressure Crystal Chemistry of Mixed Valence Iron Oxides

FeO

Fe_4O_5 ($2FeO \cdot Fe_2O_3$)

Fe_3O_4 ($FeO \cdot Fe_2O_3$)

Fe_5O_7 ($FeO \cdot 2Fe_2O_3$)

ppv-Fe_2O_3

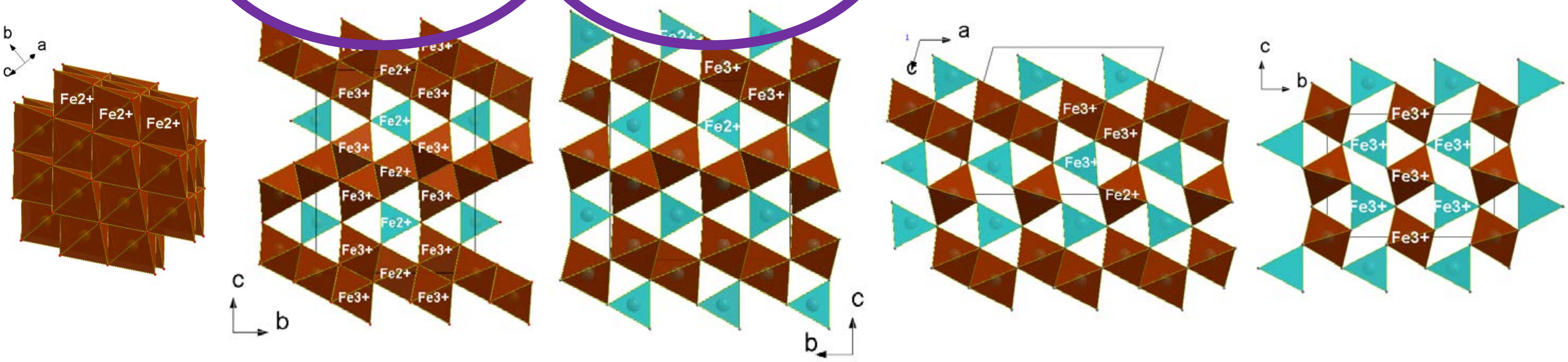

Fe_6O_7 Fe_7O_9 $Fe_{25}O_{32}$

Bykova et al., Nature Comm., 2016

High Pressure Crystal Chemistry of Mixed Valence Iron Oxides

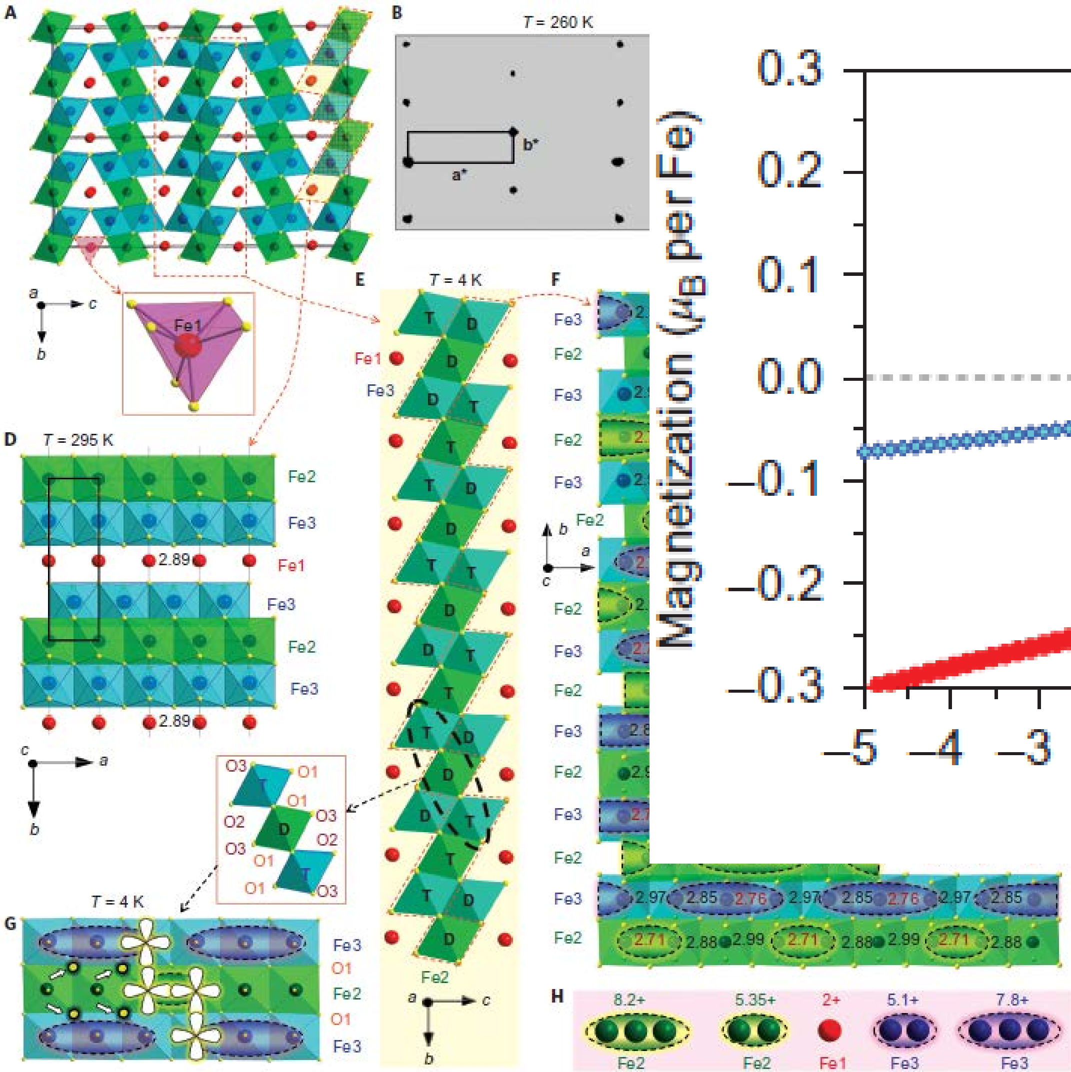

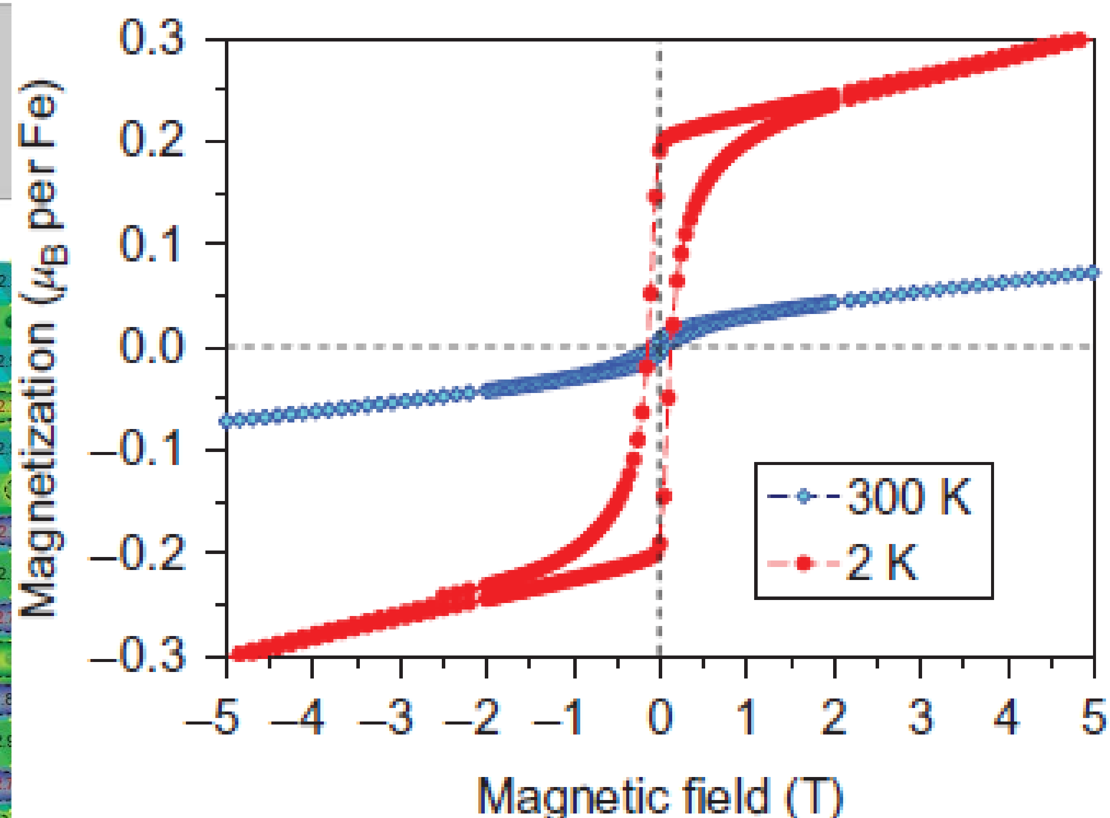

Ovsiannikov et al., Nature Comm., 2016
Nature Chemistry, 2017

Decomposition of iron oxides at HPHT

$Fe_{0.94}O$

92 GPa and 2550 K

$32 \cdot Fe_{0.94}O \rightarrow Fe_{25}O_{32} + 5.08 \cdot Fe$

126 GPa and 3150 K

$4 \cdot Fe_{0.94}O \rightarrow Fe_3O_4 + 0.76 \cdot Fe$

Fe_3O_4

80 GPa and 2900 K

$25 \cdot Fe_3O_4 \rightarrow 3 \cdot Fe_{25}O_{32} + 2 \cdot \mathbf{O_2}$

Fe_2O_3

71 GPa 2700-3000 K

$5 \cdot Fe_2O_3 \rightarrow 2 \cdot Fe_5O_7 + 0.5 \cdot \mathbf{O_2}$

above 200 GPa and 3000 K

$3 \cdot Fe_2O_3 \rightarrow 2 \cdot Fe_3O_4 + 0.5 \cdot \mathbf{O_2}$

$13 \cdot Fe_2O_3 \rightarrow 2 \cdot Fe_{13}O_{19} + 0.5 \cdot \mathbf{O_2}$

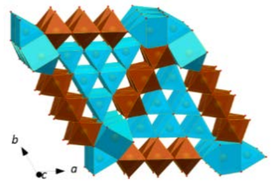

$Fe_{25}O_{32}$

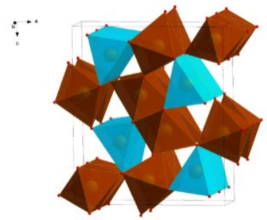

Fe_3O_4
$CaFe_2O_4$-type

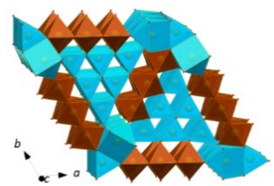

$Fe_{25}O_{32}$

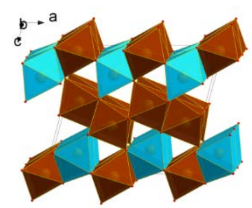

Fe_5O_7

Fe_3O_4 distorted Th_3P_4-type

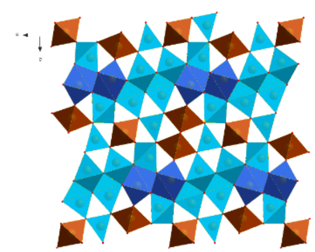

$Fe_{13}O_{19}$

High Pressure iron oxides in the presence of oxygen

Fe(II) vs Fe(III) vs Fe(IV)

O^{2-} vs O_2^{2-} vs O_2^{3-} vs ???

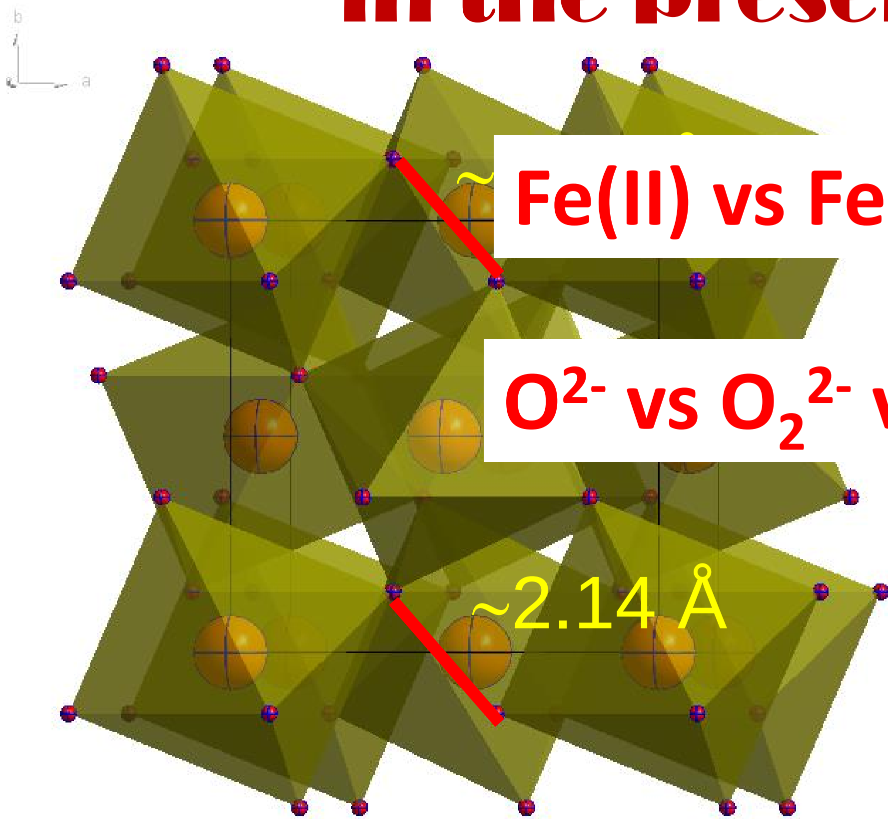

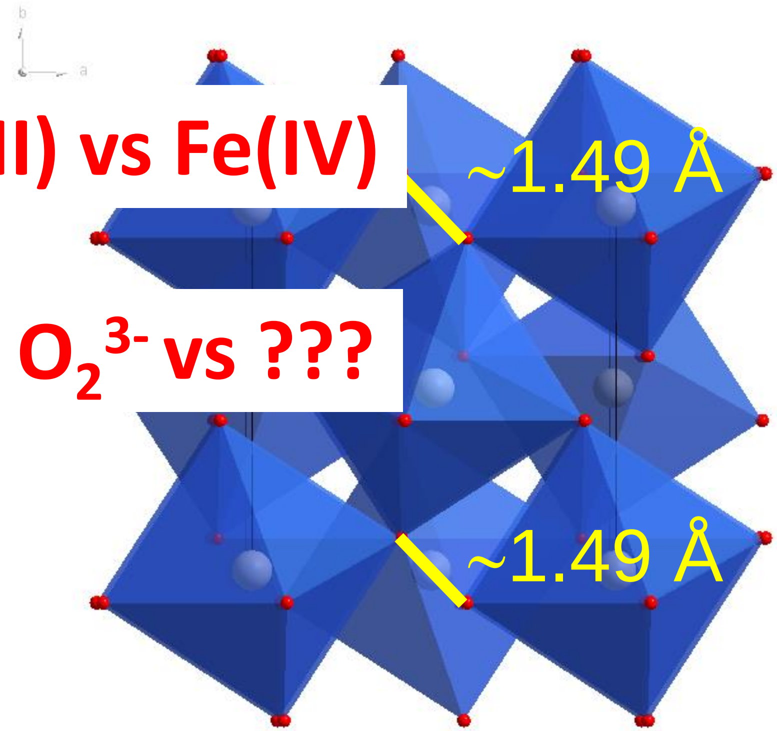

FeO_2, 68(1) GPa

HP-PdF_2-type structure

MgO_2, 0 GPa

Pyrite-type structure

O_2^{2-}

E. Koemets et al., 2019

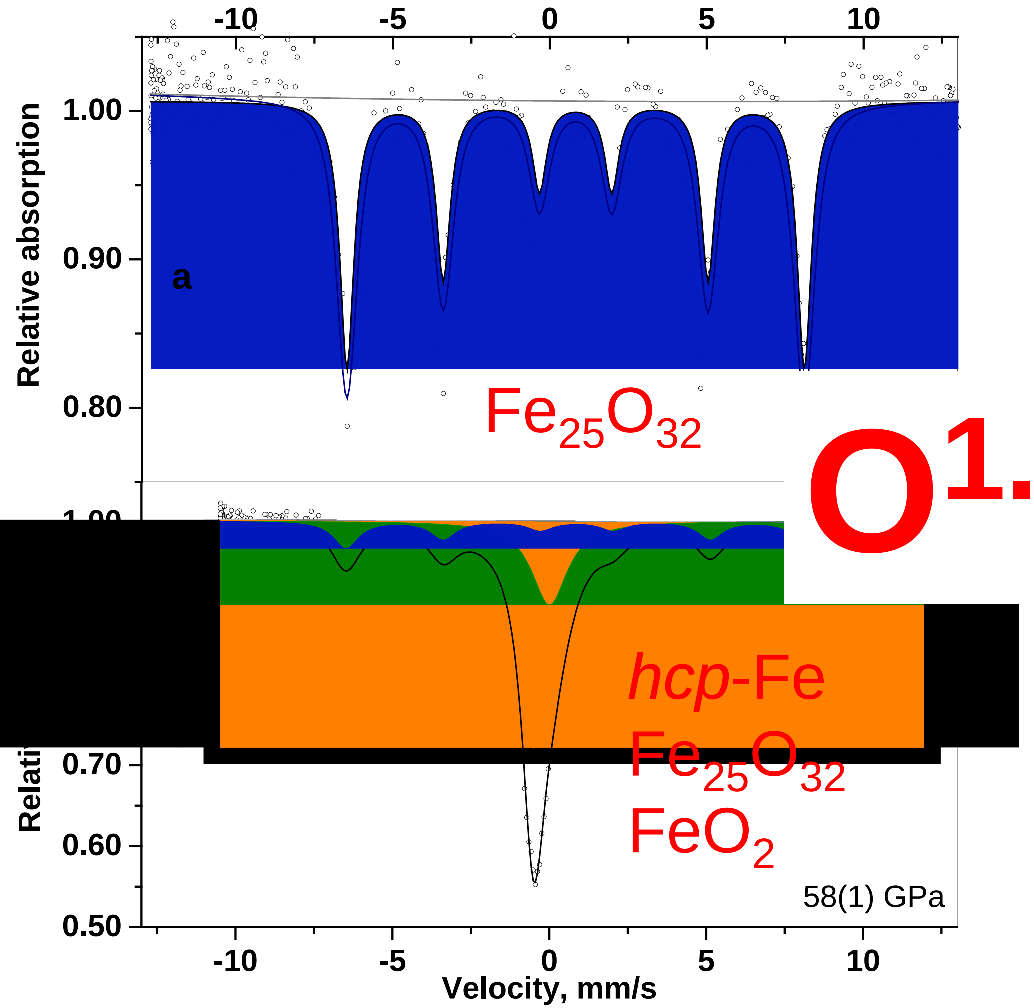

$O^{1.5-}$

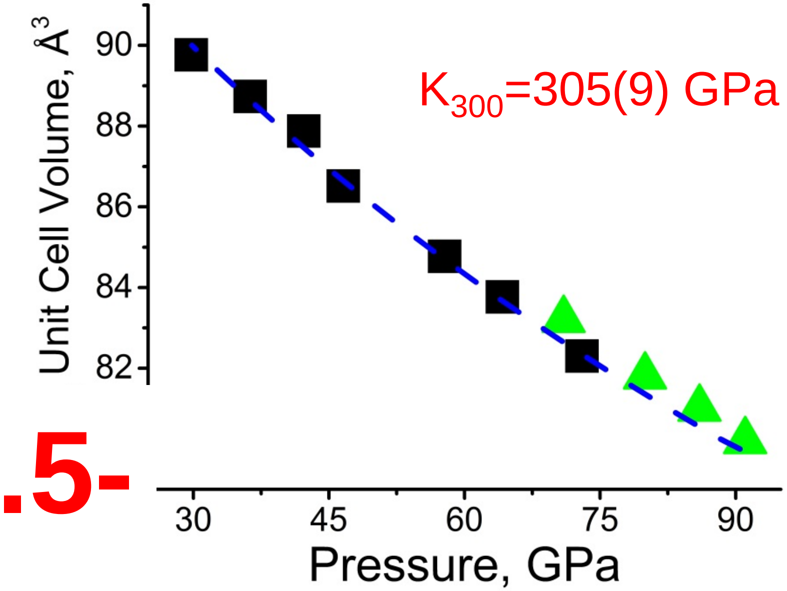

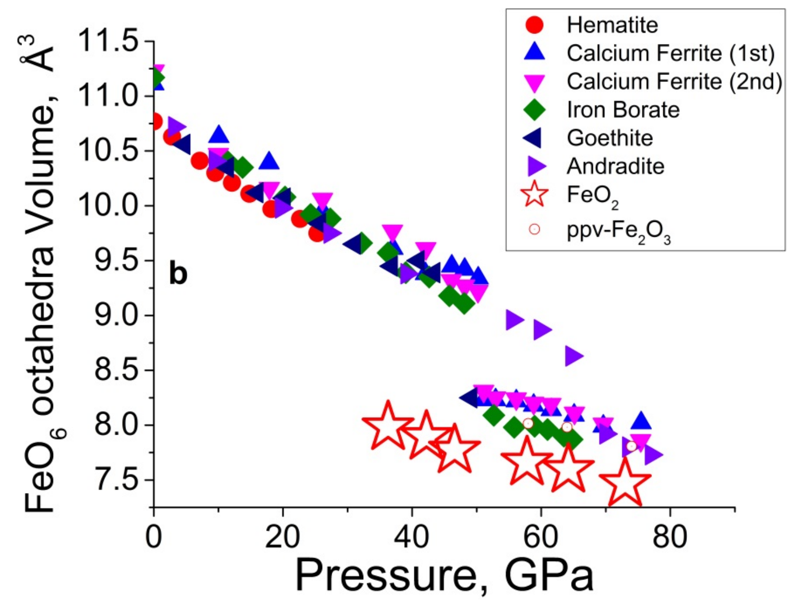

ID18, ESRF

E. Koemets et al., 2019

Iron oxides in the deep Earth's interiors

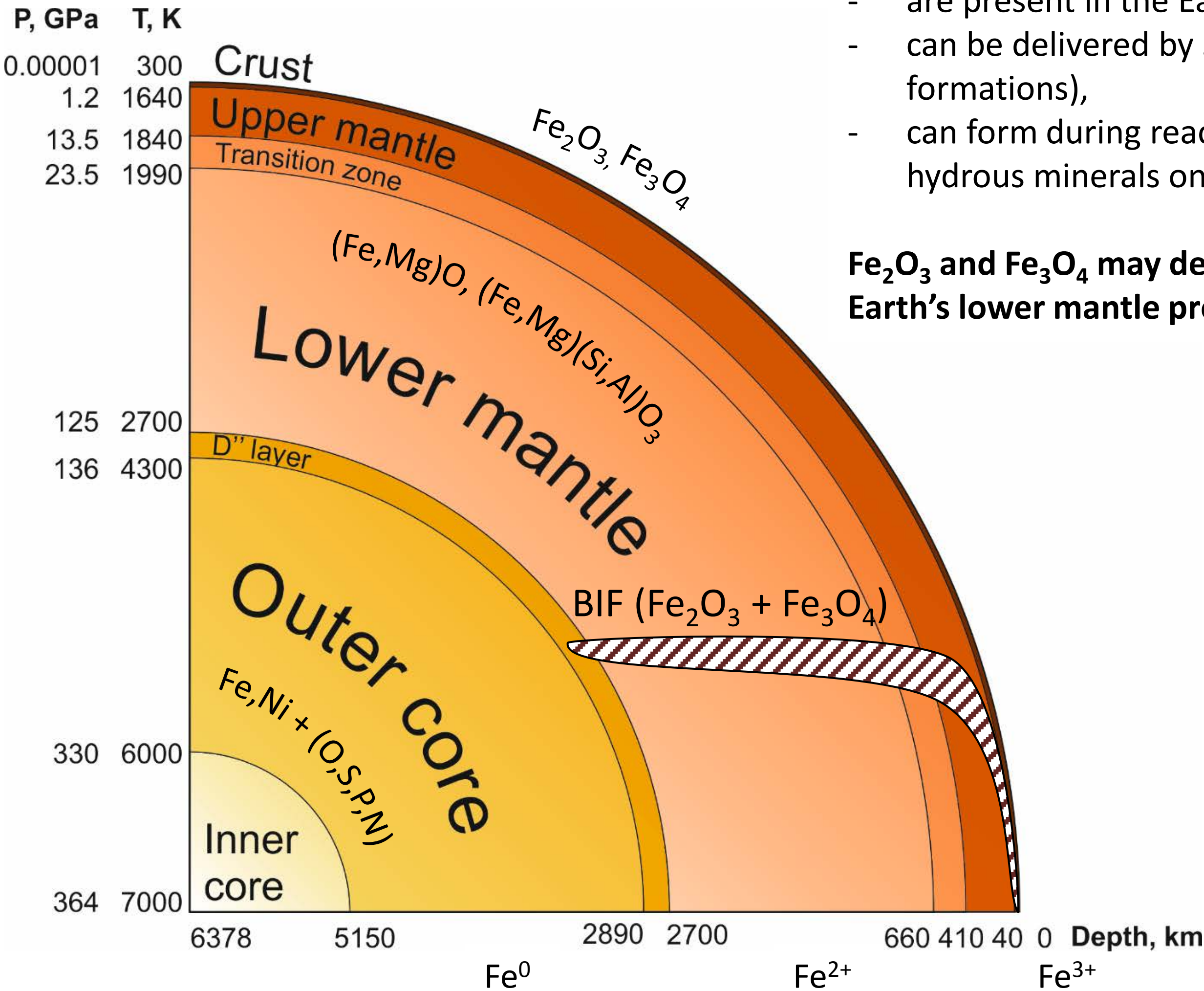

Oxides of iron:

- are present in the Earth's deep interiors (mainly Fe^{2+}),
- can be delivered by subducting slabs (banded iron formations),
- can form during reaction with water from subducted hydrous minerals on the border with core (D'' layer).

Fe_2O_3 and Fe_3O_4 may decompose at the conditions of the Earth's lower mantle producing oxygen fluids

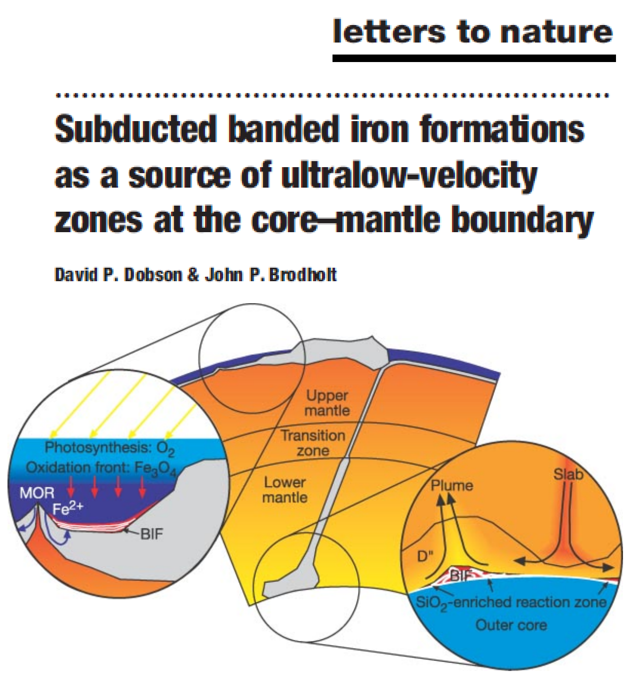

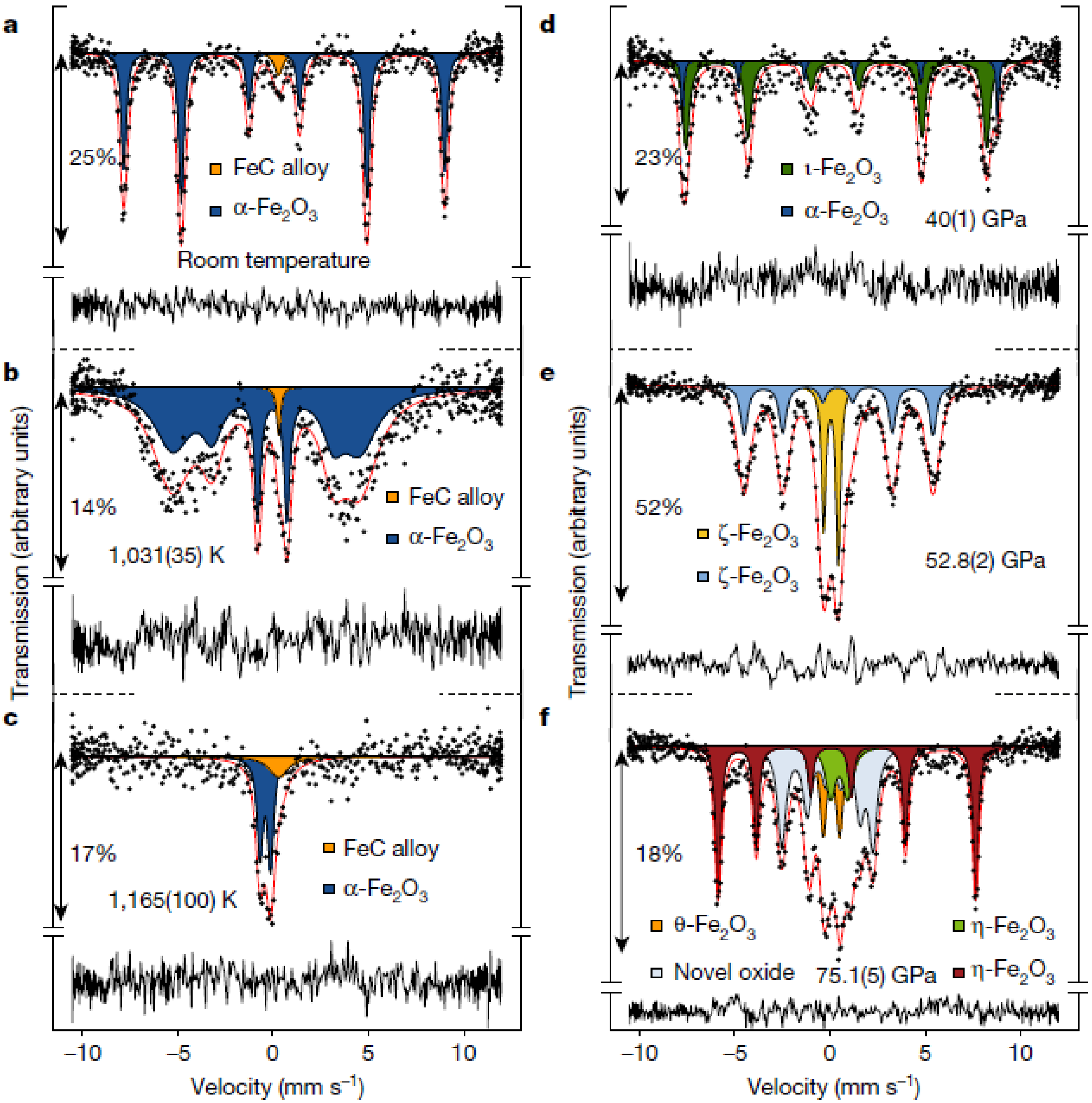

I. Kupenko et al., Nature, 2019

Oxides and nitrides applications

Electronic applications

High energy density materials HEDM applications

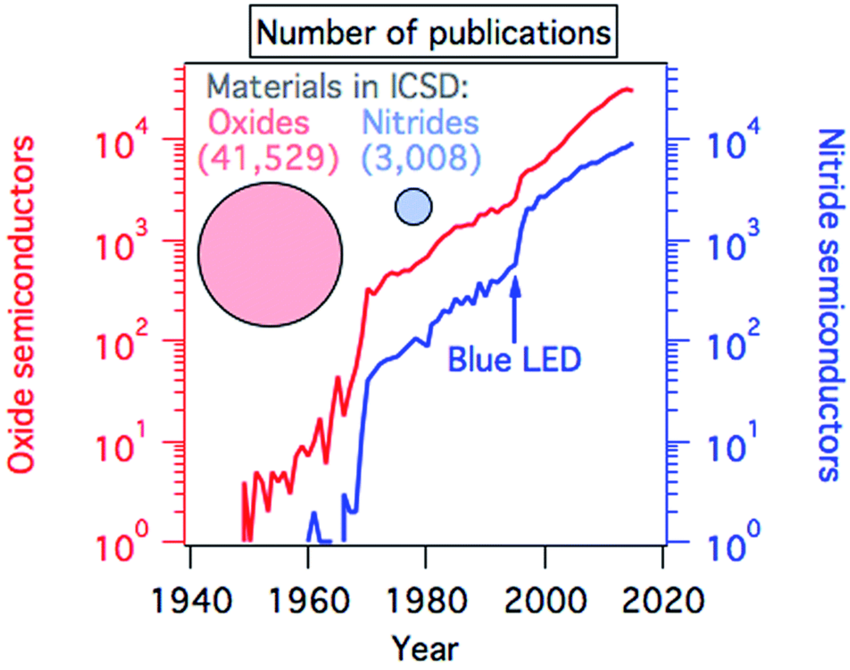

Number of indexed publications in Scopus in the fields of semiconducting oxides and nitrides as a function of year, demonstrating the increased importance of these materials in electronic applications. Inset: the number of entries in ICSD, proportional to the area of the circles, also illustrates the relatively unexplored character of the nitrides (3008) compared to the oxides (41 529).

Zakutayev. *J. Mater. Chem. A*, 2016,**4**, 6742-6754

Oxides and nitrides applications

Electronic applications

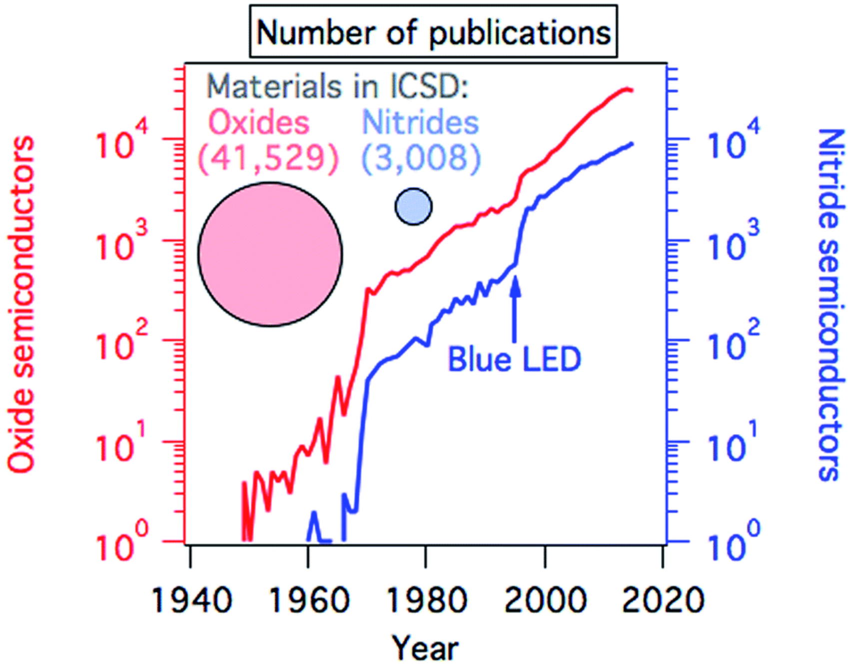

Number of indexed publications in Scopus in the fields of semiconducting oxides and nitrides as a function of year, demonstrating the increased importance of these materials in electronic applications. Inset: the number of entries in ICSD, proportional to the area of the circles, also illustrates the relatively unexplored character of the nitrides (3008) compared to the oxides (41 529).

Zakutayev. *J. Mater. Chem. A*, 2016,**4**, 6742-6754

High energy density materials HEDM applications

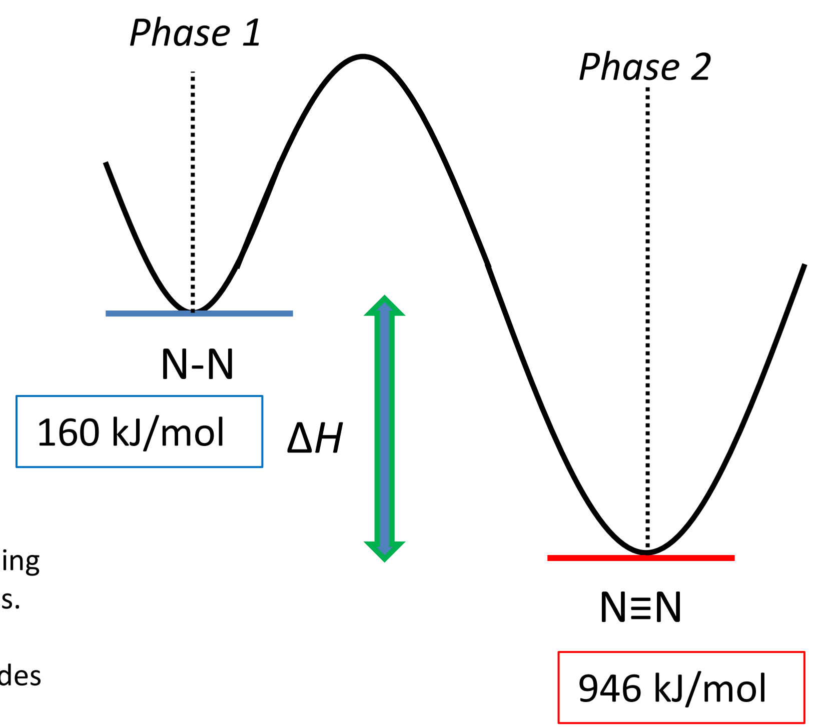

Novel nitrides synthesized at high-pressure high-temperature conditions

Inorganic Chemistry

Stable Calcium Nitrides at Ambie

Shuangshuang Zhu,[†] Feng Peng,[*,‡,§] Hanyu Liu,[⊥]

[†]Institute of Atomic and Molecular Physics, Sichuan University,
[‡]College of Physics and Electronic Information, Luoyang Norm
[§]Beijing Computational Science Research Center, Beijing 10084
[⊥]Geophysical Laboratory, Carnegie Institution of Washington, 5
[‖]Department of Physics and Engineering Physics, University of
[#]Canadian Light Source, Saskatoon, Saskatchewan S7N 2V3, C

Supporting Information

ABSTRACT: The knowledge of stoichiometries of alkaline earth metal nitrides, where nitrogen can exist in polynitroge forms, is of significant interest for understanding nitroge bonding and its applications in energy storage. For calciun nitrides, there were three known crystalline forms, CaN_2, Ca_2N and Ca_3N_2, at ambient conditions. In the present study, w demonstrated that there are more stable forms of calciun nitrides than what is already known to exist at ambient an high pressures. Using a global structure searching method, w theoretically explored the phase diagram of CaN_x and discov found a new CaN phase that is thermodynamically stable at Ca_2N. Four other stoichiometries, namely, Ca_2N_3, CaN_3, Ca predicted CaN_x compounds contain a rich variety of polynitr extended chains (N_∞). Because of the large energy difference CaN_x crystals with polynitrogens is expected to be highly exc

Inorganic Chemistry

Communication

pubs.acs.org/IC

High Pressure Synthesis of Marcasite-Type Rhodium Pernitride

Ken Niwa,[*,†] Dmytro Dzivenko,[‡] Kentaro Suzuki,[†] Ralf Riedel,[‡] Ivan Troyan,[§] Mikhail Eremets,[§] and Masashi Hasegawa[†]

[†]Department of Crystalline Materials Science, Nagoya University, Furo-cho, Chikusa-ku, Nagoya 464-8603, Japan
[‡]Fachgebiet Disperse Feststoffe, Fachbereich Material- und Geowissenschaften, Technische Universität Darmstadt Jovanka-Bontschits-Str. 2, 64287 Darmstadt, Germany
[§]Department of Biogeochemistry, Max-Planck-Institut für Chemie, Hahn-Meitner-Weg 1, 55128Mainz, Germany

Supporting Information

ABSTRACT: Marcasite-type rhodium nitride was successfully synthesized in a direct chemical reaction between a rhodium metal and molecular nitrogen at 43.2 GPa using a laser-heated diamond-anvil cell. This material shows a low zero-pressure bulk modulus of K_0 = 235(13) GPa, which is much lower than those of other platinum group nitrides. This finding is due to the weaker bonding interaction between metal atoms and quasi-molecular dinitrogen units in the marcasite-type structure, as proposed by theoretical studies.

Nitrides are attractive materials not only in the field of fundamental crystal chemistry but also in industrial applications.[1] In the 2000s, platinum group nitrides (PtN_2, OsN_2, IrN_2, and PdN_2) were remarkably discovered in a direct chemical reaction between platinum group elements and molecular fluid nitrogen at high pressures and temperatures.[2−7] The new class of compounds attracted much attention due to the unusual crystal chemistry as well as intriguing mechanical properties (e.g., K_0 = 428 GPa for IrN_2) owing to the strong bonding interaction between noble metals and nitrogen.[2−7] However, to the best of our knowledge, there has been no experimental evidence of a successful synthesis of rhodium nitride so far, although theoretical studies suggest that rhodium is likely to form RhN_2 with a marcasite-type structure.[8,9]

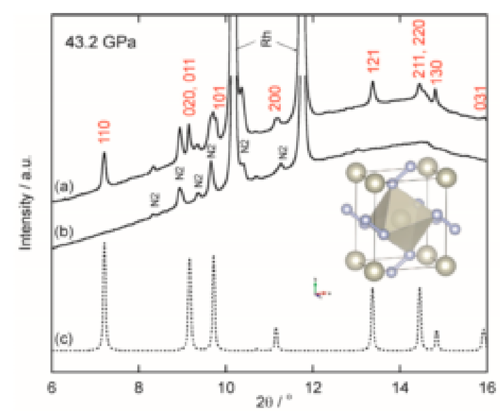

Figure 1. (a) XRD pattern of the sample measured after heating at 43.2 GPa. The diffraction peaks, which are labeled with the Miller indices, correspond to marcasite-type rhodium nitride, RhN_2. Other peaks are due to the residual rhodium metal[10] and solid nitrogen.[11] (b) XRD pattern of the unheated region. N2 represents the solid nitrogen with a rhombohedral structure.[11] (c) Simulated XRD pattern of marcasite-type RhN_2 at 43.2 GPa together with a schematic illustration of the crystal structure for marcasite-type RhN_2. Large and small balls represent rhodium and nitrogen atoms, respectively. The lattice constants and atomic positional parameters were taken from the present results and from the theoretical calculation study,[8] respectively.

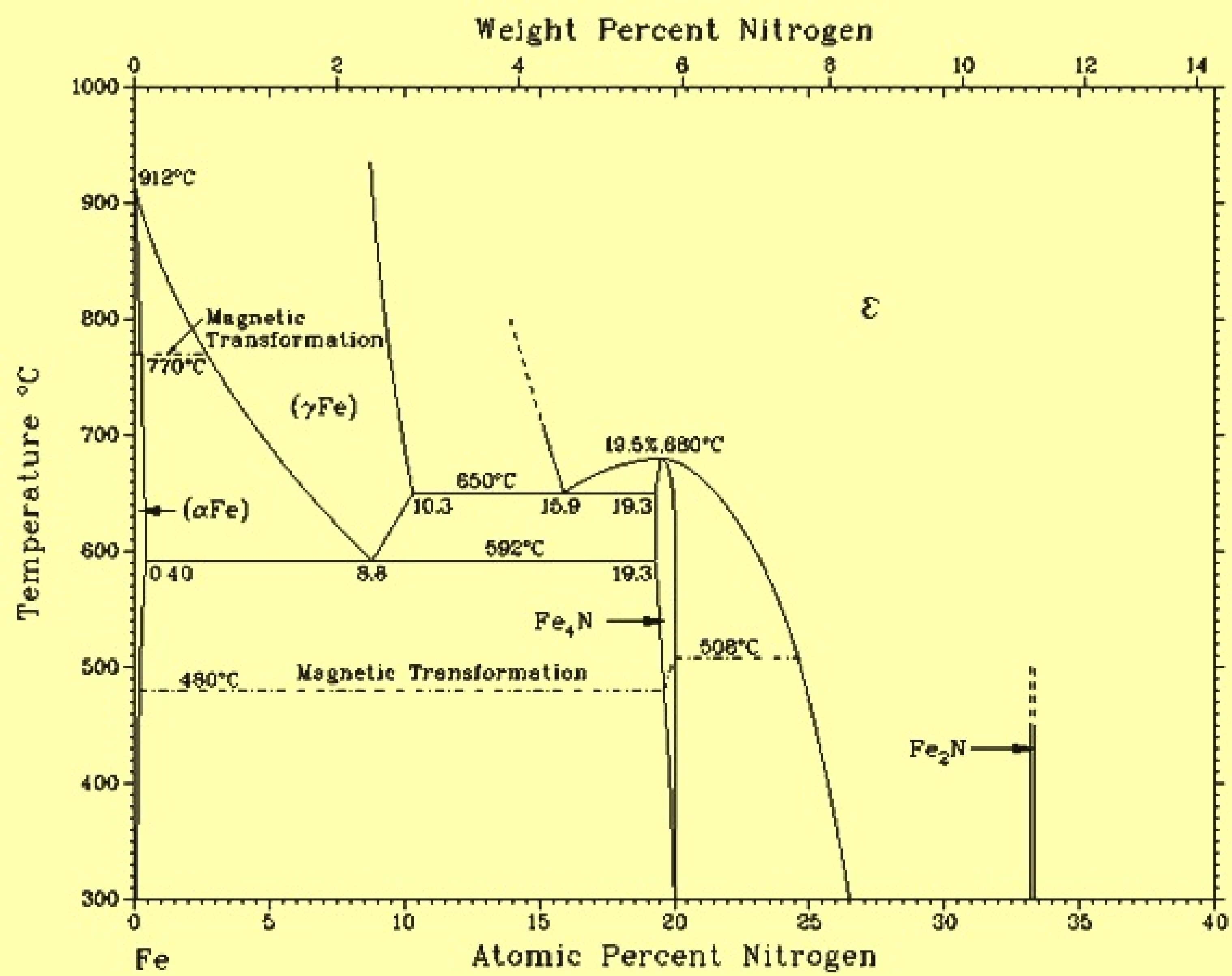
Weight Percent Nitrogen
0
2
4
6
8
10
12
14
1000
900
800
700
600
500
400
300
Temperature °C
912°C
Magnetic
Transformation
770°C
(γFe)
ε
19.5%,680°C
650°C
10.3
15.9
19.3
(αFe)
592°C
0.40
8.8
19.3
Fe4N
506°C
480°C
Magnetic Transformation
Fe2N
0
5
10
15
20
25
30
35
40
Fe
Atomic Percent Nitrogen

Novel iron nitrides

Fe_3N_2 ~50 GPa 1900(100) K

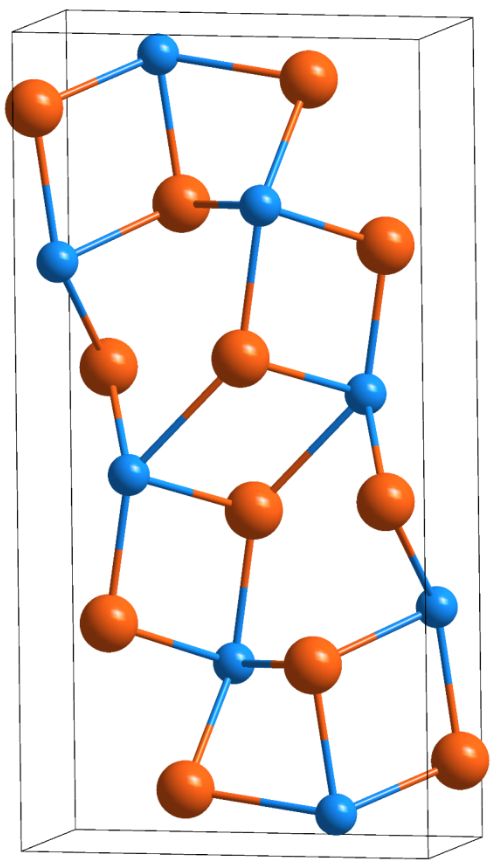

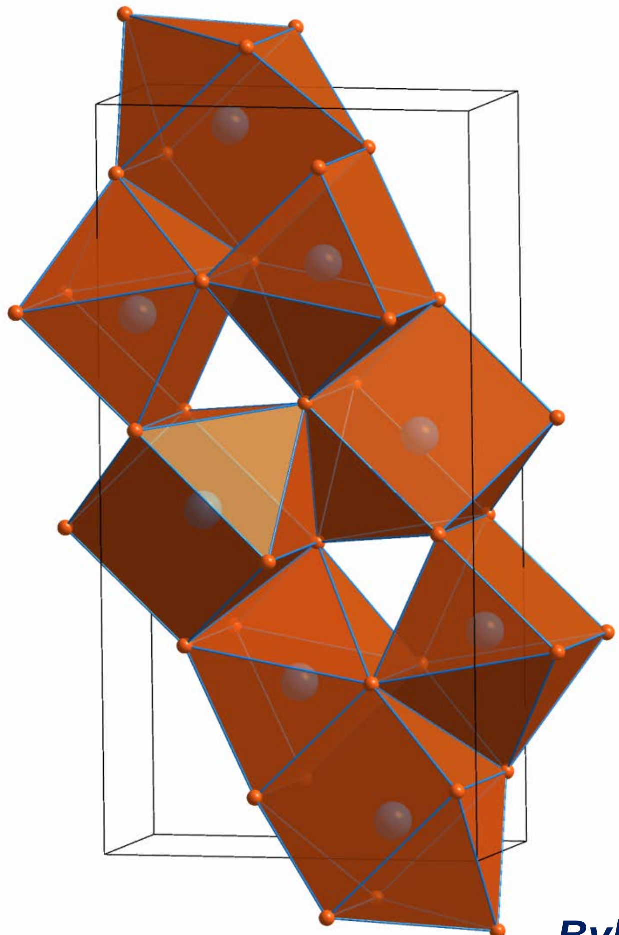

Structure type of Cr_3C_2

Pnma
a =5.4227(6) Å
b=2.6153(3) Å
c=10.590(11) Å

R_1 = 3.1%

Bykov et al. Nat. Comm. (2018)

Novel iron nitrides

B8-type FeN

50 GPa

P6₃/mmc → $P6_3/mmc$
a = 2.6392(4) Å
c = 4.8142(15) Å
V = 29.04(1) $Å^3$

R_1 = 4.3%

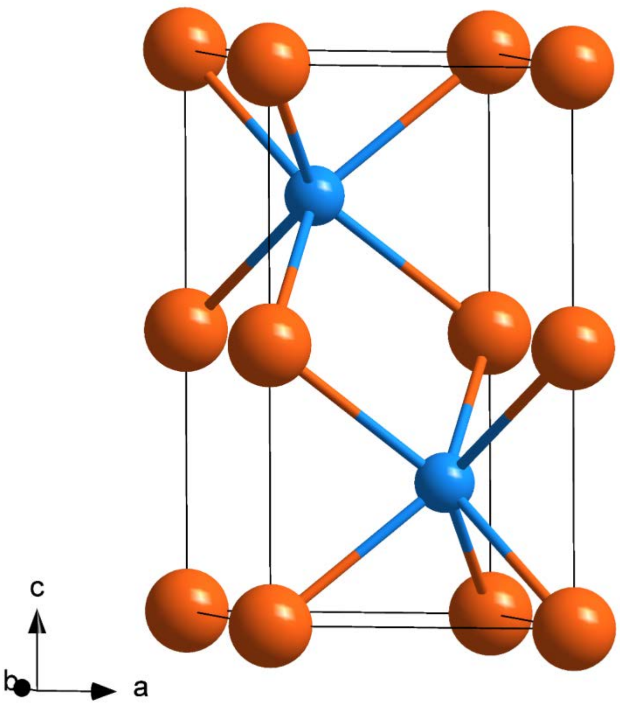

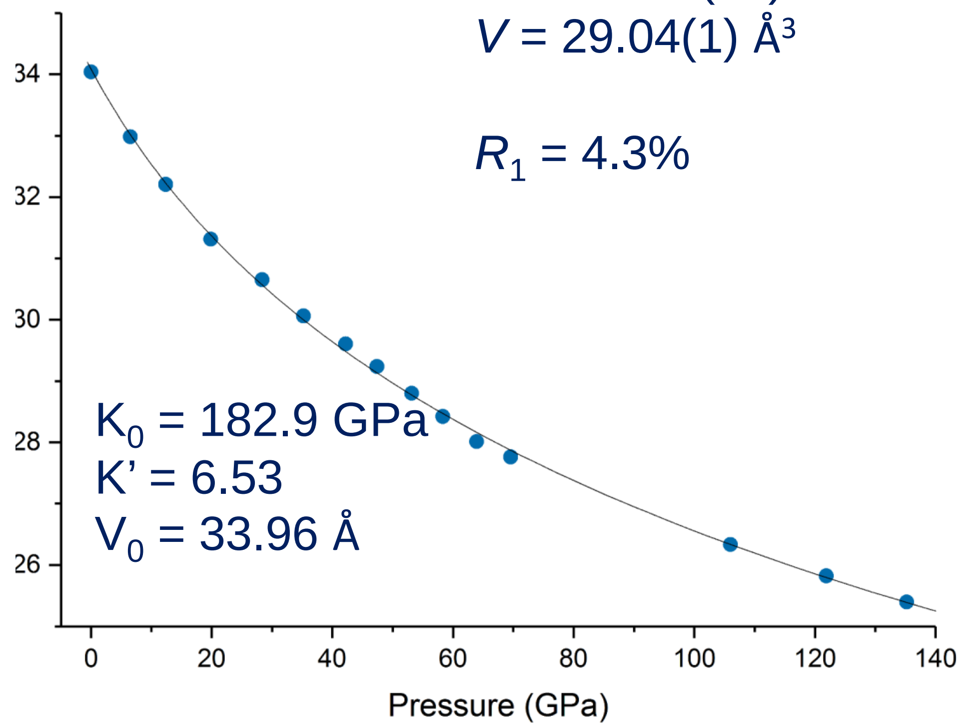

Clark et al. Angew. Chemie Int. Ed. (2017)

Novel iron nitrides

Marcasite-type FeN_2

~58 GPa

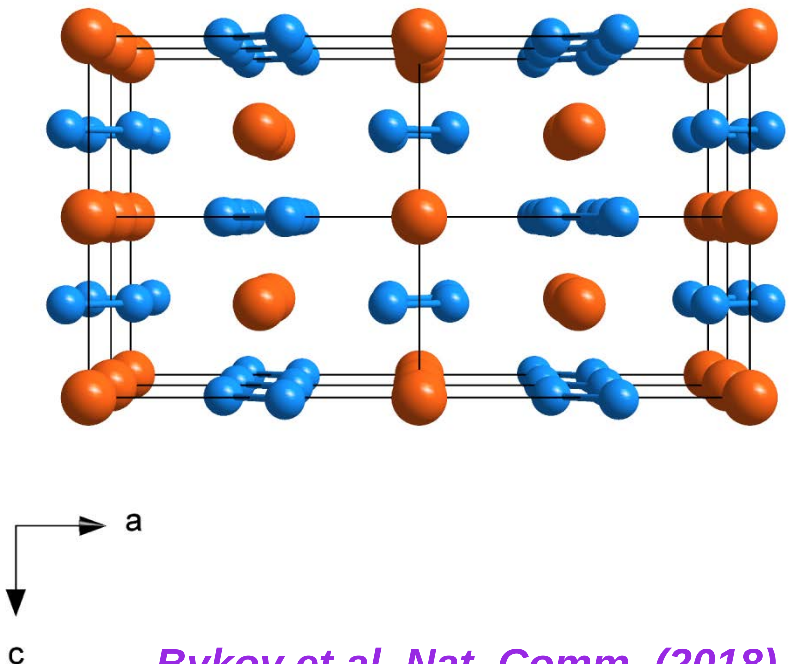

Bykov et al. Nat. Comm. (2018)

K_0 = 270 GPa,
K' = 3.4
V_0 = 47.32 Å^3

$Ti^{4+}N_2$: K_0 = 360 GPa
$Ir^{4+}N_2$: K_0 = 428 GPa

Young et al. PRL 2006
Bhadram et al. Chem Mater. 2016

Pnnm
a = 4.4308 Å *b* = 3.7218 Å *c* = 2.4213 Å
R_1 = 5.7%

d(N-N) = 1.317 Å at 60 GPa

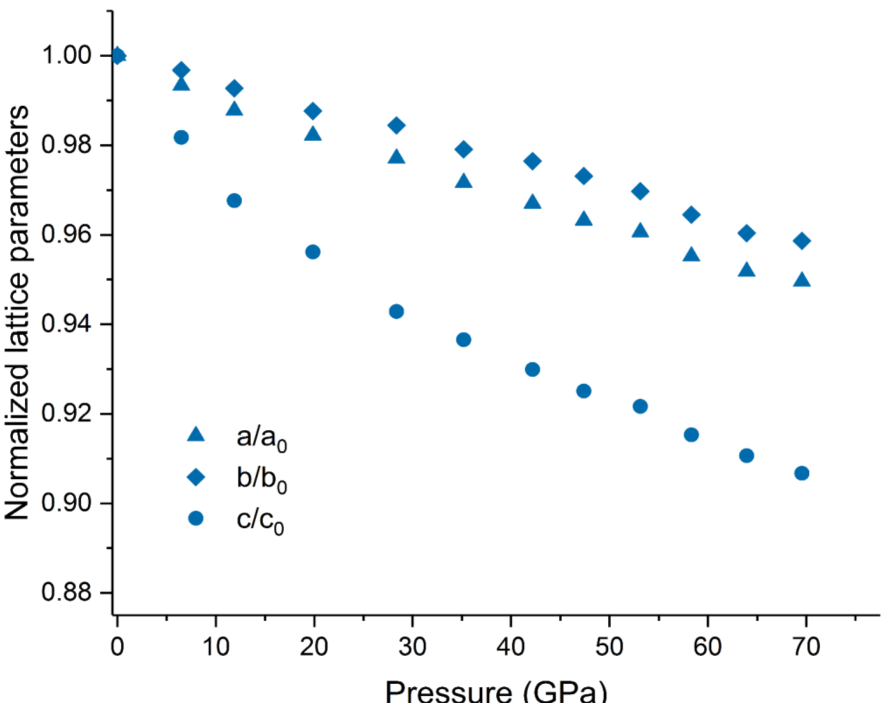

Novel iron nitrides

FeN_4

135 GPa, 2700(200) K

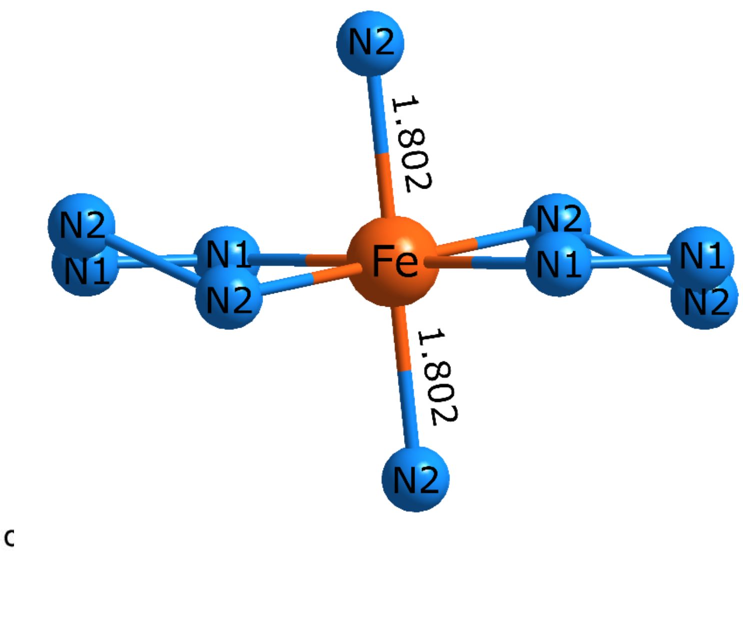

catena-poly[tetraz-1-ene-1,4-diyl] anions

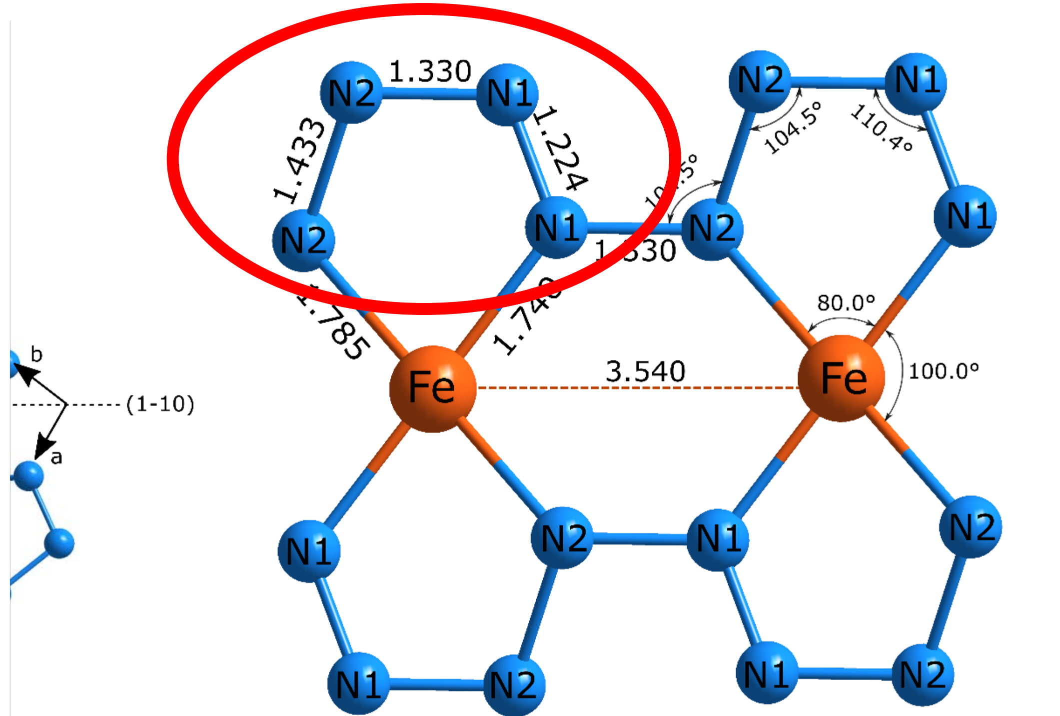

P-1
a = 2.5079(5), *b* = 3.5270(14), *c* = 3.5402(6) Å
α=105.08(2), β=110.231(16), γ=92.05(2)°
R_1 = 7.2%

Bykov et al. Nat. Comm. (2018)

FeN_4 – nitride with polymeric nitrogen chains

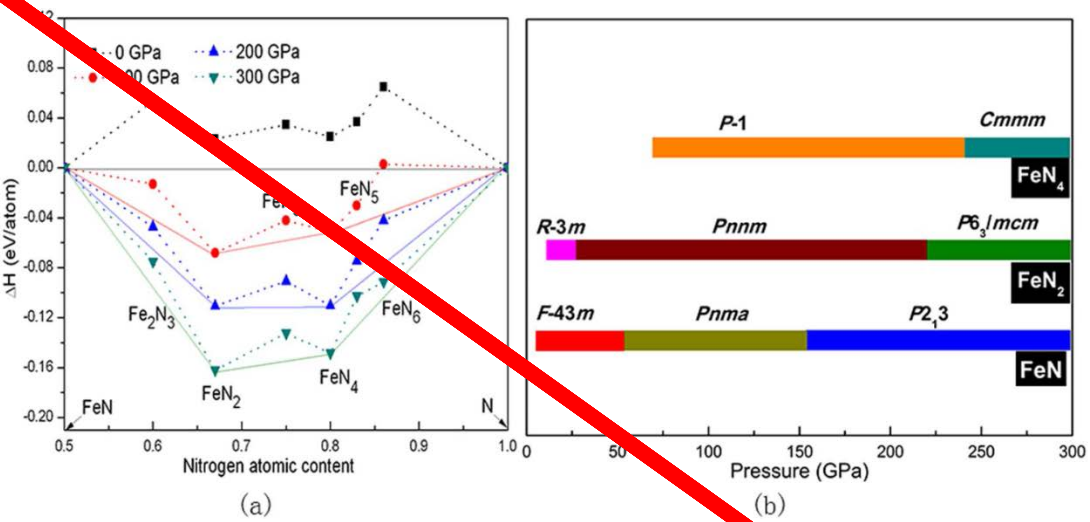

(a) (b)

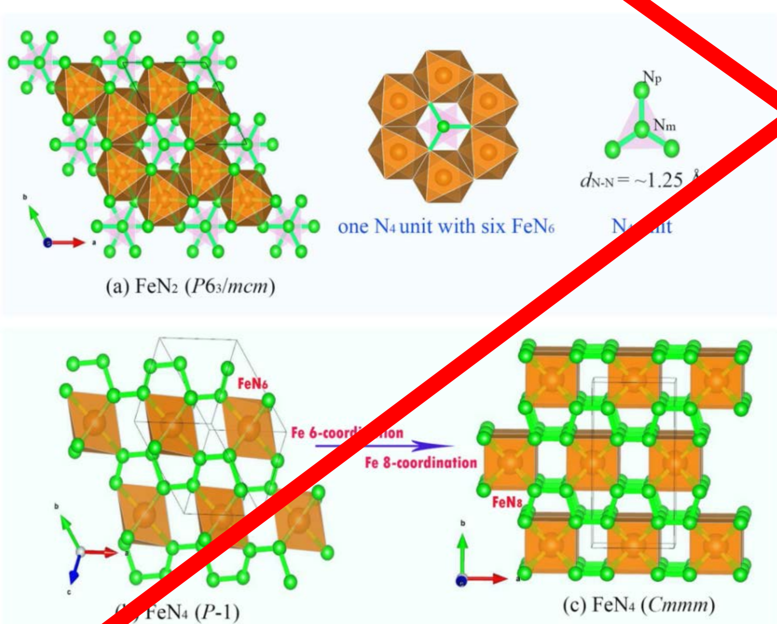

(a) FeN2 (P63/mcm)

(b) FeN4 (P-1)

(c) FeN4 (Cmmm)

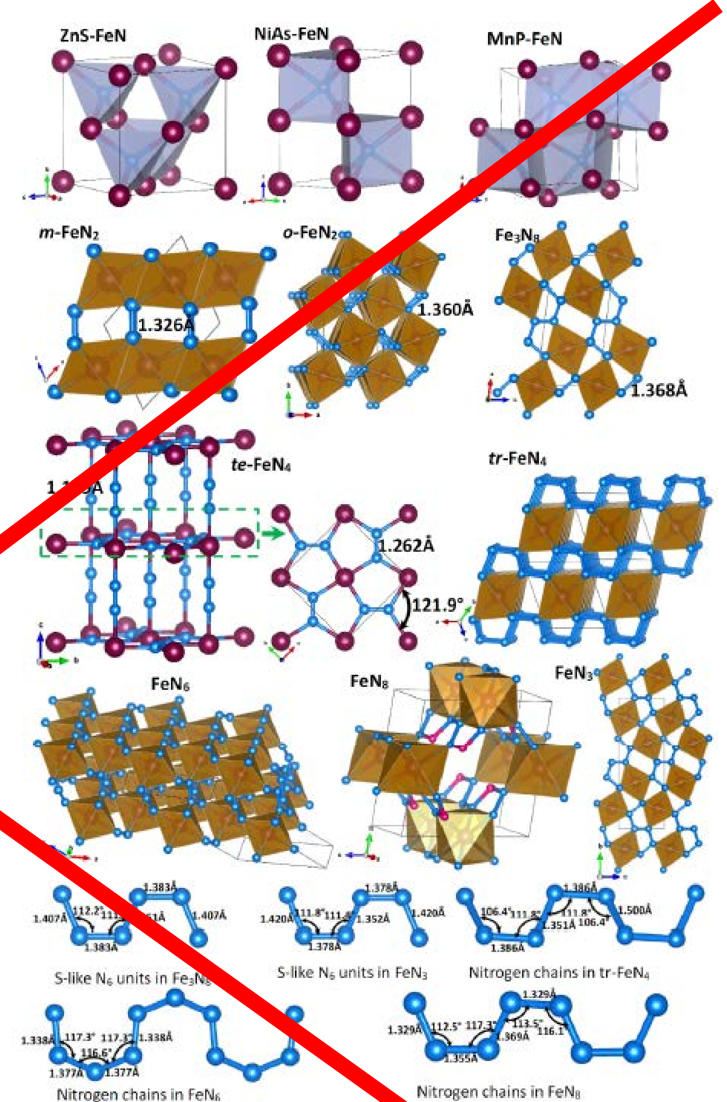

Chen et al, 10.1038/s41598-018-29038-w Wu et al., 10.1021/acs.chemmater.8b02972

Synthesis and crystal structure of $ReN_8 \cdot xN_2$

Synthesized at 106 GPa and 2700 K

Space group *Immm*
Structure at *135* GPa*:*

a = 3.4475 (7) Å
b = 6.491(11) Å
c = 6.048 (3) Å

R_1 = 6.8%

Chemical formula $ReN_8 \cdot 0.7N_2$

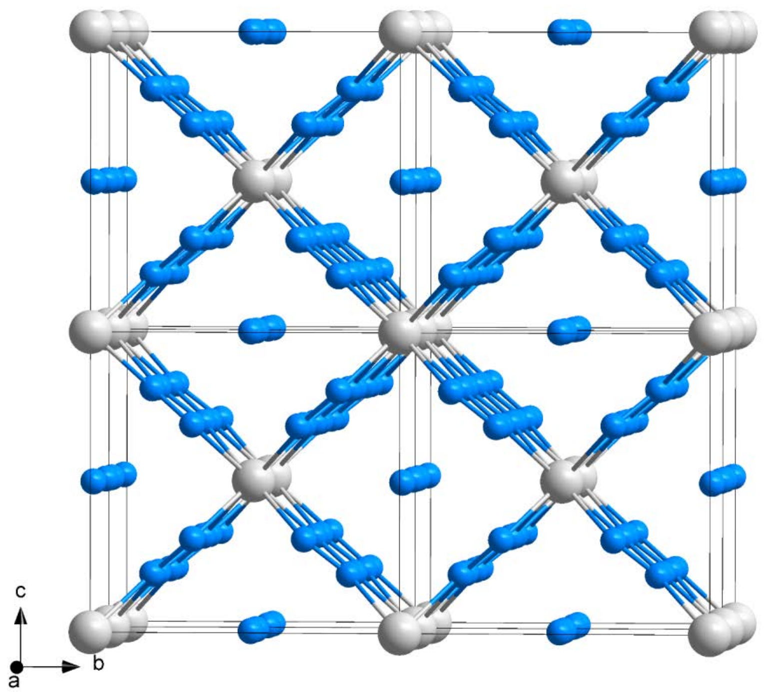

M. Bykov et al. Angewandte Chemie (2018)

Synthesis and crystal structure of $ReN_8 \cdot xN_2$

A high-pressure inclusion compound

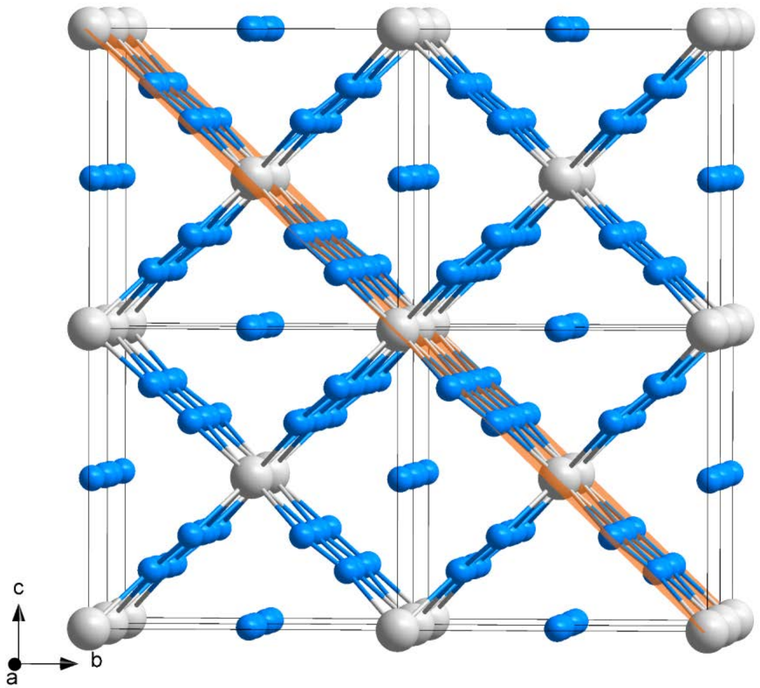

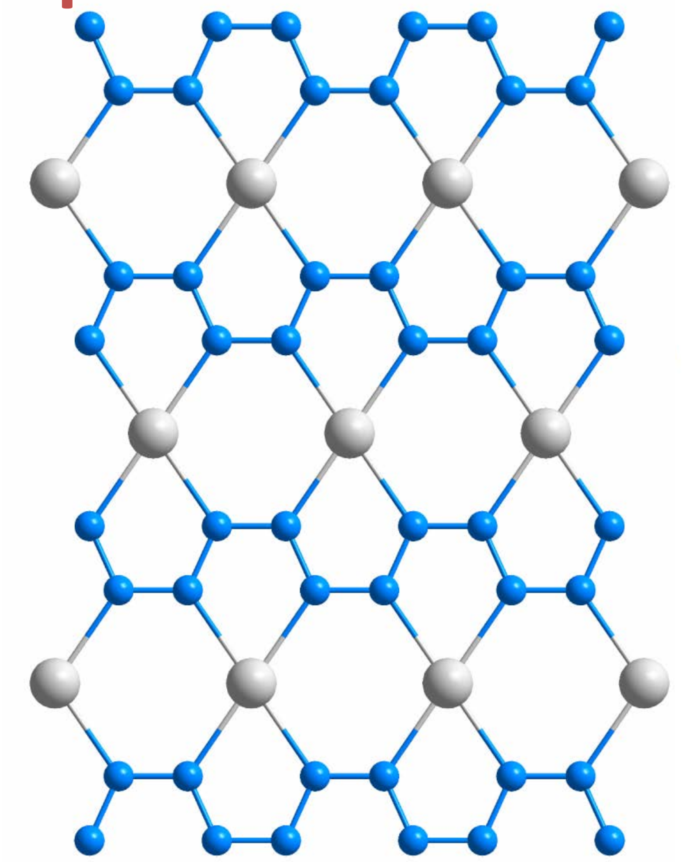

Polydiazenediyl [-N=N-]$_\infty$

Plane (0 1 1)

M. Bykov et al. Angewandte Chemie (2018)

Rhenium nitride pernitride $Re_2(N_2)N_2$ stable at ambient conditions

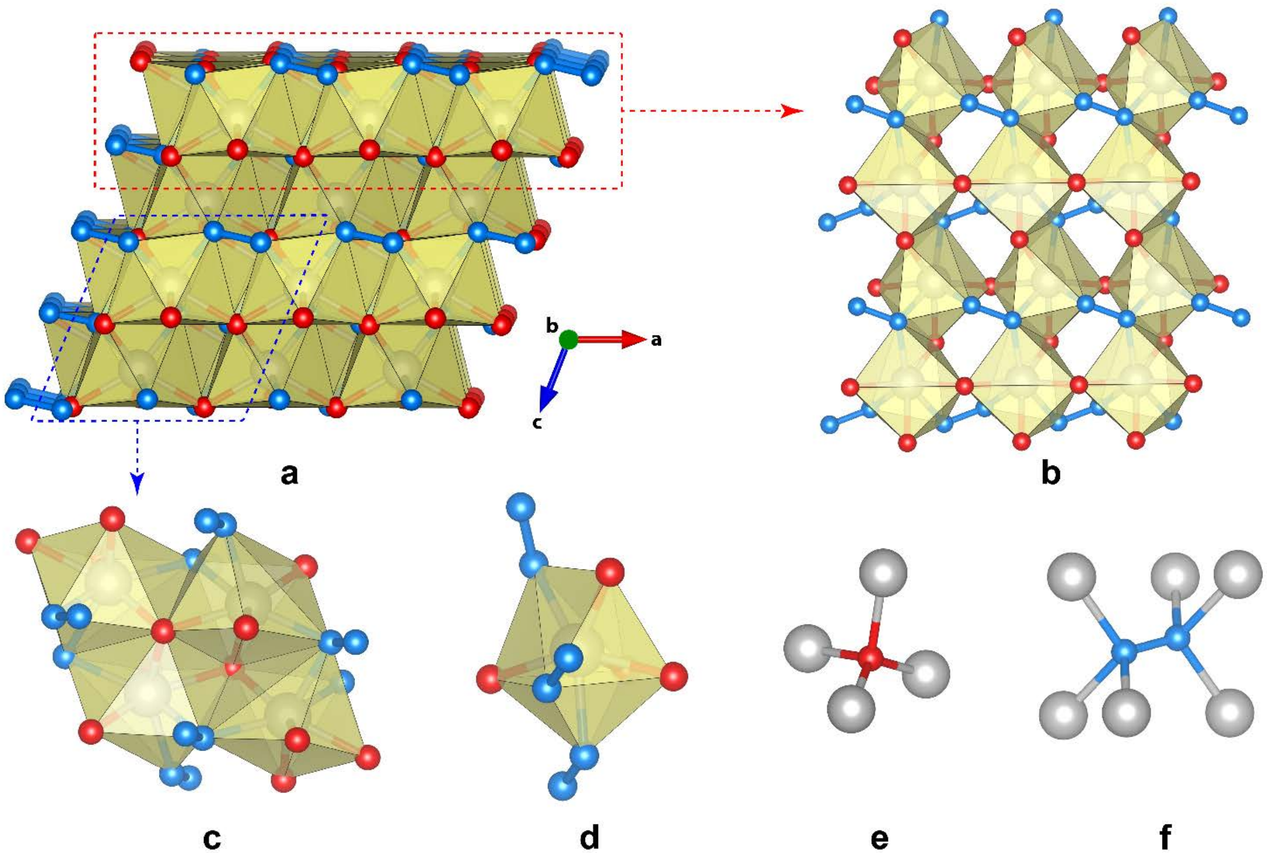

Re atoms – gray, N1 atoms – blue, N2 atoms – red.

Space group $P2_1/c$ (No. 14)
a = 3.6254(17)
b = 6.407(7)
c = 4.948(3) Å
β = 111.48(6)°.

(a) The projection of the crystal structure along the *b*-axis. ,
(b, c) Fragments of the crystal structure of ReN_2 showing how ReN_7 polyhedra are connected with each other.
(d) Separate ReN_7 coordination polyhedron.
(e) Coordination of N2 atoms.
(f) Coordination of N1-N1 dumbbells.

Bykov et al. (2019), Nat Comm, accepted
https://arxiv.org/ftp/arxiv/papers/1902/1902.09249.pdf

Physical properties of $Re_2(N_2)N_2$

Ultraincompressible and superhard

V_0=107.21(4) A^3

K_0=428(10) GPa

K'=1.6(5)

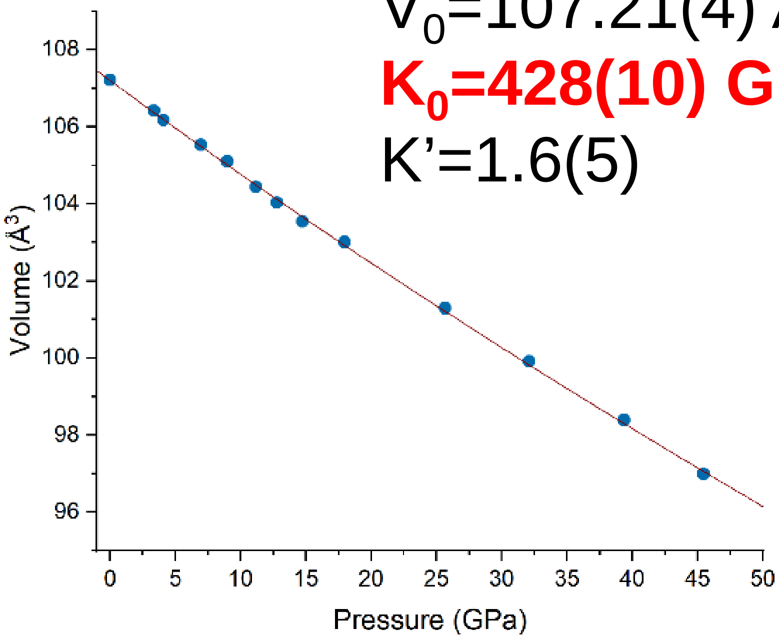

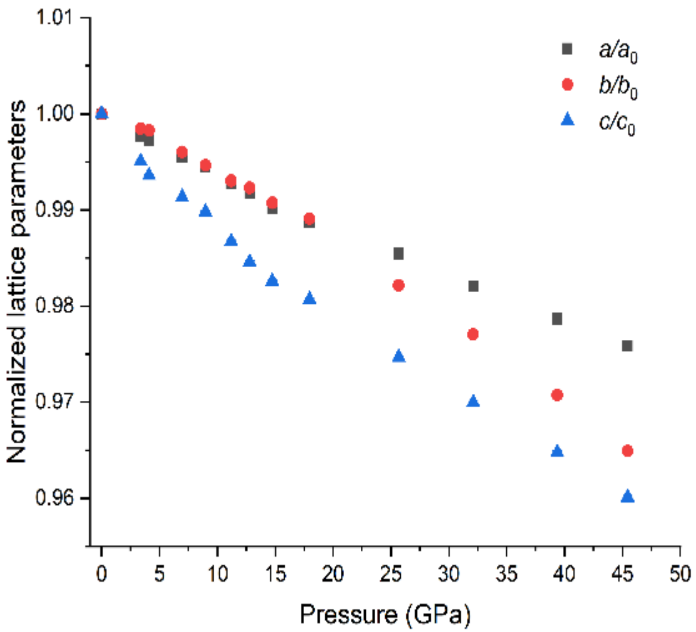

Pressure-dependence of the unit-cell volume and normalized lattice parameters of ReN_2

Bykov et al. (2019), Nat Comm, accepted
https://arxiv.org/ftp/arxiv/papers/1902/1902.09249.pdf

Nanoindentation on Re and ReN_2

Ultraincompressible and superhard

Hardness 36.7(8) GPa

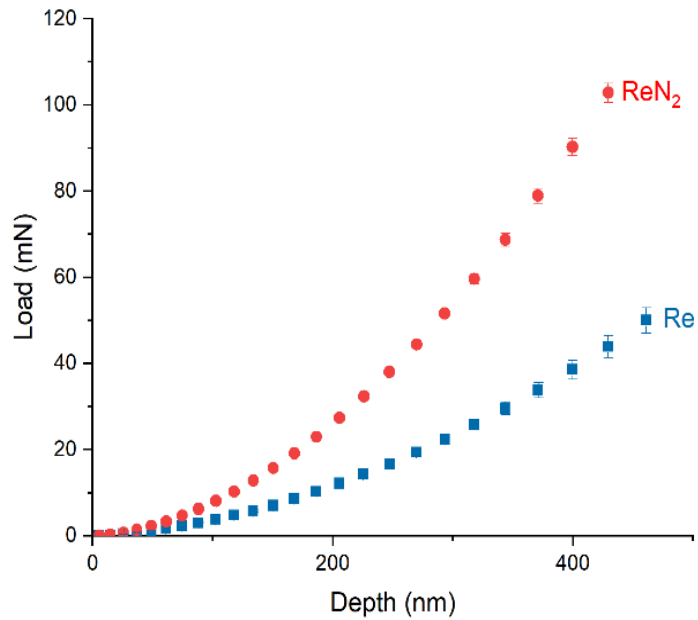

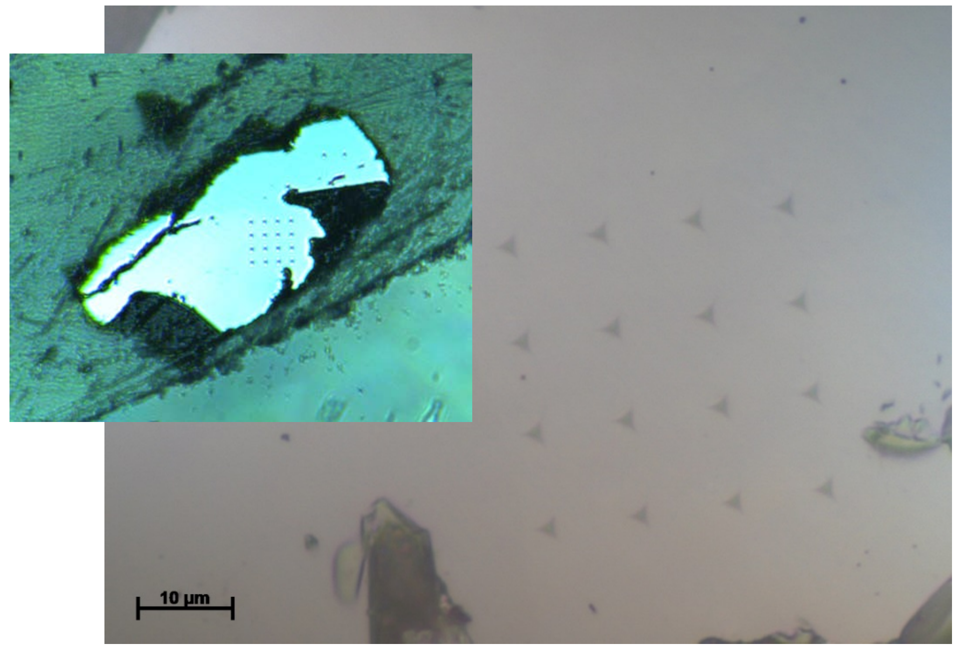

Averaged indentation load-displacement data.

Nanoindenter G200 platform (KLA-Tencor, Milpitas, CA, USA), equipped with a Berkovich diamond tip (Synton MDP, Nidau, Switzerland) and featuring the continuous stiffness based method (CSM)

Bykov et al. (2019), Nat Comm, accepted

https://arxiv.org/ftp/arxiv/papers/1902/1902.09249.pdf

Phonon and electronic structure calculations for ReN_2

- Pernitride N1-N1 unit (N_2^{4-} anion)
- Different electronic properties of N2
- Metallic nature of the material

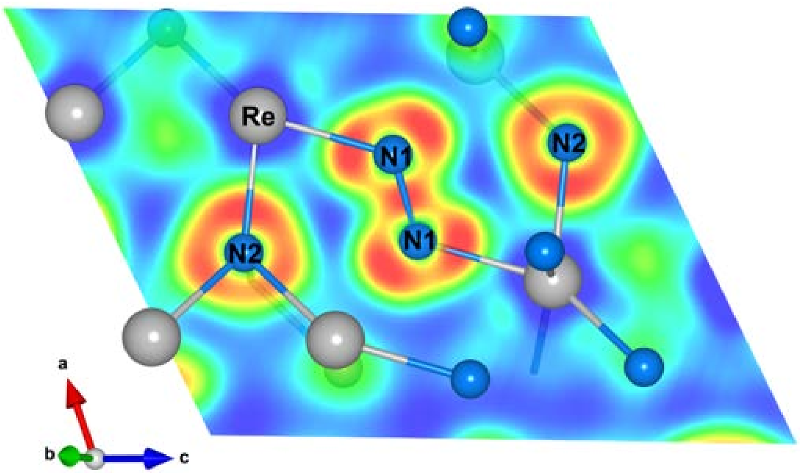

electron localization funciton

Bykov et al. (2019), Nat Comm, accepted
https://arxiv.org/ftp/arxiv/papers/1902/1902.09249.pdf

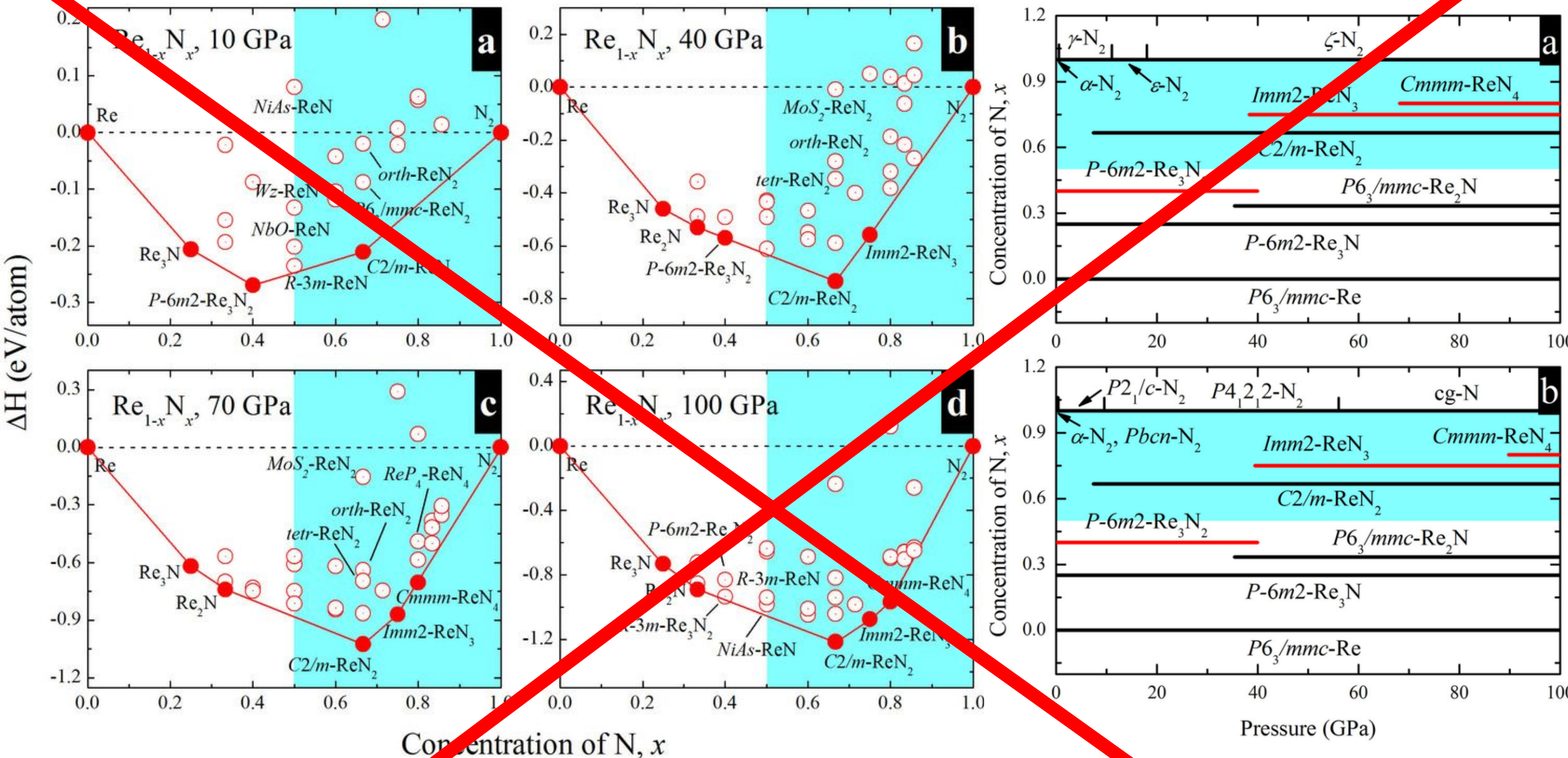

Zhao et al., 10.1038/srep04797

Double-stage DAC (dsDAC)

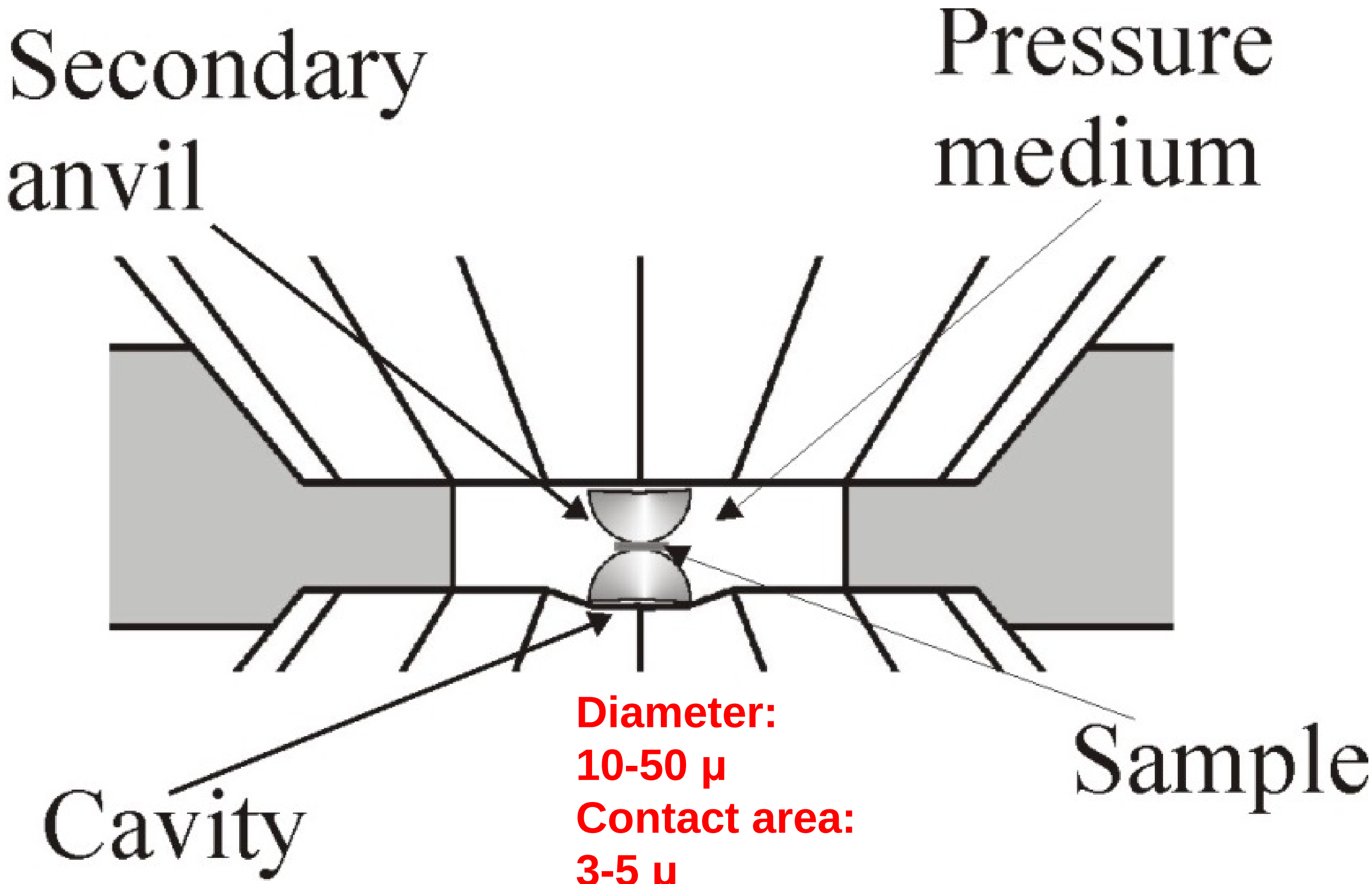

Diameter:
10-50 μ
Contact area:
3-5 μ

Dubrovinsky et al. Nature Comm. 2012

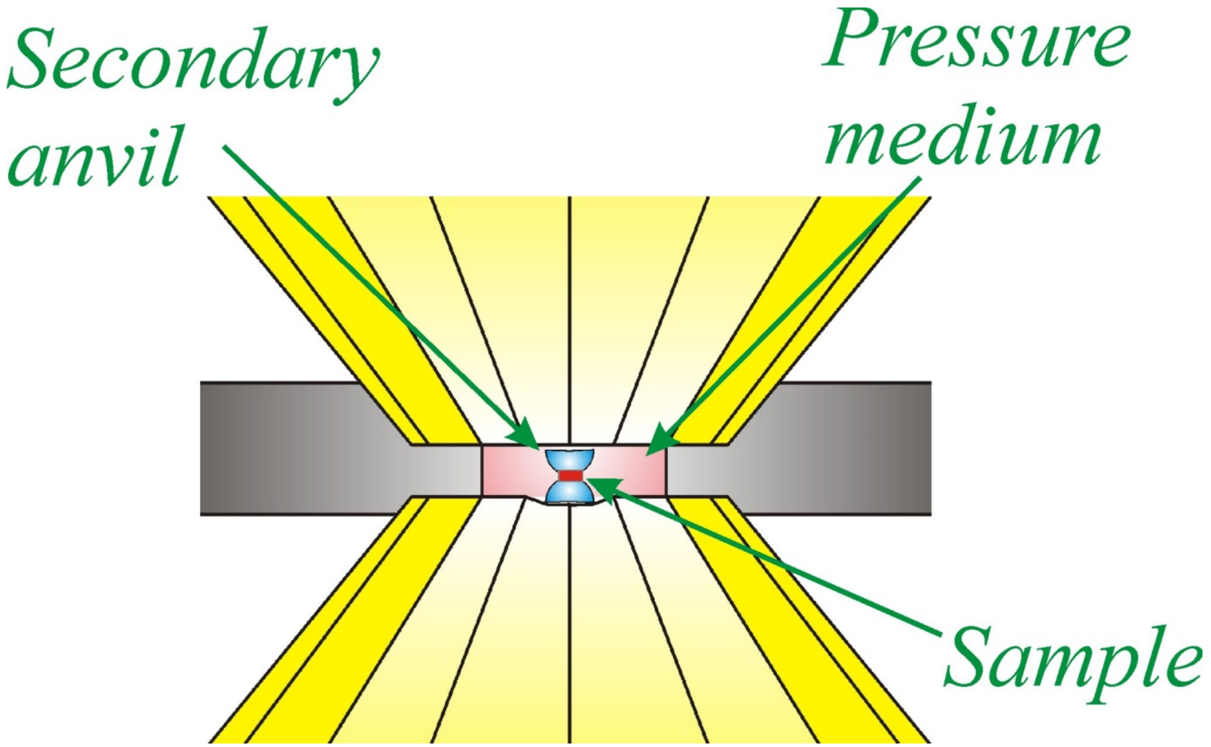

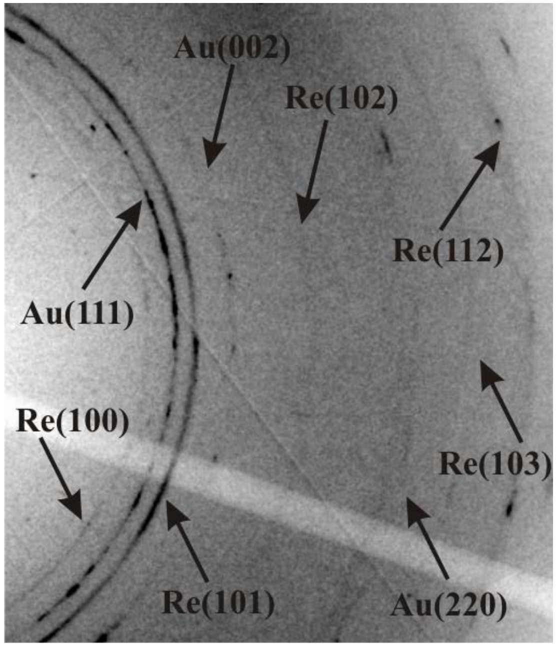

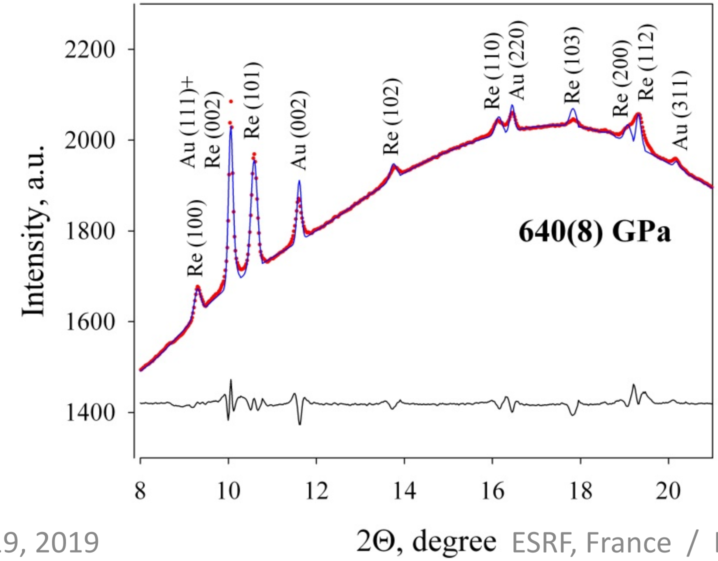

Dubrovinsky et al., Nature Commun. 2012

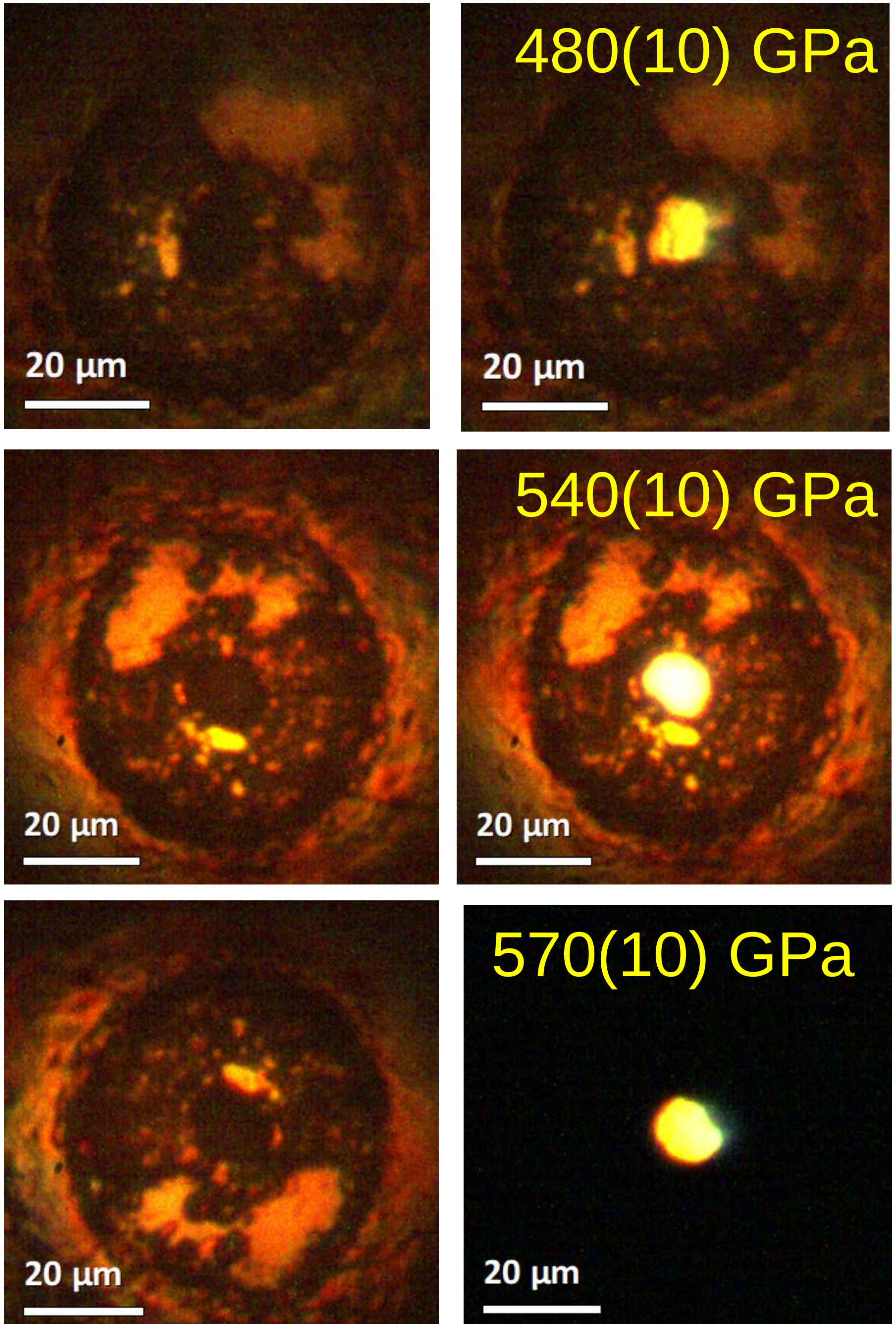
480(10) GPa
540(10) GPa
570(10) GPa
20 µm

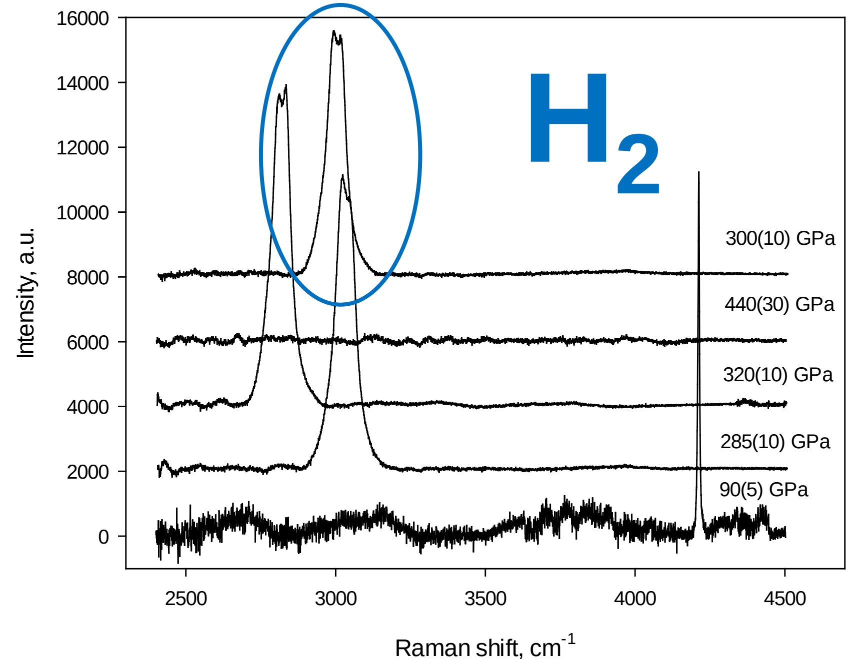
H_2
Intensity, a.u.
Raman shift, cm^{-1}
300(10) GPa
440(30) GPa
320(10) GPa
285(10) GPa
90(5) GPa

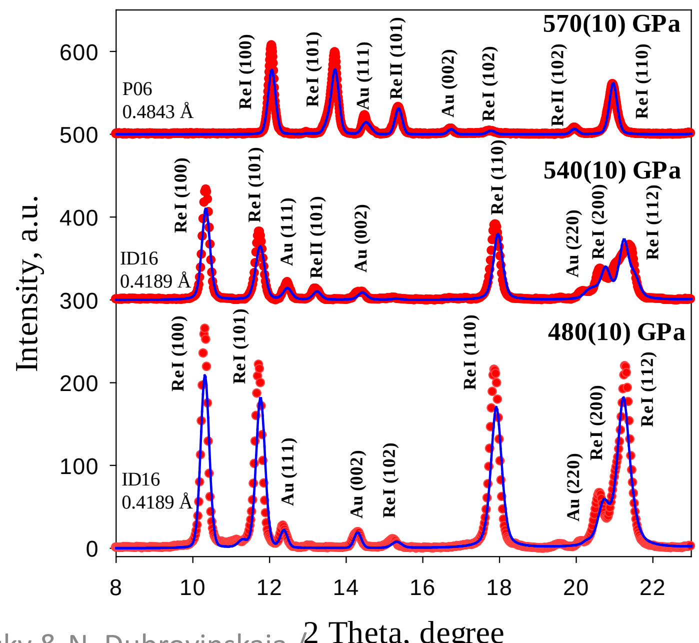
570(10) GPa
540(10) GPa
480(10) GPa
P06
0.4843 Å
ID16
0.4189 Å
ReI (100)
ReI (101)
Au (111)
ReII (101)
Au (002)
ReI (102)
ReII (102)
ReI (110)
Au (220)
ReI (200)
ReI (112)
Intensity, a.u.
2 Theta, degree

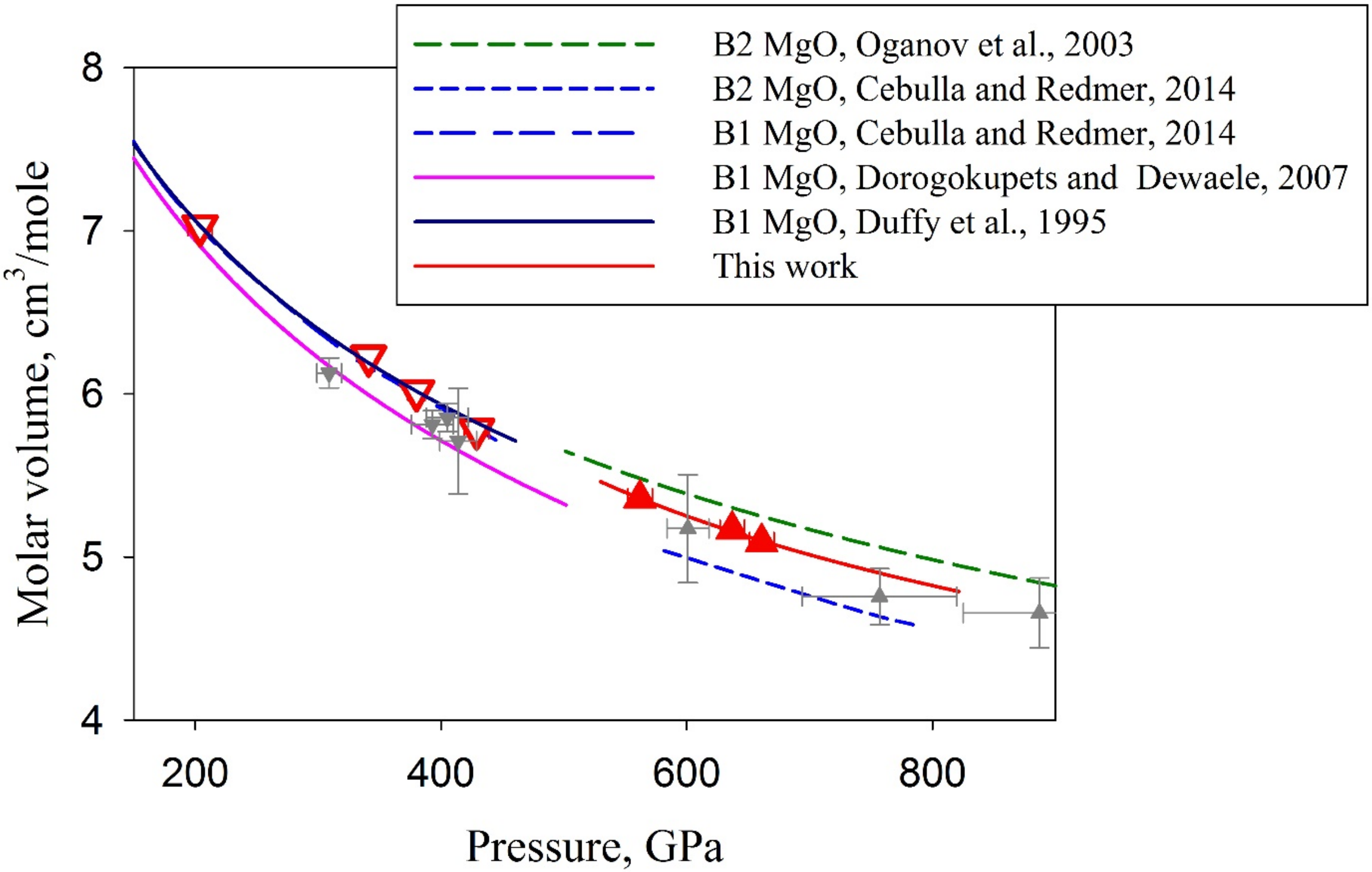

Dubrovinskaia et al., B1-B2 phase transition in MgO at ultra-high static pressure, PRB, revised

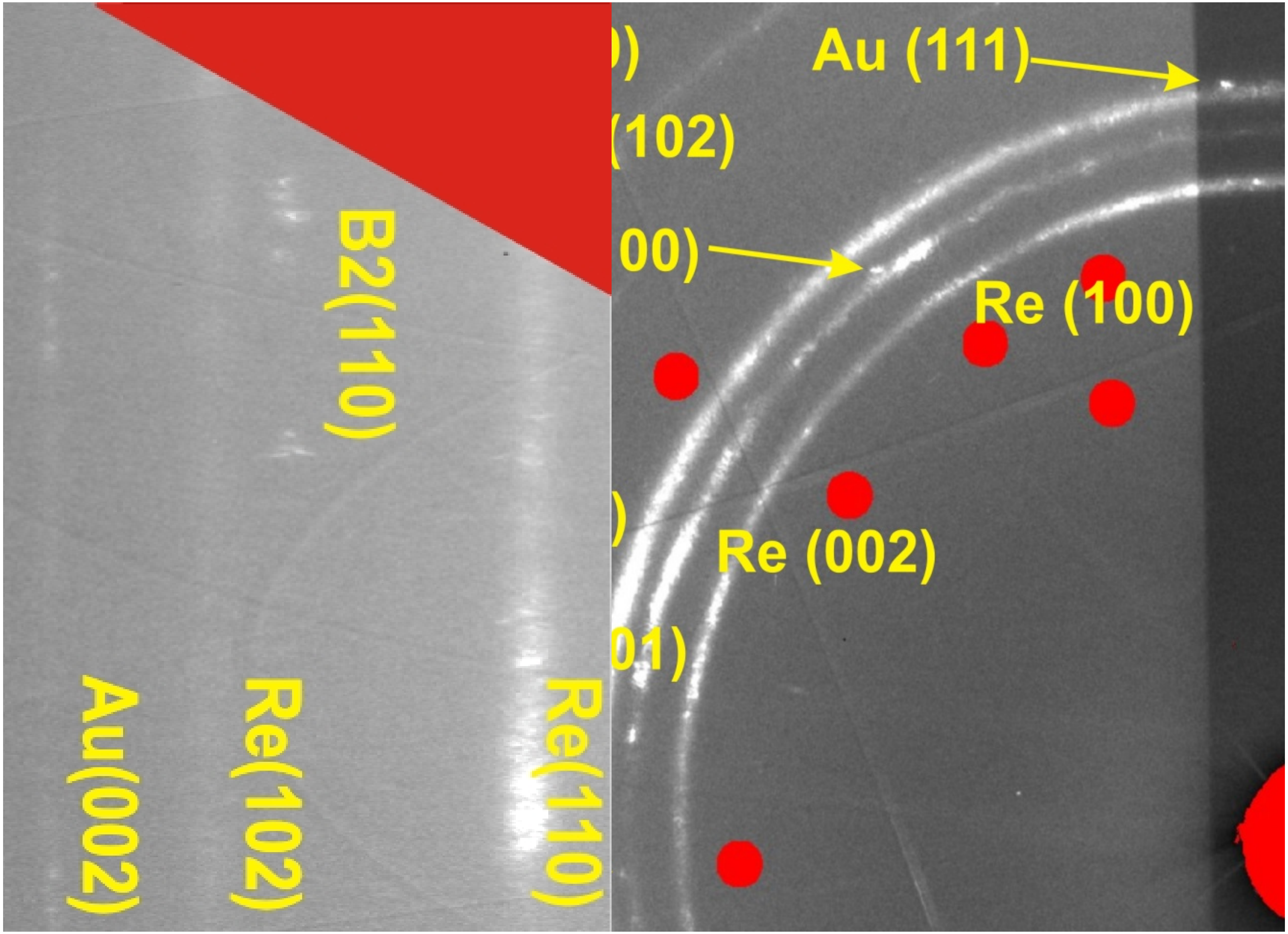

Dubrovinskaia et al., B1-B2 phase transition in MgO at ultra-high static pressure, PRX, revised

Distribution of several iron oxides in DAC at 215 GPa

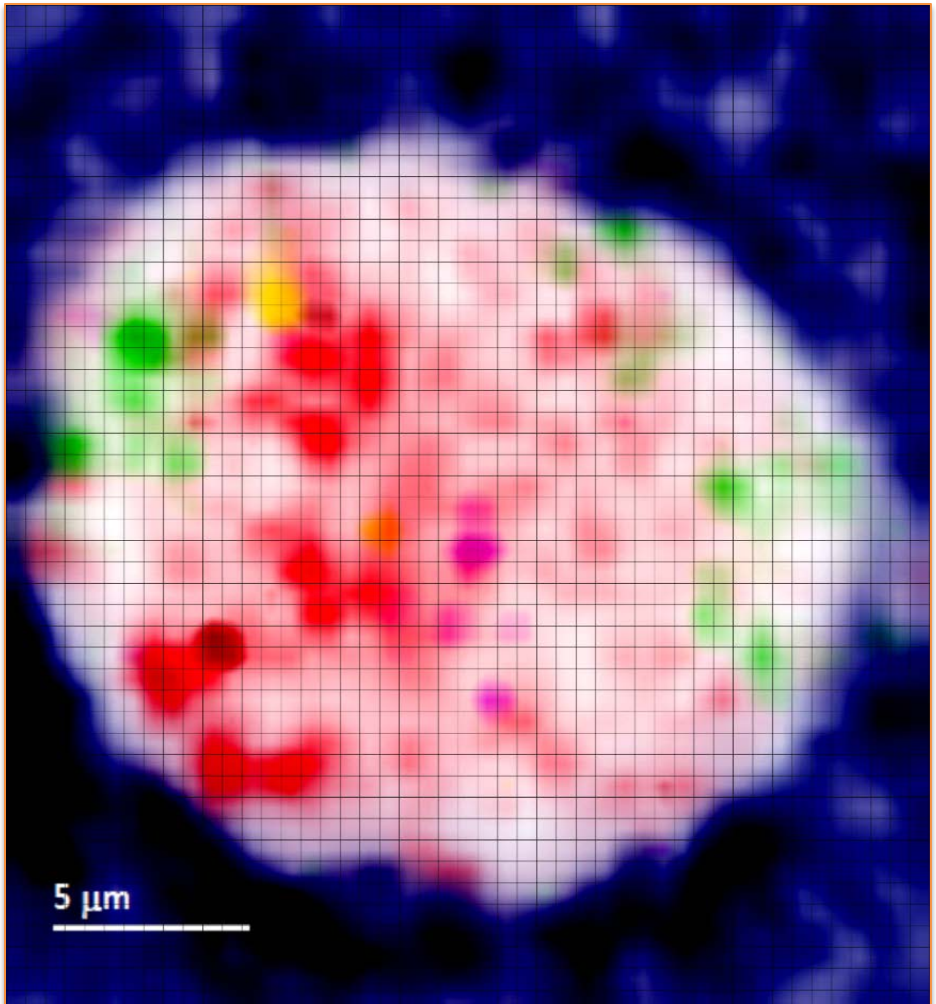

- Re
- PPv-Fe_2O_3
- Fe_3O_4 ($CaTi_2O_4$-type)
- Fe_3O_4 ($CaFe_2O_4$-type)
- $Fe_{13}O_{19}$
- Fe_7O_{12}

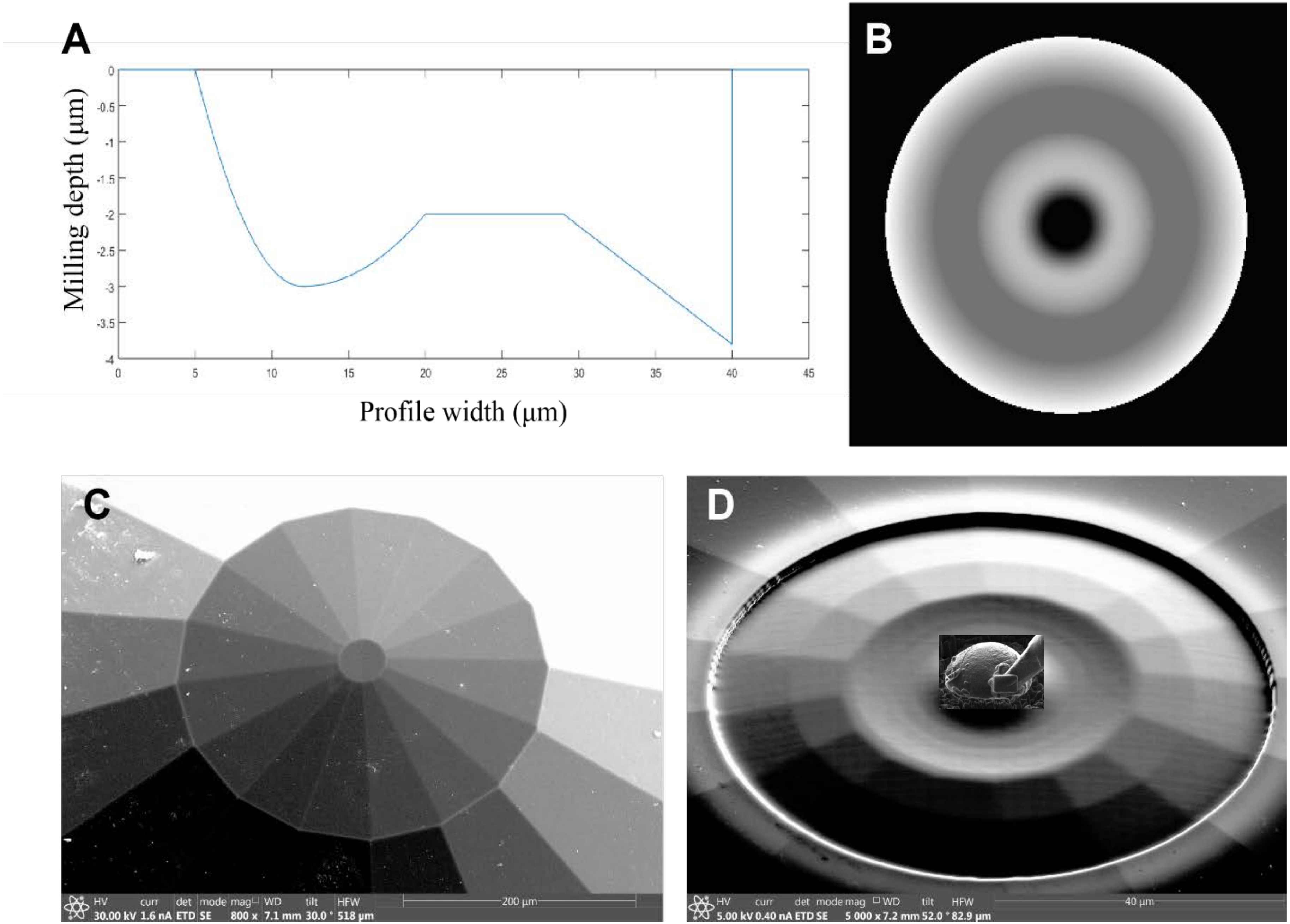

Pictures: S. Petitgirard

New LH setup design

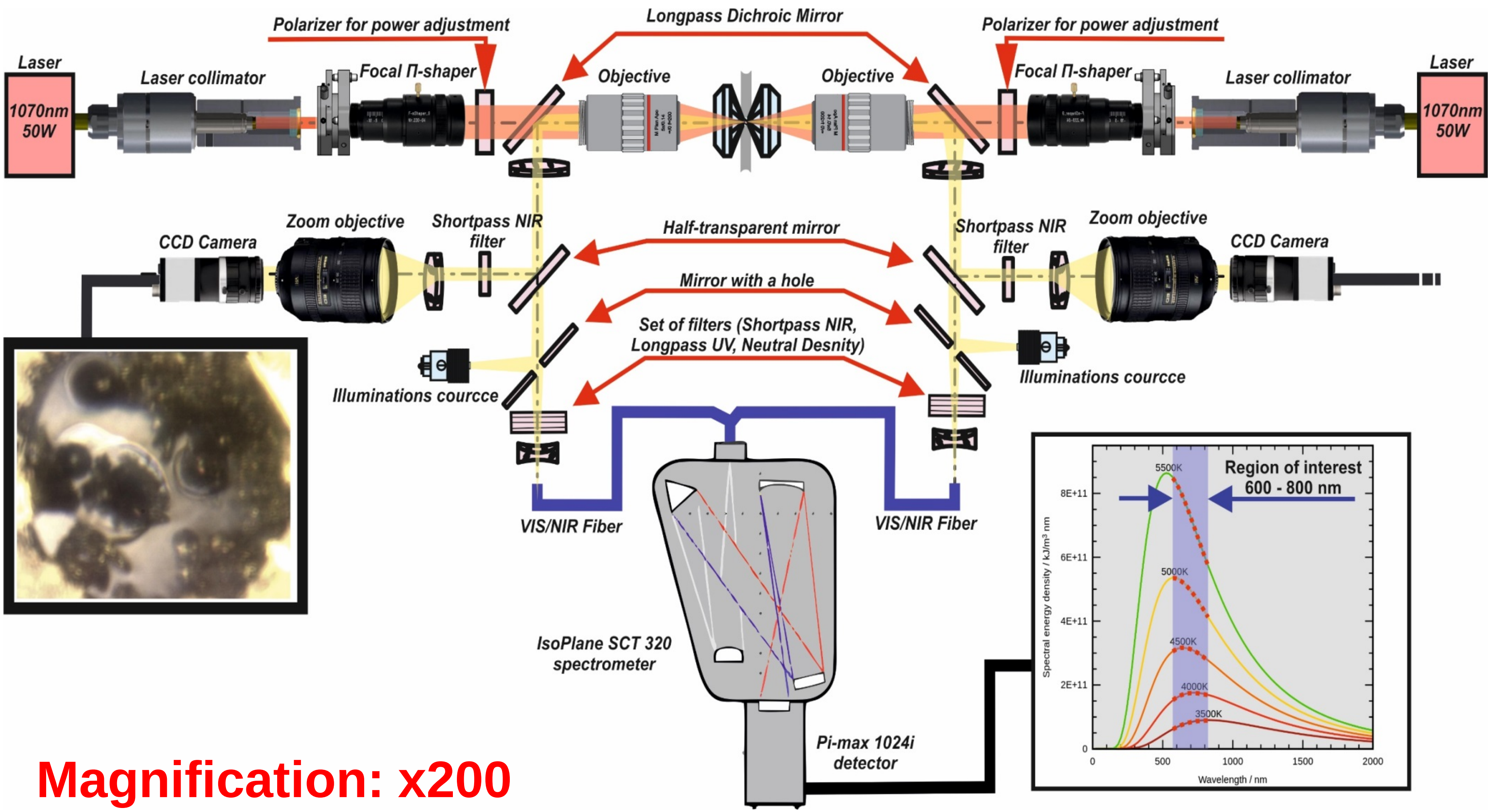

Magnification: x200

Beam-size: ~6 μm flat-top

Fedotenko et al., 2019; in preparation

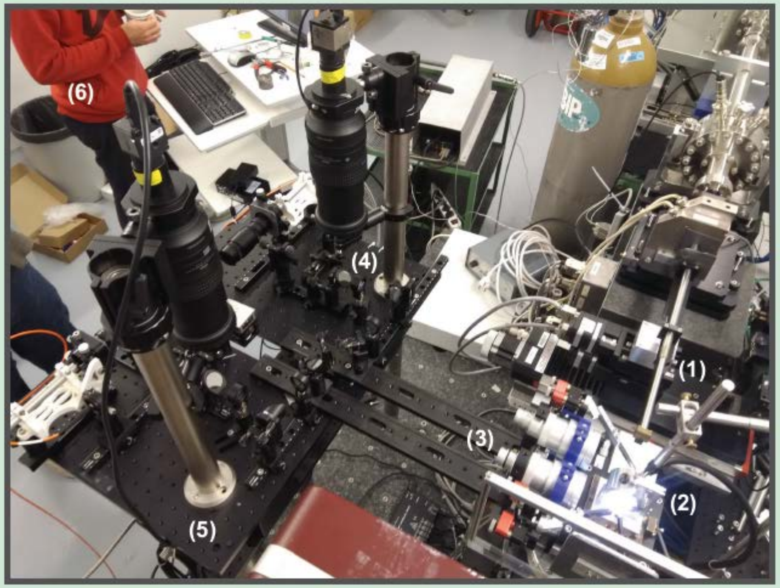

(1) X-Ray Pinhole; (2) DAC; (3) Focusing and Targeting optics;
(4) Upstream LH part; (5) Downstream LH part; (6) Egor Koemets (just a nice guy)

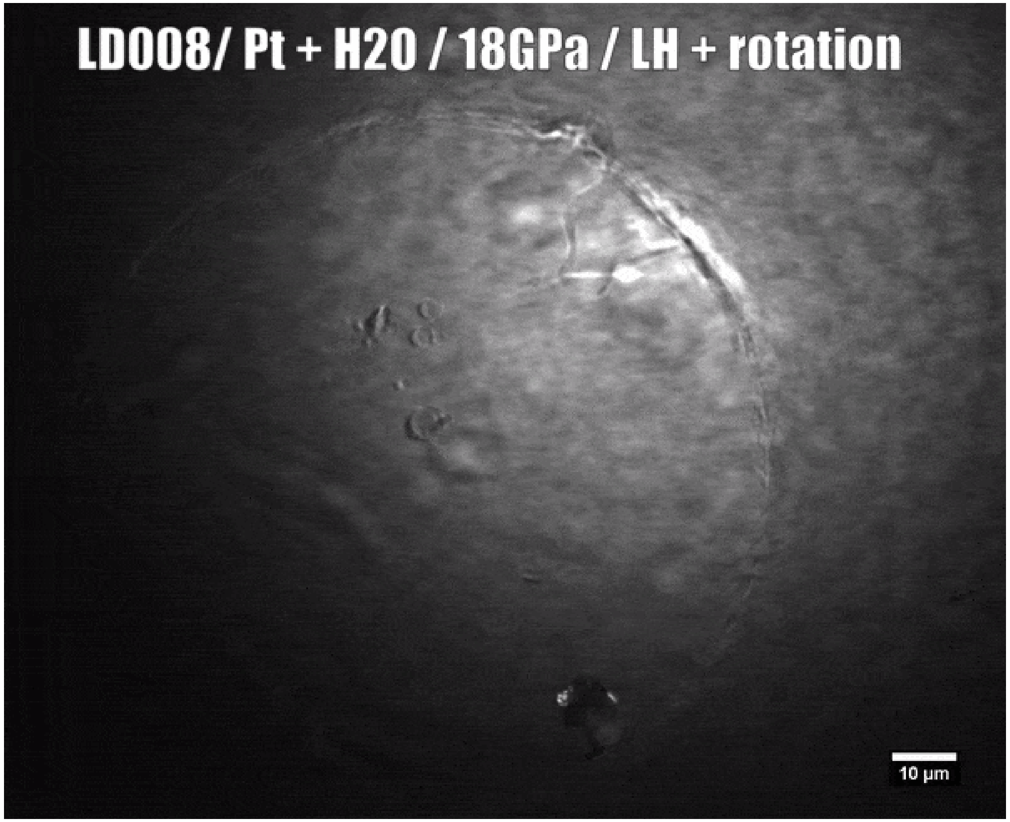

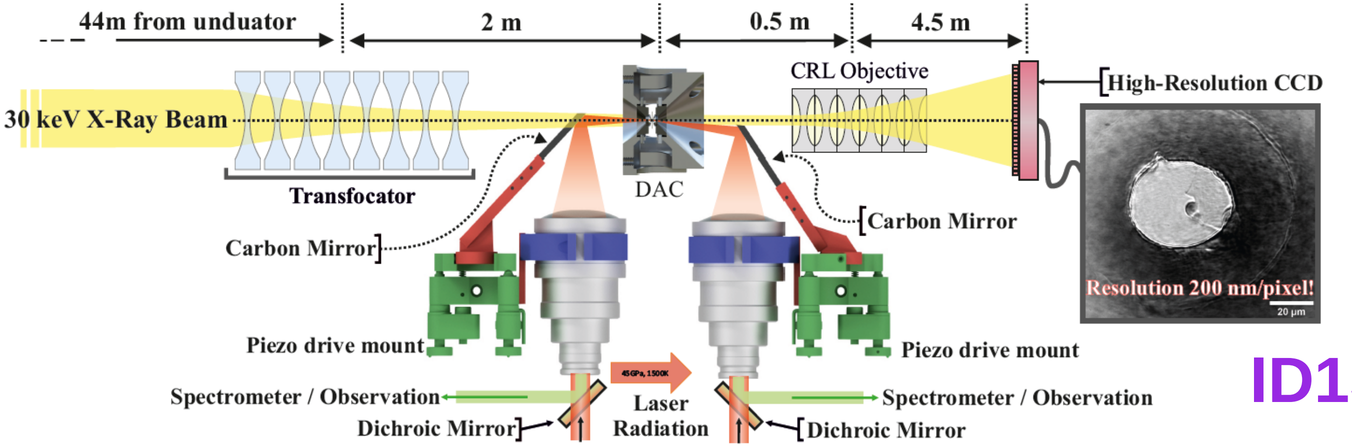

ID15, ESRF

Fedotenko et al., 2019; in preparation

Heating of Re-N in dsDAC

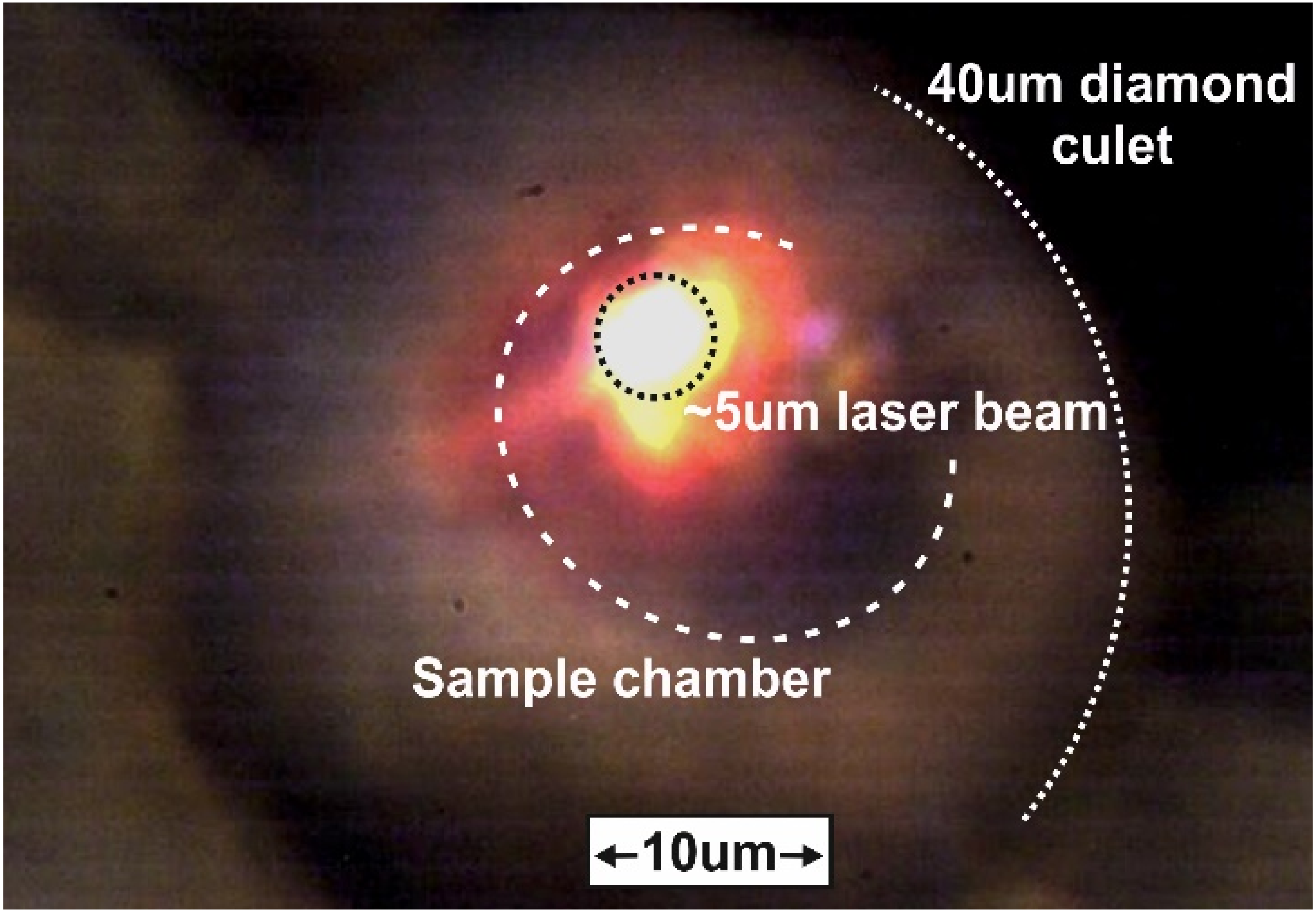

903(10) GPa (Anzellini et al., 2014)
1155(10) GPa (Dubrovinsky et al., 2012)

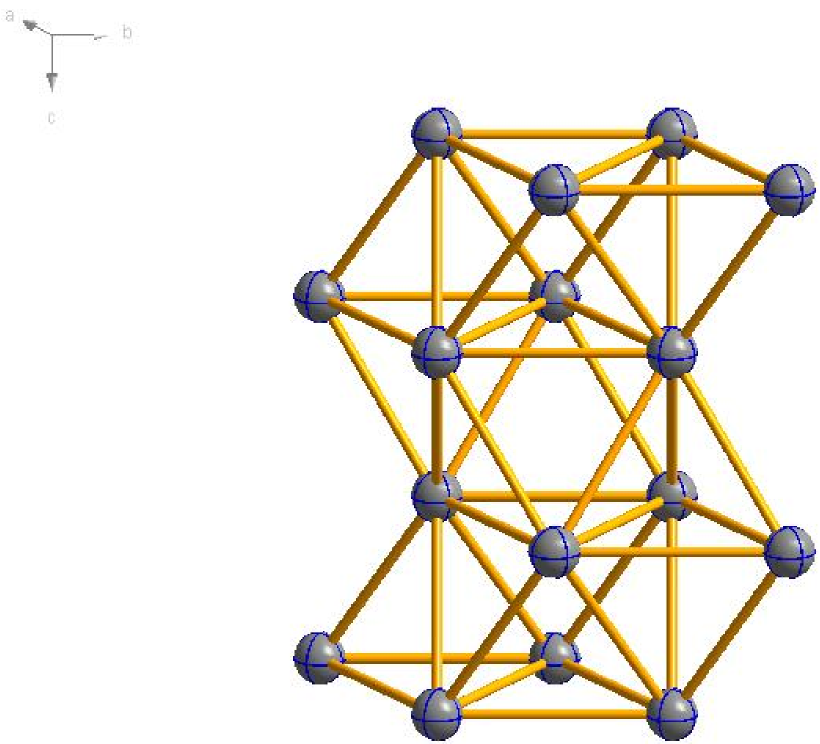

p

Re

P6₃/mmc

a=2.2556(4) Å

c=3.6127(4) Å

V=15.92(2) $Å^3$

Z=2

75 reflections

Rint=5.6%

R1=6.2%

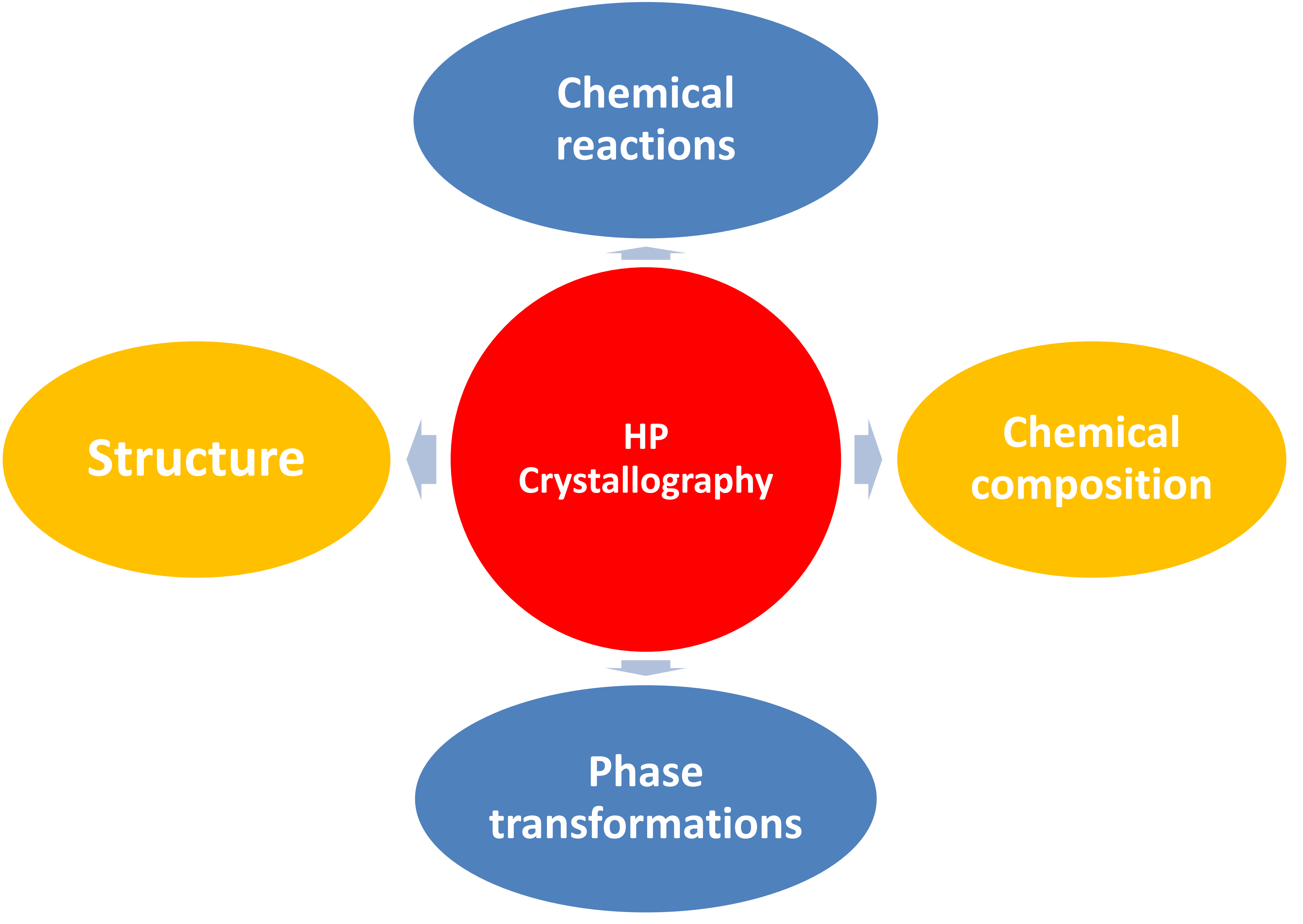
Chemical reactions
Structure
HP Crystallography
Chemical composition
Phase transformations

Acknowledgments

Bayreuth, Germany:

- Dr. Maxim Bykov
- Dr. Alexander Kurnosov
- Timofey Fedotenko
- Egor Koemets
- Sayana Khandarkhaeva
- Georgius Aprilis

P02.2, Petra III, DESY, Hamburg, Germany

- Dr. Elena Bykova
- Dr. Konstantin Glazyrin
- Dr. Hanns-Peter. Liermann

ESRF, France

- Dr. Michael Hanfland (ID 15B)
- Dr. Pavel Sedmak (ID11)
- Dr. A. Chumakov (ID18)
- Dr. M. Mezouar (ID27)

GSECARS, Chicago, USA

- Dr. Vitali Prakapenka

LIU, Linköping, Sweden

- Prof. Igor A. Abrikosov

Photo: E. Bykova